2002

Development of an evaluation test of the coated wire feedstock for cold heading products

Mario Ernest Epler
Lehigh University

Epler, Mario Ernest

Development of an Evaluation Test of the Coated Wire Feedstock for Cold Heading Products

January 2003

DEVELOPMENT OF AN EVALUATION TEST OF THE COATED WIRE FEEDSTOCK FOR COLD HEADING PRODUCTS

by

Mario Ernest Epler

A Thesis
Presented to the Graduate and Research Committee
of Lehigh University
in Candidacy for the Degree of
Master of Science

in

Materials Science and Engineering

Lehigh University

January, 2003

Certificate of Approval

This thesis is accepted and approved in partial fulfillment of the requirements for the Master of Science.

12/3/02

Date

Wojciech Z. Misiolek
Thesis Advisor

11/26/02

Slade Cargill
Chairperson

Acknowledgements

This work was approximately two and a half years in the making, and during that time I received assistance from a great number of people. This partial list of acknowledgements includes those most influential in my success.

The author would like to thank Mike Rex for designing and fabricating numerous rigs, parts, and accessories used in rehabilitating the old hydraulic drawing bench. He also lent his tools fairly freely to me, a big undertaking on his part due to problems in the past of his tools disappearing.

Alex Bandar has provided innumerable hours of help in designing experiments, assembling electronics for the wire-drawing bench, and trouble shooting the numerous problems that we encountered. Although the 1% rule of his may not work, I am still humored by his daily applications of it.

Derrick Rockosi has stood by me in all my many years at Lehigh, and held me up while I was falling, so I owe much gratitude to him. He has taught me to appreciate ice hockey, especially as a distraction to research.

Brian Gish has provided support for me since I met him in nursery school, and has also provided me with many antics since then. He is a great motorcycle rider and a great riding buddy. Be sure to vote for him when he runs for office.

Both Neil Hurley and Dermot Stratton helped take the monotony out of never ending testing performed on both the wire drawing bench and the Instron tensile tester. Without their help, I would have never completed the myriad of tests that I had to perform to complete this work. They humored me as I tried to humor them. After all, it is boring work.

To those who have lived with me throughout my graduate career (Frank Gift, Patrick King, Phil Anderson, Dominik Zurakowski, Shen Dillon, and Greg Vincent), I thank you, even if you provided squalid living conditions for me.

The students and members of the IMF deserve the highest honors. They are hard working and intelligent people that provide a challenge to me to do better and become greater.

To the rest of my gang, I cannot forget you. The hometown crew: Tony, Nate, Jimmy, and Steve (Metal), thank you for countless good times. Brian Newbury has been a great friend that seems to always get me fired up. We have had great radio shows and excellent road trips. He'll always be the punkest guy that I know. I hope he will allow me to continue to be his official bicycle mechanic in the future. Thanks to Dick Yuengling and family for providing me with the means to stimulate creativity. Kathleen has stood by my side and I will not forget her unrelenting support.

Carpenter Technologies has provided me with the opportunity to do great research and assisted me on the way. Thank you to Tom Balliett, Charlie Polinko, Ken Dabbs, and Mohamed Mohamdein.

Arlan Benscoter may be the greatest educator that I have ever met. I doubt that there is a metals related problem that he cannot solve.

My greatest thanks are to Wojciech Misiolek. He has taught me many lessons and provided limitless knowledge and opportunity. I view him not only as a mentor, but as my colleague and more importantly, as a friend. Although his jokes may not always be great, I will always laugh with him.

Table of Contents

TABLES AND FIGURES

Tables

Figures

Abstract

Friction plays a great role in the formability of metals. Often, a value of coefficient of friction is assigned to a material deformed under contact with a specific tooling material. The means to obtain this value is often a test that does not accurately describe the deformation conditions that are encountered in production, which often are different and more complicated.

Cold-heading is the process where wire "blanks" are formed through a series of steps into final products such as fasteners. The steps include wire drawing, forging, extrusion, piercing, and shearing. Friction between deformed material and tooling, next to material ductility and applied state of stress, is a very significant factor in material formability. Lubricants, coatings, and parting agents are used to extend tooling life and facilitate the ability to form parts of greater geometric complexity.

This thesis focuses on developing a series of tests that simulate the actual process and can be used quantitatively and qualitatively to rate coating performance. The first test is a wire drawing test, where drawing force values are captured and a value of coefficient of friction is determined by using theoretical equations. The second test is a trapped extrusion test. In this test, wire blanks were partially extruded using a standard mechanical testing unit. Maximum extrusion force and its standard deviation were used to characterize coating performance along with the shape (footprint) of the force versus stroke of the extrusion. The maximum extrusion force is composed of the force necessary to upset the material in the die and to overcome the static friction of the blank in the die chamber. Standard deviation of this value is

used to measure the coating adherence and assign a rating of adherent, semi-adherent, or non-adherent. The footprint of the curve provides perhaps the most important data. Three distinct footprints were observed, and can be attributed to: 1) typical extrusion, 2) extrusion where the part becomes stuck in the die due to packing of the deformation zone with coating/lubricant, and 3) a curve attributed to non-uniform friction during deformation. It was found that the coatings that exhibited the highest coefficient of friction in the drawing test also exhibited die packing in the extrusion test.

1.0 Cold Heading Introduction

Cold heading is the process where wire feed stock is formed through a series of metal forming operations into a useful, value-added part or component. The term encompasses a wide variety of forming operations. Often, the finished products are small fasteners and related components. Figure 1.1 shows examples of the many different complex geometries that can be formed via cold heading. Many different materials can be cold-headed today, including stainless steels and high temperature alloys.[1, 2] Often, the compositions are modified slightly to lower work hardening coefficient.[1]

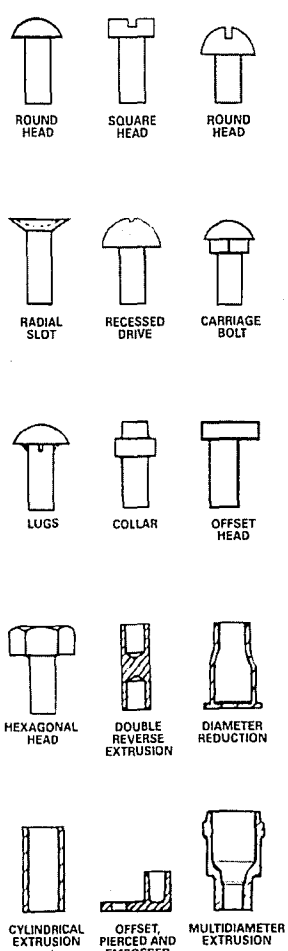

Figure 1.1 Different geometries achievable using cold heading.[1]

Forming operations that fall under the umbrella of cold heading include, but are not limited to: upsetting, forging, shearing, forward extrusion, backward extrusion, and piercing. A brief definition of each follows.

In **backward extrusion** the force is applied to a blank that is constrained on one end by an angular punch. The material flows outward and along the surface of the punch, leaving a hollow cross-section.

Forging is similar to upsetting in that a piece of wire is subjected to compressive forces to initiate flow of the material. However, in forging, the material flows into a defined geometry given by the die that it is constrains it.

Forward extrusion occurs when the wire blank is forced to enter a die with diameter smaller than itself. The cross-sectional area is reduced, while the length is increased due to conservation of volume.

Piercing is very similar to backward extrusion, but generally, the amount of metal flow is less. It is used to produce holes or small slots (such as screw head slots) in the blank.

Shearing is the process where wire blanks are cut from a continuous coil by a die. The cutting occurs by high shear forces applied by the die, and is the first step in the heading process after any pre-drawing that may be applied to the coiled wire.

Upsetting is the process where piece of stock wire constrained only at its free ends is subjected to compressive forces. The material shortens and flows outward in the unconstrained regions forming a portion of upset material that is of larger cross-section than initially. It is a controlled upsetting, where careful calculations are performed to insure the desired geometry will be formed.

Typically, a cold-headed part is formed through a combination of the above processes in a series of steps, also known as "blows." These steps are carried out at a high rate of speed in automated machinery leading to high production rates. Prior to entering any heading dies, the wire is usually subject to a light wire drawing pass. In the drawing pass, the wire that is coming off the coil is put through a wire drawing die with a very small reduction that is used to help straighten the wire and remove any surface defects present on the wire in the coil and to insure the incoming wire has exactly the same diameter and is not out of round.[3]

There are many advantages to cold heading. As already mentioned, high production rates are easily achievable. There is a great amount of repeatability associated with the process, so it is ideal for high production runs. High dimensional tolerances can be maintained fairly easily and surface finish is good, as in most cold forming operations. It is a net shape forming process and therefore material is conserved unlike in machining, except in the case of piercing. The metallurgical benefits of cold heading are also very important. In the majority of cases, the material is work hardened since it is processed at room temperature, providing higher strength. The grain structure is arranged to follow the flow lines that material underwent during forming. This provides strengthening at critical points in the part. Cold forming generally results in higher strength, hardness, toughness, and fatigue resistance because of the grain size and structure.[1, 4, 5]

There are some drawbacks to cold heading. If the part that is being formed is of a more complex geometry, the number of the steps in the process increases. The more steps that are needed to form the part necessitate more complex machinery that

can transfer and orient the part for each die set, and there is a greater number of pieces of tooling for each part. Also, complicated designs may limit the material than can be cold formed. Warm or hot heading may be necessary in such a case. Also, production runs should be high to justify cold heading because of the expensive equipment and dies.

Formability of a cold-headed material can be defined as the amount of deformation that is achieved without undergoing material failure during deformation at room temperature under defined process conditions. Material failure is manifested as surface cracking or tearing or internal microvoid formation. One of the limiting factors in the process is the presence of friction. Frictional forces can prevent formation of complex geometries, can cause excessive die wear, can cause tooling fracture, and can cause workpiece failure. Lubricants and coatings are employed heavily in the cold-heading industry to help facilitate formability of the material. Coatings include parting agents such as copper, which prevents galling between the workpiece and the die and part seizing. Other coatings that are employed are low shear strength materials such as graphite, tungsten disulfide (WS_2), soaps, oxalates, and molybdenum disulfide (MoS_2).[1, 6, 7] Lubricants are employed to also reduce frictional forces. Often, proprietary combinations of these chemicals are used in a single coating.

There is a need for a way to evaluate the effectiveness of a coating in the cold-heading process.[2, 7-13] The characteristics of the coating and lubricant are important when deciding which to employ for a given forming operation. Often, the measure of the effectiveness of a coating that is presented is the coefficient of

friction. The means to determine this value is often a simple sliding or upsetting test where the testing geometry is simple enough to predict the reaction and deformation forces, and the frictional forces can be evaluated. From this, the value of coefficient of friction is determined. The drawback of this approach is that the predicted coefficient of friction value does not provide enough information to coating performance in more severe operations, such as cold heading. Interface interactions can change depending on the applied stress state, and because of the different stress states in cold extrusion (versus wire drawing) coatings may shear or perform differently. A new method of testing, utilizing both wire drawing to determine coefficient of friction and wire extrusion using production dies to measure characteristics in the more severe operations, has been developed.

2.0 Friction in Metal Working Processes

Consideration of friction is very important in metal forming processes. Static friction plays an important role in metal working at the beginning of the process, while dynamic friction conditions apply to the rest of the process. There is a great need to determine friction or friction conditions, especially in dynamic processes. Often, tribological models to evaluate dynamic friction are developed for simple systems that do not account for plastically deforming workpieces.[14, 15] Three different modes of friction are generally investigated in metal forming, along with the transitions between them: sticking friction, boundary lubrication, and thick film lubrication.[16]

Sticking friction occurs when there is some adherence between the workpiece and the die. Often, it is manifested as galling. Galling is the phenomena where the metal from the work piece sticks to the die, and due to the relative motion, shears or tears away and remains attached to the die. The shear stress for deformation is on the order of that of the material, taking into account temperature of deformation and other such factors. Typical values of coefficient of friction (μ) range from approximately 0.5 to the value of 1.0.[16]

Boundary lubrication occurs when a semi-continuous layer of coating or lubricant separates the workpiece and the tooling. A monolayer of lubricant may be on the surface of the material, but the asperities that are present may act to disrupt the layer, especially during deformation. Localized contact occurs, resulting in coefficient of friction values on the order of 0.1 – 0.15.[16] Sometimes boundary

lubricant conditions are referred to as "stick-slip," where sticking occurs between intimate contact between die and workpiece.[6]

Thick film lubrication is also sometimes referred to as hydrodynamic lubrication. It is desirable to have hydrodynamic lubrication to prevent excessive wear on tooling and to prevent large temperature increases in working. It occurs when there are several monolayers of lubricant separating the tooling and the workpiece. It is also facilitated by higher strain rates and specifically designed tooling geometry to promote hydrostatic pressure of the lubricant. One negative aspect of this condition is the degradation of surface quality from the large hydrostatic pressures the workpiece is subject to. These can cause localized yielding of grains because of their anisotropy in yield strength, a condition often referred to as orange peel. Values for coefficient of friction can be quite low for these conditions, which are on the order of 0.01 – 0.05.[16]

Values of coefficient of friction that fall between the stated values for the three defined conditions can be thought of as intermediate conditions that may be a combination of modes. By any means, the value of coefficient of friction alone cannot describe all the friction conditions. Such other aspects as surface finish or defects of the finished workpiece will also give insight to the conditions. Temperature rise due to friction and tool wear are also used as indicators of friction.[17]

Many theoretical equations have been devised to define or estimate the force or stress necessary to perform metal working operations. By using these theoretical equations derived from specific mechanical analysis and actual measured force data,

coefficient of friction can be estimated. Since wire drawing is an integral part of the cold heading operation and many different models have been proposed for wire drawing, part of the test to determine the effectiveness of coatings is a wire drawing test. Force is measured on a hydraulic draw bench using dies of various geometries for the coated materials.

Commonly used equations to determine drawing force or stress for a given set of conditions (material flow stress and coefficient of friction) are similar to those proposed by Schey, Sachs, and Yang. Each is discussed and presented below.

From Schey[6]

$$P = \sigma_m A_2 (1 + \frac{\mu}{\alpha}) \ln(A_1 / A_2) \tag{1a}$$

$$\frac{\mu}{\alpha} \approx \mu \cot \alpha \tag{1b}$$

Where P is the load for drawing, σ_m is the mean flow stress (0.2% offset yield stress measured from tensile test), A_1 and A_2 correspond to initial and final cross-sectional area respectively, α is the die half angle (6° for all dies used in this study), and μ is the coefficient of friction.

Sachs gives a commonly used equation[18]

$$P = \sigma_m A_2 \left[\frac{1+B}{B} \left\{ 1 - \left(\frac{d_2}{d_1} \right)^{2B} \right\} \right] \tag{2a}$$

$$B = \mu \cot \alpha \tag{2b}$$

To illustrate the effect of the bearing length, a theoretical equation for draw-stress (σ_2) from Yang[19] is used in equation set 3.

$$\sigma_2 = \left\{ \sigma_0 \left(\frac{C}{1-C} \right) \left[\left(\frac{A_1}{A_2} \right)^{1-C} - 1 \right] - \sigma_0 \right\} e^{\frac{-4\mu}{d_2} l_2} + \sigma_0 \qquad (3a)$$

$$C = \frac{1 + \mu \cot \alpha}{1 - \mu \cot \alpha} \qquad (3b)$$

Where σ_0 is the yield stress at the elastic and plastic boundary (0.2% offset yield stress), l_2 is the bearing length (or land), and d_2 refers to the diameter of the wire after drawing. σ_2 is simply the drawing force divided by the wire diameter after drawing.[5]

Only the equation set proposed by Yang (of those selected for this study) takes into account all aspects of the drawing die geometry. It accounts for the bearing length of the die, which the other equations neglect, that accounts for a great deal of friction during the process.[5]

Another approach that is proposed by Avitzur[20] is the limit analysis to predict drawing stress. Through mechanical analysis of the process, an upper- and lower-bound approach is used to determine the maximum and minimum theoretical drawing stress for a given material and die geometry to provide a window of predicted drawing stresses, with the actual solution lying between the two calculated values. The upper bound equation derived by Avitzur for wire drawing is as follows[20]:

$$\frac{\sigma_{xf}}{\sigma_0}=\frac{\sigma_{xb}}{\sigma_0}+2f(a)\ln\left(\frac{R_0}{R_f}\right)+\frac{2}{\sqrt{3}}\times\left[\frac{\alpha}{\sin^2\alpha}-\cot\alpha+m\cot\alpha\ln\left(\frac{R_0}{R_f}\right)+m\frac{L}{R_f}\right] \quad (4a)$$

where

$$f(a)=\frac{1}{\sin^2\alpha}\left(1-(\cos\alpha)\sqrt{1-\frac{11}{12}\sin^2\alpha}+\frac{1}{\sqrt{11\times12}}\ln\frac{1+\sqrt{\frac{11}{12}}}{\sqrt{\frac{11}{12}}\cos\alpha+\sqrt{1-\frac{11}{12}\sin^2\alpha}}\right) \quad (4b)$$

To develop upper- and lower-bound solutions, great care must be taken to properly account for material characteristics and identify the exact friction conditions.[20] Since this work is focused on determining friction conditions for various coatings, limit analysis is not a suitable approach. No lower bound solution equations were investigated because of the unknown friction conditions prior to testing.

3.0 Wire Drawing Test

3.1 Introduction

Drawing of wire is an integral process to many industrial applications including cold heading. It provides for high dimensional control and surface finish and is generally a continuous process. Wire can be used as a final product, or as in this case, can be further formed through processes such as heading to reach the final desired geometry. Much research has been performed on the process. Using a drawing test, a first approximation can be made to the friction characteristics of the coatings. Also, insight to coating adherence is provided, however the ability for a coating to last through multiple forming steps cannot be easily evaluated by this test alone.[14] The coefficient of friction that is calculated using the drawing test will provide a more standard measurement of effectiveness that is often used.

Friction is a limiting factor of the wire drawing process. Friction affects total amount of deformation achievable, deformation forces, surface finish, and distribution of strain and therefore mechanical properties of the deformed wire or tube. According to Dieter[5], friction occurs in the "bell" portion of the die (Figure 3.1), but its effect is seen much more in the land (or bearing) portion of the die. The shape of the bell and the approach angle are designed to promote the flow of lubricant into the die and increase the hydrostatic pressure of the lubricant[5] while the bearing portion of the die is necessary to refine the surface of the wire and remove any damage that may have been caused by die wear[4, 5].

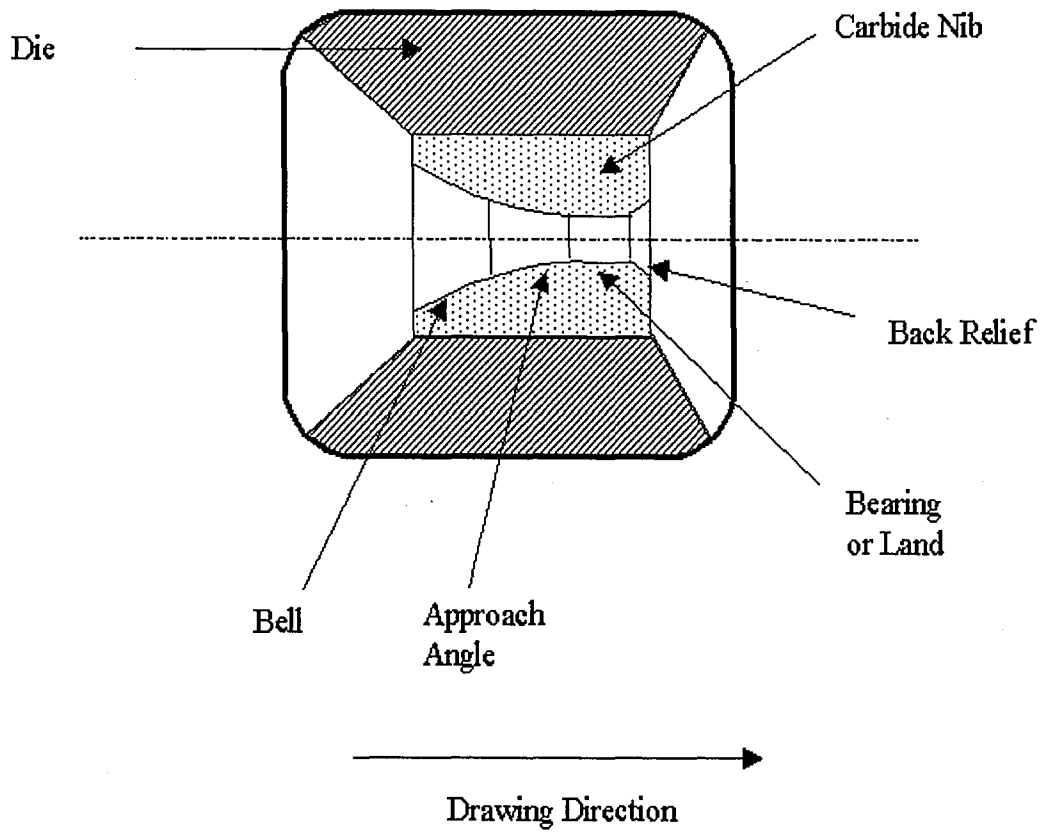

Figure 3.1. Cross-section view of drawing die

Workability, also often referred to as formability, can be defined as the amount of deformation a material can be subjected to without undergoing surface deterioration (cracking, tearing, etc) or the formation of internal microvoids. For any given metal working process, a basic workability function can be defined as:[21, 22]

$$W_k = F[f_1 \text{ (material)}, f_2 \text{ (process)}] \qquad (5)$$

where W_k is defined as workability.

The material function, "f_1," includes material properties such as flow stress, strength, strain-rate dependence on ductility, and stress and microstructure dependence on temperature. The process function, "f_2," defines variables such as state of stress and

its distribution, amount of strain and its localization, temperature gradients, heat transfer, and friction conditions. Since final product often dictates the workpiece material, the process function will be investigated. For wire drawing, the major process variables are amount of strain (cross-section reduction), die design, lubrication, and drawing speed. Die design includes the approach angle, amount of deformation, and bearing length. One of the easiest parameters to change to influence deformation characteristics is the lubricant used in the process.

When dealing with lubricants, there is a general "wish list" for which minimum criteria apply. The lubricant should not react excessively with the work material or the die material. It should sufficiently wet the surface and adhere enough to properly lubricate the workpiece. As a result of the use of a lubricant, there should be a significant reduction of sliding friction, deformation forces, and deformation temperature. Temperature rise due to friction conditions can be quite a significant factor in the processing of metals.[17] A measure of a lubricant's effectiveness in reducing sliding friction is often expressed by the coefficient of friction, μ. The Coulomb coefficient of friction, μ, ranges in value from 0 to 1. There is another approach with use of the friction factor "m." This idea is based upon shear strength of the contact of the interface between the die and the workpiece[5, 16]. According to Dieter[5], the use of μ is well established for wire drawing both in industry and the research community and therefore friction factor, m, is not considered in this analysis.

The evaluation of coatings/lubricants in wire drawing is based upon the value of μ for this study. Dies with varying bearing lengths with similar reductions and die half angles (α) are used to measure drawing force. Because the bearing length

changes, the amount of surface contact with the wire changes, and therefore frictional forces also change. By using a mechanical force balance, a value for μ can be calculated for each die and for each coating/lubrication combination.

To include the effect of the bearing length on draw-stress, a theoretical equation for draw-stress (σ_2) proposed by Yang[19] is used, as shown in equation set 6.

$$\sigma_2 = \left\{ \sigma_0 \left(\frac{C}{1-C} \right) \left[\left(\frac{A_1}{A_2} \right)^{1-C} - 1 \right] - \sigma_0 \right\} e^{\frac{-4\mu}{d_2} l_2} + \sigma_0 \qquad (6a)$$

$$C = \frac{1+\mu\cot\alpha}{1-\mu\cot\alpha} \qquad (6b)$$

Where σ_0 is the yield stress at the elastic and plastic boundary (0.2% offset yield stress). Because of the deformation geometry of wire drawing, σ_0 has been defined as the mean yield stress of un-drawn and drawn wire in this study. l_2 is the bearing length (or land), and d_2 refers to the diameter of the wire after drawing. Drawing stress σ_2 is simply the drawing force divided by the wire diameter after drawing.[5] A_1 and A_2 are the cross-sectional areas before and after drawing, respectively. α refers to the die-half angle.

In order to calculate the value of μ, a Matlab™ program was written that incremented values of μ until the right hand side of the equation was equal to the left hand side. This was done by calculations using measured drawing force. Drawing force measurements were considered to be accurate to five significant figures (a tenth of a pound for the 5000 pound load cell and a hundredth of a pound for the 500 pound

load cell), while tensile testing data was accurate to four significant figures. Coefficient of friction μ was calculated out to four significant digits so that comparison could be made between different coatings that exhibited similar coefficient of friction values. For each coating/substrate combination, comparison of coefficient of friction is made for a given die geometry. Values of coefficient of friction may change between the various die geometries (bearing length) as an artifact of an error in the equation set (6) in calculating exact values of μ. However, the rankings of the various coatings can still be used as a measure of the effectiveness of the coating.

3.2 Wire drawing procedure

Commercial quality 302-HQ, A286, and T430 stainless steel wires were drawn through various dies of the same reduction and the same die half angle (α) with different bearing lengths on a Waterbury-Farrel hydraulic drawing bench. Chemical compositions of the tested steel grades can be seen in Table 3.1. Five samples of each coating were drawn on four dies for the 302HQ material, and five samples of each coating were drawn on one die for the T430 and A286 materials.

Table 3.1: Chemical Compositions of Stainless Steel Alloys Used in Study

302-HQ			
Carbon (max)	0.060 %	Manganese (max)	2.0 %
Phosphorus (max)	0.0400 %	Sulfur (max)	0.140 %
Silicon (max)	1.0 %	Chromium	16.0 – 19.0 %
Nickel	9.00 – 11.0 %	Copper	1.3 – 2.4 %
Iron	Balance		
A-286			
Carbon (max)	0.080 %	Manganese (max)	2.0 %
Silicon (max)	1.0 %	Chromium	13.5 – 16.0 %
Nickel	24.0 – 27.0 %	Molybdenum	1.0 – 1.5 %
Titanium	1.9 – 2.3 %	Aluminum (max)	0.35 %
Vanadium	0.10 – 0.50 %	Boron	0.00300–0.0100%
Iron	Balance		
T-430			
Carbon (max)	0.12 %	Manganese (max)	1.0 %
Phosphorus (max)	0.0400 %	Sulfur (max)	0.0300 %
Silicon (max)	1.0 %	Chromium	16.0 – 18.0 %
Iron	Balance		

An approximately three-foot (0.9144 m) un-drawn section of coated and uncoated wire was used for each test. Coating designations are outlined in Appendix A. Black Coatings A and B are proprietary coatings that are composed of a mixture of MoS_2 and other agents. Precoat soap is a proprietary soap coating, as is oxalate a proprietary oxalate coating. Die bearing lengths were 0.1887, 0.1622, 0.122, and 0.039 inch [4.793, 4.120, 3.10, and 0.991 mm]. The die bearing lengths are also expressed as a percentage of the drawn wire diameter for the rest of the report, resulting in 148%, 127%, 96%, and 31% bearing length dies respectively. Experimental setup is shown in Figure 3.2 and full listing of equipment modifications is listed in Appendix G. Draw speed of approximately 6.5 feet/min [1.98 m/min] was

used. Initial wire diameter was 0.1343" [3.411 mm] (except the S72714-Precoat soap, which was pre-drawn to apply coating to 0.131" [3.327 mm]), which was reduced by drawing to 0.1270" [3.226 mm], resulting in a reduction of 10.5%. Before drawing, the wire was pointed at Carpenter Technologies so that a portion could be inserted through the die into the drawing grips. A special lubricant box was constructed so that the wire would be fully submerged in the lubricant prior to entering the die (see Figure 3.2). Commercial Hammidraw 1846-B drawing grease was used to lubricate the wire.

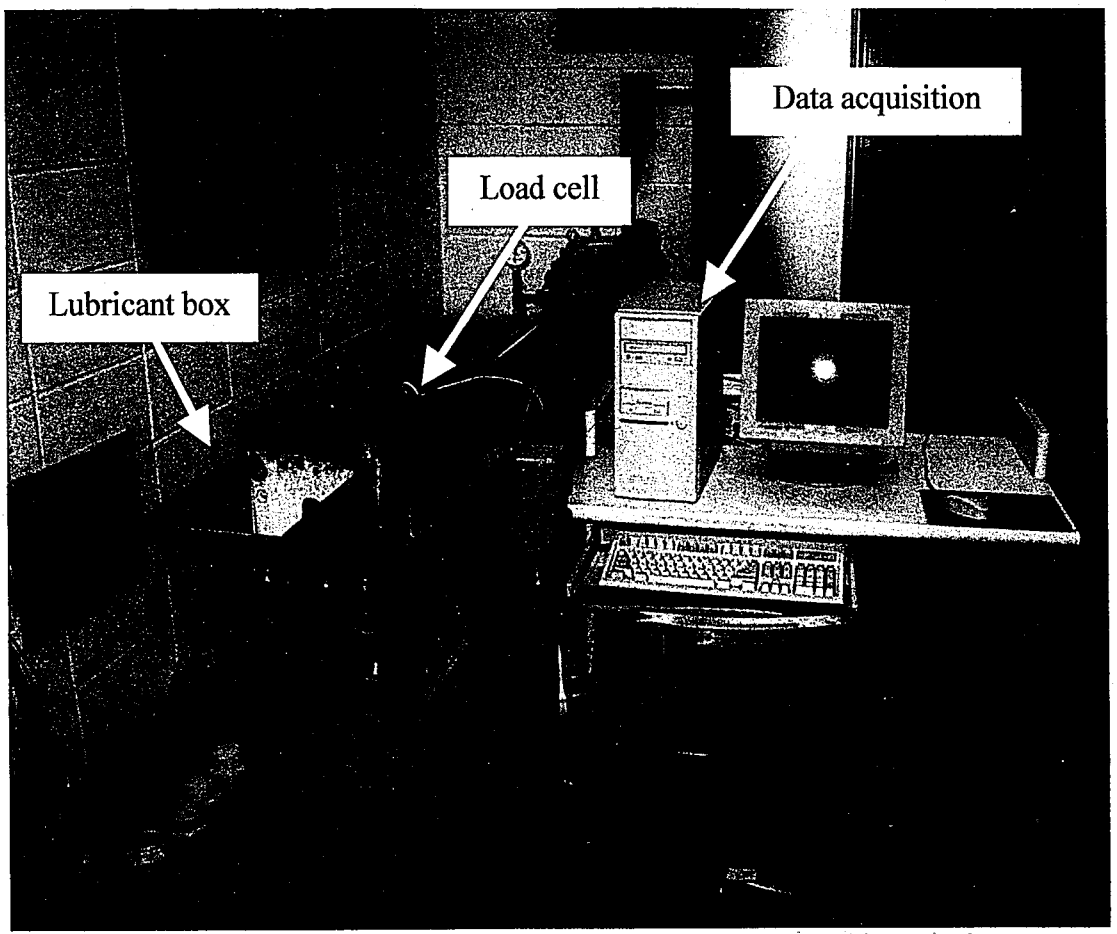

Figure 3.2. Wire drawing bench and data acquisition system used in experiment

Drawing force was measured using either a 5000 or 500-lb (22,241 or 2,224.1 N) capacity load cell (depending on bearing length and substrate material flow stress) manufactured by Entran. A special rig was constructed so that the load cell was located between the ram and the wire grips (Figure 3.2). Output from the load cell is voltage that is linear in relation to the applied load. The signal is amplified and then read by a National Instruments data acquisition card implemented with the National Instruments LabView software. Voltages are recorded for the entire stroke of the bench, and by using a Microsoft Excel spreadsheet, drawing force is determined. A sample of output from the load cell as the computer collects it is seen in Figure 3.3.

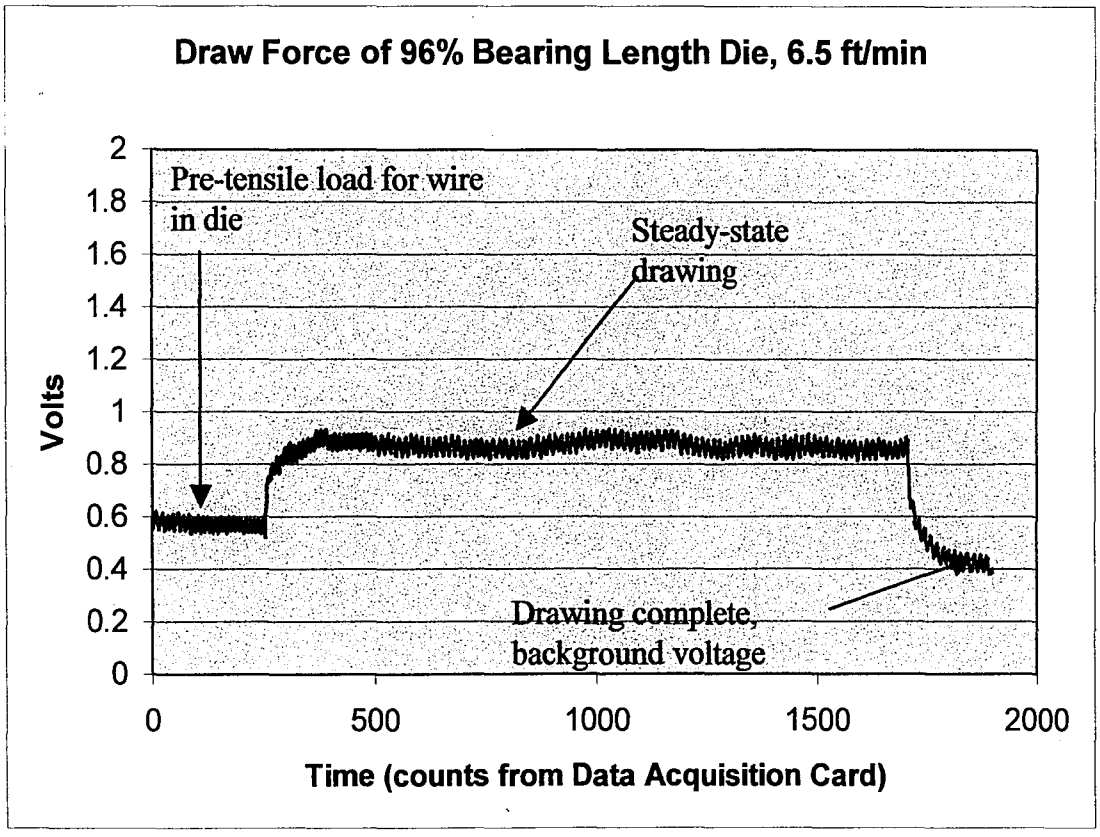

Figure 3.3. Example output from load cell during wire drawing experiment

The pre-tensile load on the wire in the die occurs because the wire must first be pulled a slight amount to ensure that the grips will hold the pointed end. The waviness or thickness of the data is caused by electronic noise. This noise remained constant at approximately 0.075 volts for all the tests. After the drawing is complete, there is some background voltage that the data acquisition card still reads. To calculate the drawing force, the average value of the no load region (background after drawing) is subtracted from the average of the steady state region. This value (in volts) is divided by 10 volts (total output available from the load cell), and multiplied by either 5000 or 500 lbs (capacity of load cell). The result is force for drawing in pounds. 50 counts were collected for each second of drawing.

Samples of the drawn and un-drawn wire were tested according to the ASTM E 8 / ASTM A 370 tensile testing standard to determine the drawn and undrawn 0.2% offset yield strength. The mean value of the two was used as the flow stress of the material in the subsequent coefficient of friction analysis.

3.3 Drawing Test Results

Wire identification and coating descriptions can be seen in Appendix A. Wire was tensile tested before and after drawing from 0.1343 inch [3.411 mm] down to 0.1270 inch [3.226 mm] according to the ASTM E 8 / ASTM A 370 testing method. Tensile results are presented in Appendix B.

Results for calculation of coefficient of friction μ for the die with various bearing lengths can be seen in Appendix C. Samples are listed in order from lowest coefficient of friction to the highest value in each table. It is important to note that for the 302HQ material for the dies with 31, 96, and 127% bearing length the order of

coefficient of friction obtained from these tests does not change although the values do. The A286 and T430 materials were only tested on the 96% bearing length die because there was not sufficient material to test on multiple dies, and 96% bearing length was the most intermediate die, where the bearing portion is nearly the same length as the diameter of the drawn wire.

4.0 Extrusion test

4.1 Introduction

The second test developed to characterize coating performance for cold heading is based upon using actual cold heading production dies. It is a trapped-forward extrusion; meaning that there is no room in the upper, larger diameter bore of the die for the wire to upset freely other than to fill the chamber before extruding. Figure 4.1 shows a schematic drawing of a typical trapped extrusion die for cold heading.

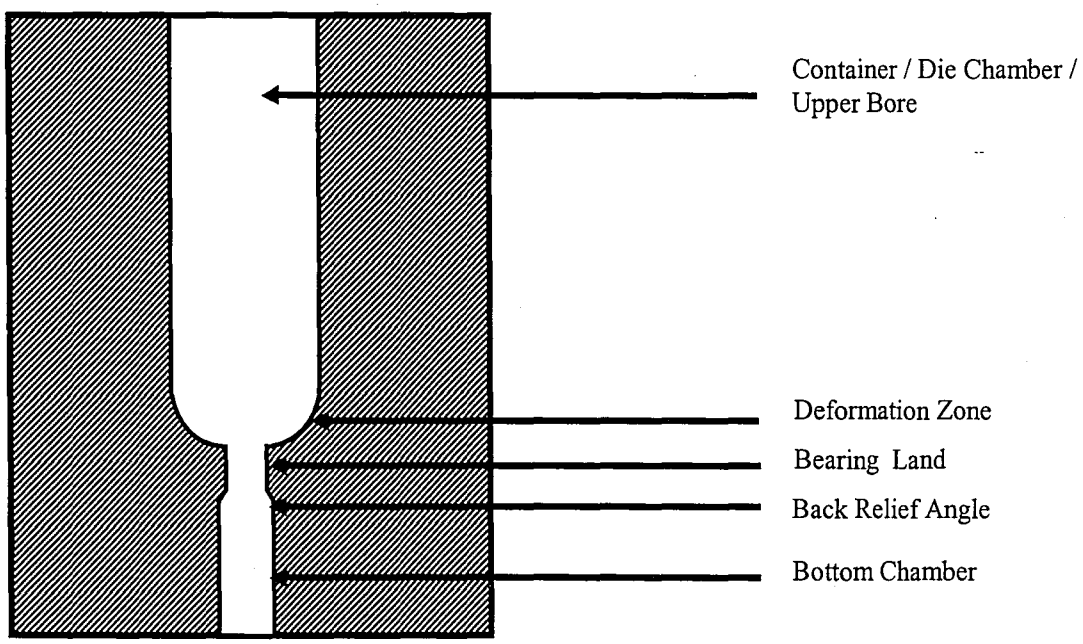

Figure 4.1. Schematic view of the cross-section of a trapped-forward extrusion die.

The container of the die is where the undeformed blank is placed prior to extrusion. This is where maximum friction occurs because of the contact between the surface of the blank and the die. The deformation zone of the die is the radial portion of the container leading to the bearing portion. These two areas cause the wire to be reduced in diameter during the application of a compressive load from the top of the

die. The back relief angle has the same function as in the wire drawing die: to relieve and elastic deformation of the material at a strain rate that will not cause surface tearing. The knock out pin is inserted through the bottom chamber to remove the partially extruded billet.

A comparison between trapped and open extrusion scenarios can be seen in Figure 4.2. In an open extrusion, Figure 4.2a, the blank is not contained entirely in the die prior to extrusion. Typically, open extrusions are more common than trapped extrusions, but there are several drawbacks.[1] If frictional forces and deformation forces in the deformation zone are too high, the material will upset above the lower portion of the die, where the reduction is performed. Reduction is typically limited to 30% or less depending on the flow stress of the material, otherwise the sample tends to upset above the die. By using trapped forward extrusion dies, much greater reductions can be performed (sometimes as high as 75%).[1] Figure 4.3 shows the steps in the experimental extrusion process.

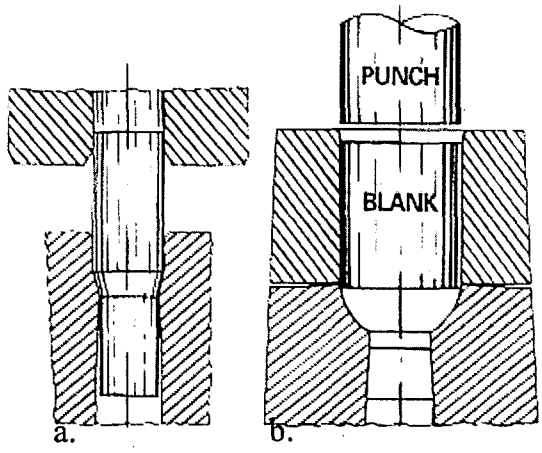

Figure 4.2. Comparison of a) Open forward extrusion and b) Trapped forward extrusion[1]

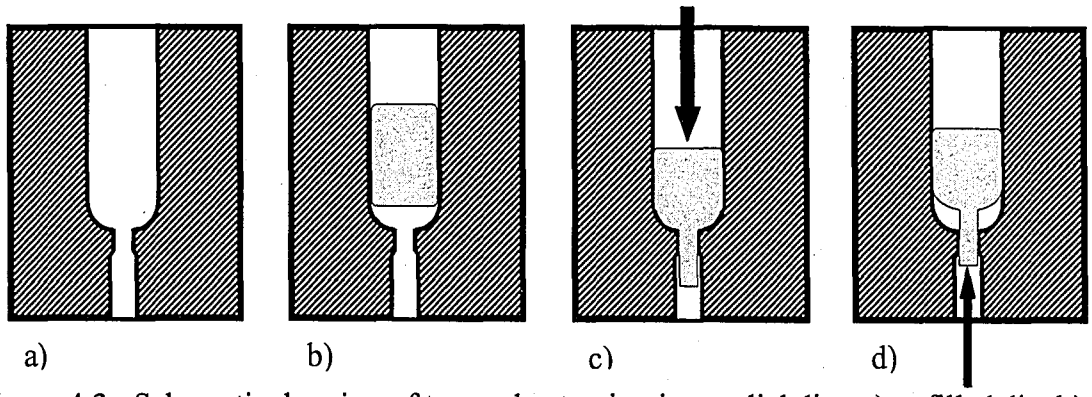

Figure 4.3. Schematic drawing of trapped extrusion in a radial die. a) unfilled die b) die with extrusion blank c) arrow represents force applied by punch (not shown) to extrude blank d) arrow represents force applied by knock out pin (not shown) to remove partially extruded blank

To simulate the actual step of extrusion in a heading-operation, an existing punch and die set were obtained from an industry partner company, with proprietary geometry. A special die holder was designed and machined so that the punch and die could be fitted to an instrumented Instron testing unit. This allows for a full load versus stroke curve to be captured for the extrusion process.

The extrusion process has both important and significant deformation and friction components that have been well studied.[23] A typical load versus stroke graph for direct and indirect (not focused upon in this study) hot extrusion can be seen in Figure 4.4. Hot extrusion exhibits similar characteristic curve shapes to cold extrusion, although the magnitudes of the various components may be different. The initial portion of the graph shows a rapid increase in load as the billet or blank (in the case of cold heading) fills the die chamber upon upsetting. A maximum load is reached, which is the breakthrough force initiating actual flow of the billet material through the die orifice. Several components contribute to the breakthrough value. Among them are friction components of static friction of sample in the container of

the die and maximum surface contact between the undeformed sample and the container.[23] Also, upsetting of the sample maybe necessary to fill the chamber before extrusion occurs, although at such a small extrusion ratio, this may not be a large component of the value. Finally, the material flow stress is another component of this value. The rest of the curve's shape is based upon several different phenomena, one of which is friction and any changing friction conditions. See Figure 4.4(b).

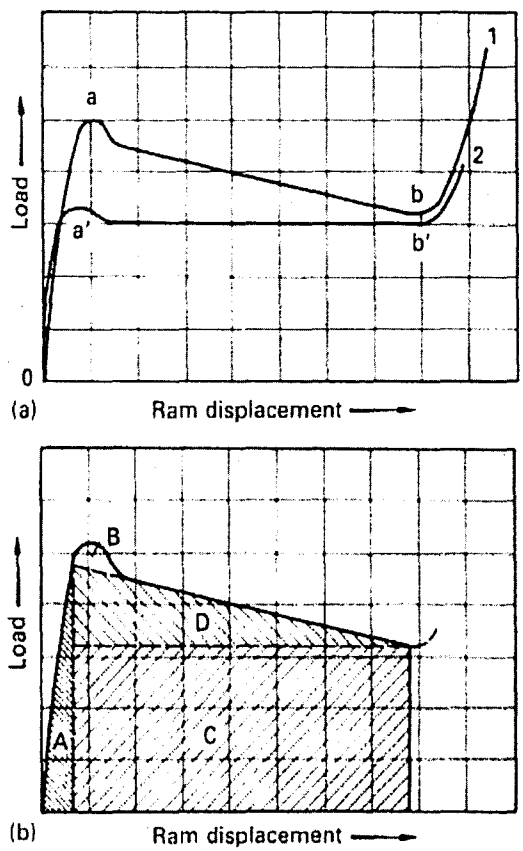

Figure 4.4. (a) Typical load versus displacement curves for extrusion. Curve a-b showing direct extrusion process. Curve a'-b' shows indirect extrusion process. (b) Components of direct extrusion load versus displacement curve: A = work of upsetting billet, B = work needed to initiate deformation (breakthrough force), C = work of deformation, D = work to overcome shearing and friction[24]

The shape of the force-displacement curve can give much initial information to the process. For instance, the appearance of a "double peak" in the initial portion of the curve can suggest several different phenomena, one of which is non-uniform metal flow due to "die packing." Die packing occurs when the coating of the wire comes off and fills the deformation area of the die including the die orifice causing a large increase in the load needed to extrude the blank. Effectively, the die packing increases the extrusion ratio R (by making the orifice smaller), hence the higher force value. The shape of the curve after the breakthrough point also gives information about the coating's performance. If the curve tapers off, it suggests proper lubrication. If the curve maintains a steady value, it suggests that lubrication is not properly occurring or friction conditions are not constantly decreasing because of less material in the upper chamber of the die as time increases.

4.2 Wire extrusion procedure

Commercial quality 302HQ, T430, and A286 wire that was pre-drawn in the drawing test was extruded using a commercial cold extrusion radial die and flat punch set. Figure 4.5 shows the punch and radial extrusion die. Figure 4.6 shows the die and punch on the Instron tensile testing unit.

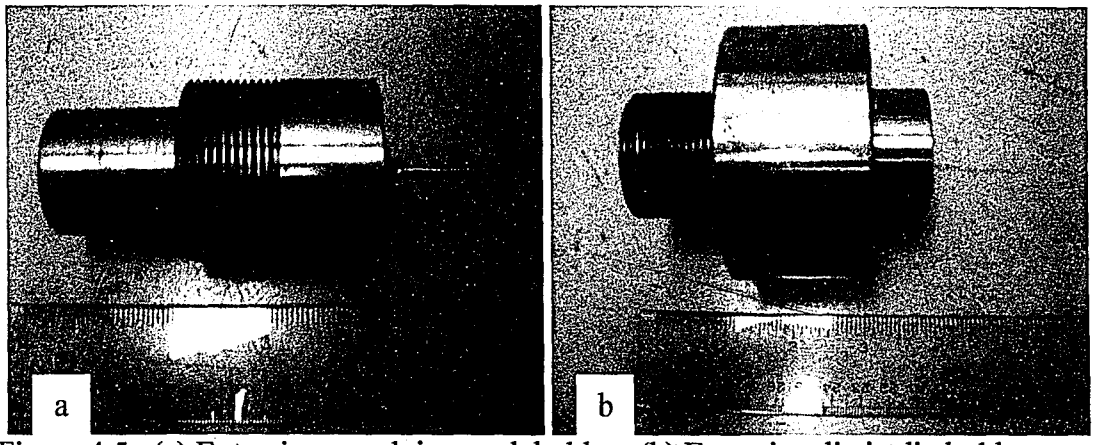

Figure 4.5. (a) Extrusion punch in punch holder. (b) Extrusion die in die holder.

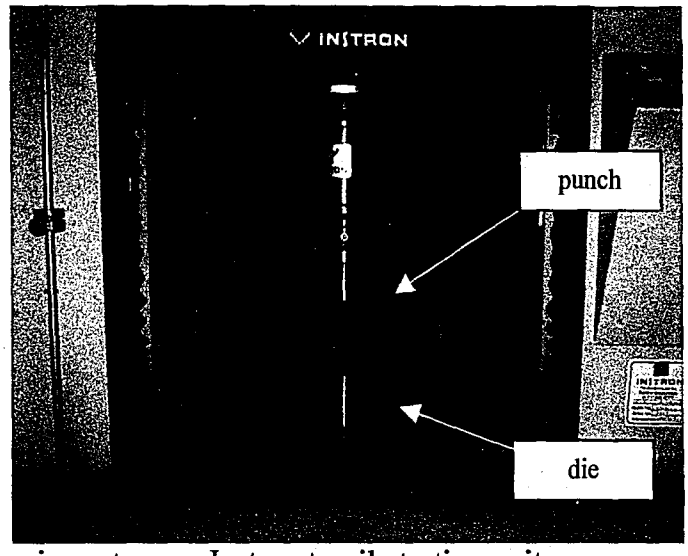

Figure 4.6. Extrusion set up on Instron tensile testing unit.

The wire used in the extrusions experiments was pre-drawn using Hammidraw 1846-B drawing grease (except S72675, S72678, and WS2 which were drawn in Sun Waylube) from 0.1343 inch to 0.1270 inch [3.411 to 3.226 mm]. The 0.127 inch [3.226 mm] wire was extruded to a final diameter of 0.101 inch [2.57 mm]. The extrusion ratio R for this test is

$$R = \frac{A_0}{A_F} = \frac{(d_0)^2}{(d_f)^2} = \frac{0.127^2}{0.101^2} = 1.58$$

The wire was sectioned into extrusion blanks of 3 lengths: 0.716, 0.587, and 0.446 inch [18.2, 14.9, and 11.3 mm]. Extrusion blanks were prepared by cutting freshly drawn wire with a wire shear which is pictured in Figure 4.7.

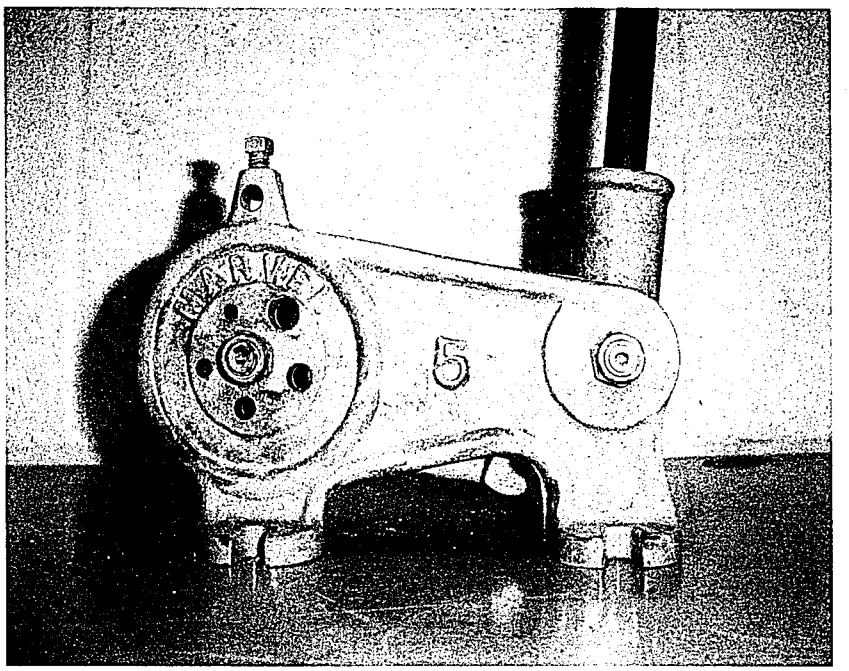

Figure 4.7. Wire shear used to cut long lengths of drawn wire into shorter extrusion blanks for the extrusion test.

Prior to loading the test sample into the extrusion die, a drop of lubricant (Hasco Stealth) was applied using an eyedropper into the bore of the die. The blank was put into the large diameter portion of the die and tapped down using a smaller diameter setting pin and a hammer to insure that the blank was seated on the face of the deformation zone portion of the die. It is important to note that this does not insure that the material was placed entirely into the deformation zone of the die. Another drop of lubricant was applied on top of the blank in the die prior to extrusion.

Once the blank was loaded into the die, the die holder was screwed into the bottom portion of the Instron unit. The punch/punch holder was placed on top of the blank in the as the Instron crosshead was jogged down to insure proper alignment of the punch to prevent breakage. Once the crosshead was at the proper position, the securing pin was inserted and the locking ring was tightened. The punch was then jogged down until a small pre-load was achieved before testing began.

Each extrusion was run at a crosshead speed of 20 inch/min [0.508 m/min]. Three different length extrusions were performed, designated as long, medium, and short. Corresponding to these designations are cut off lengths (blank lengths) and strokes (respectively) of:

0.716 inch blank – 0.3700 inch stroke	(18.2 mm blank – 9.398 mm stroke)
0.587 inch blank – 0.2500 inch stroke	(14.9 mm blank – 6.350 mm stroke)
0.446 inch blank – 0.0800 inch stroke	(11.3 mm blank – 2.032 mm stroke)

The strokes were chosen so that nearly the same amount of material was left un-extruded for each extrusion length (0.346, 0.337, and 0.366" respectively [8.79, 8.56, and 9.30 mm]).

The shortest blank/extrusion was paused for 0.6 seconds at full stroke in an effort to capture the maximum load, because in initial testing, a consistent breakthrough point was not noted. It was then determined that the shortest extrusion was not long enough to reach a steady state extrusion conditions where the extruded length was significantly longer than the bearing portion of the extrusion die. The stroke of the extrusion should be at least two times the bearing length to insure that steady state extrusion is reached based upon experience during testing.

During extrusion, load/stroke data was captured at a rate of 20.000 pts/sec. Load/stroke data was then exported as a comma-delimited text file to be imported into Microsoft Excel. Using an Excel spreadsheet, maximum extrusion load, extrusion footprint, and area under the curve was determined for each test.

After extrusion, the punch was removed from the die and the die holder was removed from the base of the Instron testing unit. A knockout pin was inserted into the small-bore portion of the die and was used to remove the partially extruded wire blank from the die. After any coated sample was run except copper coatings, the bore of the die was swabbed with cotton and ethanol in an effort to prevent any build up of the coating. Periodically, the die was also cleaned by submerging it in ethanol and putting it in an ultrasonic cleaner. For each coating/substrate combination, five samples were extruded for each extrusion geometry.

4.3 Extrusion Test Results

Two numerical measurements are made on the extrusion test: max extrusion load and area under the extrusion curve. Additionally, the shape/footprint of the extrusion curve, and the amount of standard deviation for the maximum load and the area under the curve are used to investigate the coatings performance. Data for all three extrusion conditions are included, but the short extrusions are not considered in the analysis. Because of the short length of the extrusion, there is uncertainty if a steady state in extrusion load was reached in all the cases. In some cases this causes a great discrepancy in maximum load when compared to the medium and long extrusions, where the maximum loads correspond for each coating/substrate

combination. Also, area under the curve is not included for the short extrusions because of the above reasoning and the fact that the short extrusion curves were captured by pausing at the end of the stroke for 0.6 seconds and steady state conditions were not met.

Appendix D shows the maximum force results for the extrusions. Also included in the tables are the standard deviations and the percentage standard deviation. Each table contains one type of substrate (302HQ, A286, or T430) and one extrusion length (short, medium, or long). Each table is arranged from lowest maximum extrusion force to the highest extrusion force.

Area under the curve (energy for extrusion) was calculated for the long and medium extrusions. The calculation was performed using a macro available in Microsoft Excel. This method was compared to a hand calculation performed by using the trapezoidal method and was found to be in satisfactory agreement. Appendix E shows the results of the area under the curve calculations. Again the tables are arranged in increasing order of area.

The third criterion used to rate coatings in the extrusion test is the shape or "footprint" of the curve. Figure 4.8 shows examples of the different footprints. Two portions of the curve give information about coating performance. For the initial part of the curve, a single maximum peak that is widely known as the typical direct extrusion curve (A-type) and a two-peaked curve that in this case indicates die packing can occur (B-type). The flat, non-sloped taper is indicative changing friction conditions or non-ideal friction conditions, which may be related to poor lubricant

carry through (C-type). Also, a characteristic breakthrough force is not evident in the C-type curve.

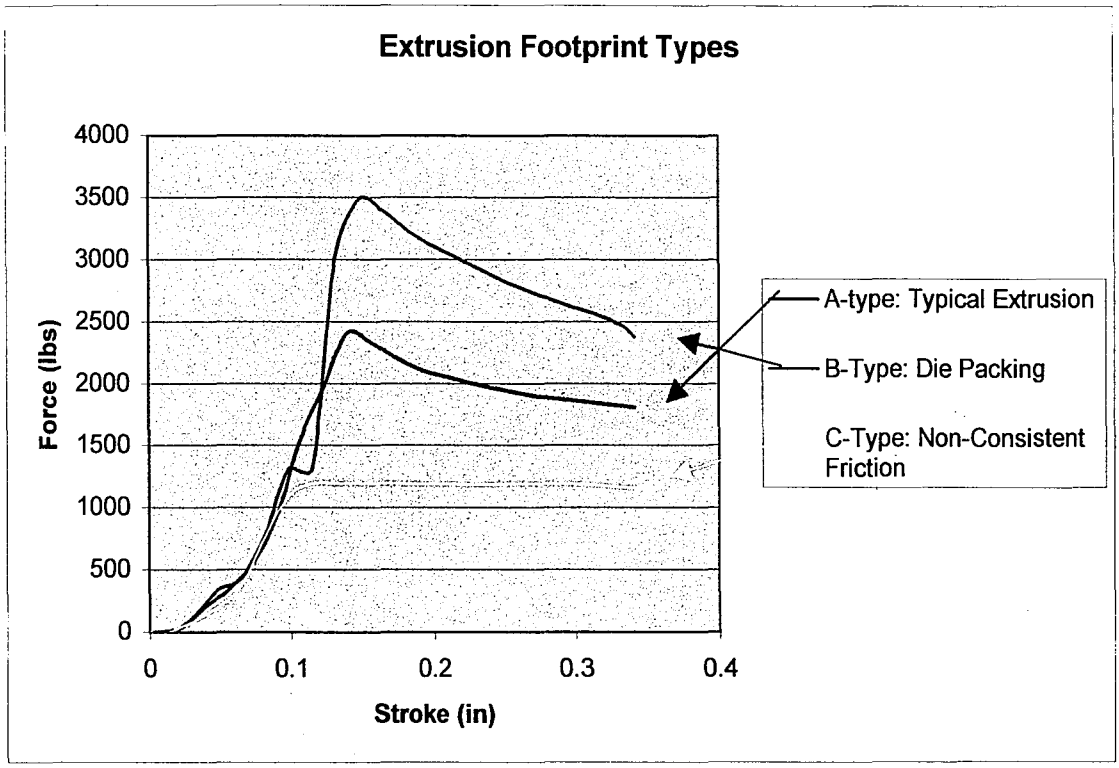

Figure 4.8. Basic extrusion footprint shapes.

5.0 Copper coating thickness measurements

To measure copper coating thickness, the following procedure was used. Measurements were only performed on S72675, S72676, and S72677 wires. Small sections of wire (drawn and undrawn) were cut approximately 0.5 inch in length. A small piece of plain carbon steel wire was tack-welded to one of the sample using 30-Volts. The wire was then hung into a Buehler Edgemet electroless nickel coating solution by the plain carbon wire so that the wire was completely submerged and kept in the solution at 80°C for approximately 3 hours. This provided a thick, hard Ni coating that helped preserve the Cu coating during subsequent metallographic polishing.

The Ni-coated wires were placed on their sides in cold-setting epoxy. Standard metallographic preparation was used to prepare the samples. Each mount was ground and then polished up to 6μm diamond paste until the centerline of the wires was reached. The un-etched wires were investigated using a light optical microscope in conjunction with a Leco-3001A image analysis system by taking coating measurements along several different points on each piece of wire. An example of an image used to measure Cu thickness can be seen in Figure 5.1. Results for copper coating thickness measurements can be seen in Table 5.1. Fairly large standard deviations are observed in the measurements, which may be a result of several factors. The Cu coating process results in inherent variations to coating thickness. In addition, errors could be made if the wire was not at the exact centerline when the coating was measured, and measurements made outside of the copper coating may both contribute to the larger standard deviation. It is important to note

that the copper coating thickness remained relatively unchanged after drawing. In some instances, it appears to be actually thicker, but when compared to standard deviation, the thicknesses are comparable for the drawn and undrawn material. Also, the thicknesses are with in standard deviation of the quoted thickness values (50, 100, 200 micro-inch).

Table 5.1. Copper Coating Thickness Results for 302-HQ Substrate Wires

Coating-ID	Copper Thickness Micro-Inches	Copper Thickness Microns
Undrawn		
S72675	121.1 ± 19.1	3.08 ± 0.49
S72676	58.36 ± 12.6	1.48 ± 0.32
S72677	172.3 ± 21.8	4.38 ± 0.55
Drawn		
S72675	109.6 ± 22.3	2.78 ± 0.57
S72676	83.9 ± 18.4	2.13 ± 0.47
S72677	203.0 ± 40.2	5.16 ± 1.0

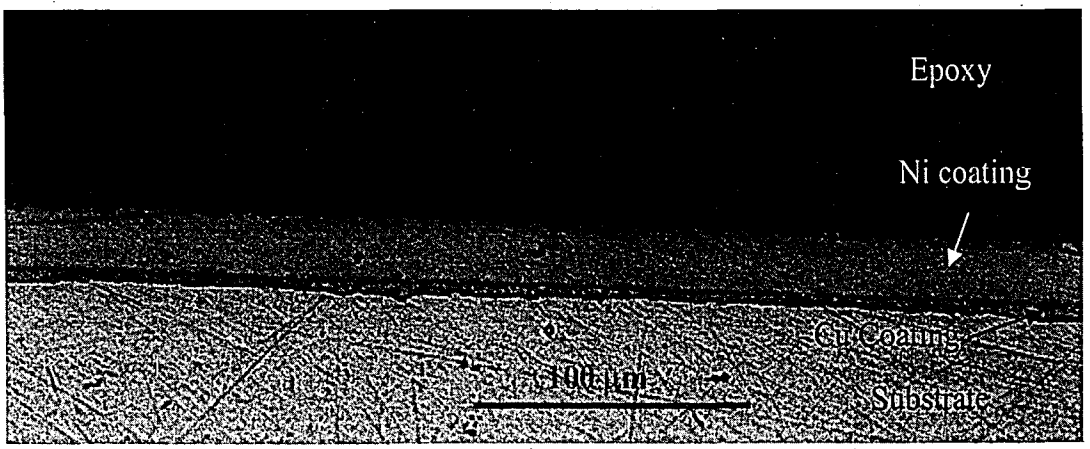

Figure 5.1. Image of Cu coating on drawn S72677 wire as used to measure coating thickness. Ni coating is present to preserve Cu coating during metallographic preparation.

that the copper coating thickness remained relatively unchanged after drawing. In some instances, it appears to be actually thicker, but when compared to standard deviation, the thicknesses are comparable for the drawn and undrawn material. Also, the thicknesses are with in standard deviation of the quoted thickness values (50, 100, 200 micro-inch).

Table 5.1. Copper Coating Thickness Results for 302-HQ Substrate Wires

Coating-ID	Copper Thickness Micro-Inches	Copper Thickness Microns
Undrawn		
S72675	121.1 ± 19.1	3.08 ± 0.49
S72676	58.36 ± 12.6	1.48 ± 0.32
S72677	172.3 ± 21.8	4.38 ± 0.55
Drawn		
S72675	109.6 ± 22.3	2.78 ± 0.57
S72676	83.9 ± 18.4	2.13 ± 0.47
S72677	203.0 ± 40.2	5.16 ± 1.0

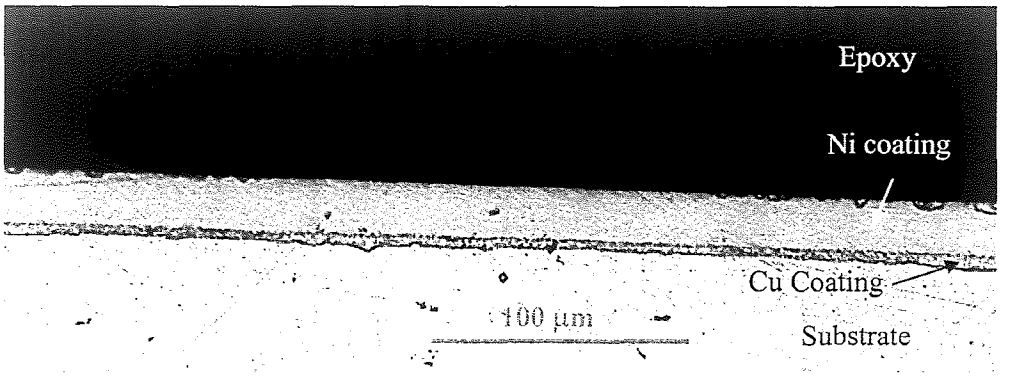

Figure 5.1. Image of Cu coating on drawn S72677 wire as used to measure coating thickness. Ni coating is present to preserve Cu coating during metallographic preparation.

6.0 Discussion

6.1 Wire Drawing Test

In order to rank coating performance, a calculated coefficient of friction was used to compare the various materials. The lower the value of coefficient of friction, the less force necessary to deform a material in a given process due to lower friction forces. Although deformation forces may be lower, this test did not evaluate any effect of coating on die wear or temperature effects for sustained periods of drawing at high speeds. These are two other important considerations for coatings. Several different methods are available to estimate coefficient of friction in the wire drawing process, such as the different methods proposed by Schey, Sachs, and Yang.[5, 6, 18, 19] By using the Yang equation, any differences in flow stress (evident in Appendix B) are accounted for, and die geometry is accounted for to provide a more accurate coefficient of friction. The differences in flow stress of the coated material arise because of the various coating processes and the amount of cold work from bending and coiling associated with each. By changing the bearing length of the drawing die, any changes that might be associated with geometry can be noted. This allows for a recommendation for a standard die geometry and test setup to compare various coatings and substrate materials by imposing a severe enough test to differentiate between coatings.

One interesting result obtained by varying the wire drawing die geometry (changing bearing length) was that at the higher bearing lengths (127 and 148%) the drawing force for some of the coatings did not change. This is illustrated in Figure 6.1. Specifically, the copper only coated samples and the non-coated sample showed

essentially the same drawing force for the 96, 127, and 148% bearing length. The coatings that are considered not as adherent (black coatings A and B, oxalate, and WS_2) show a sudden increase in drawing force for the 148% bearing length die. Although this phenomenon is not entirely understood or well documented in the literature, when the Yang equation is plotted for a given set of conditions (flow stress, reduction, die angle, and coefficient of friction) and bearing length is varied, a similar result is observed, as plotted in Figure 6.2. The steady state value of drawing force is achieved at higher bearing lengths when the equation is evaluated. One proposed mechanism for the sudden increase in the drawing force for certain coatings at high bearing lengths is that there is such a demand on the coating that it shears from the substrate material, and packs into the die. This may cause additional resistance to deformation by making the die orifice smaller. Future work is needed to more thoroughly quantify this phenomenon.

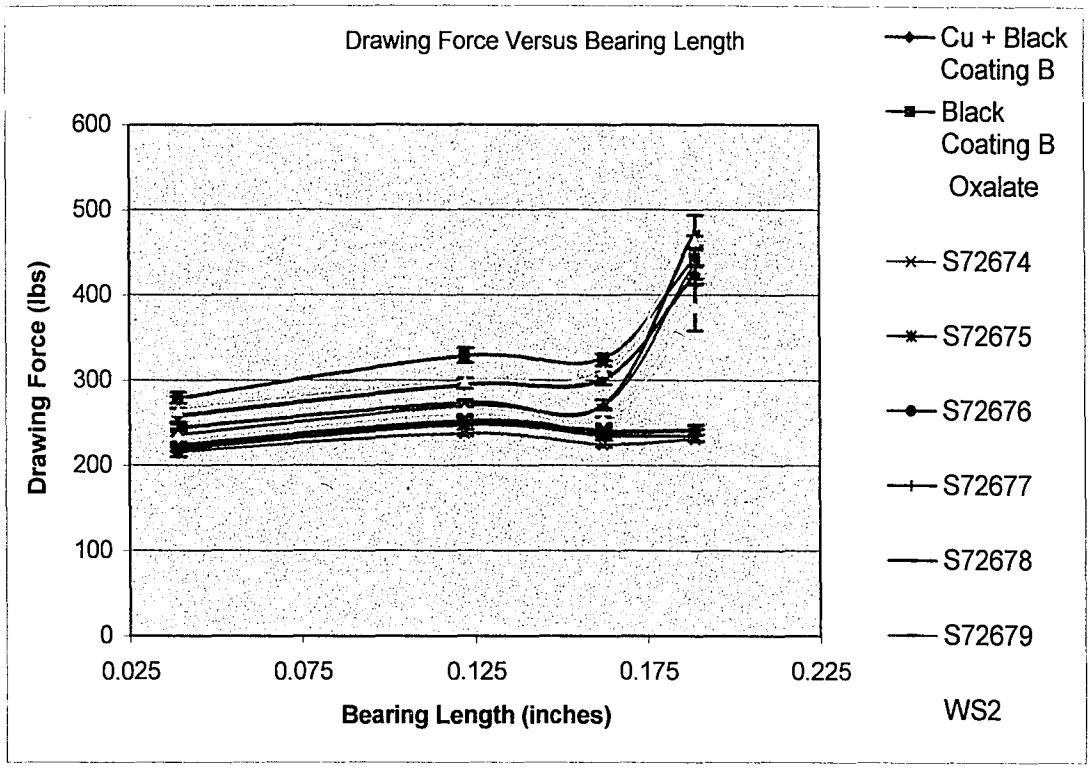

Figure 6.1. Drawing force data versus bearing length for different coatings 302HQ stainless steel wires.

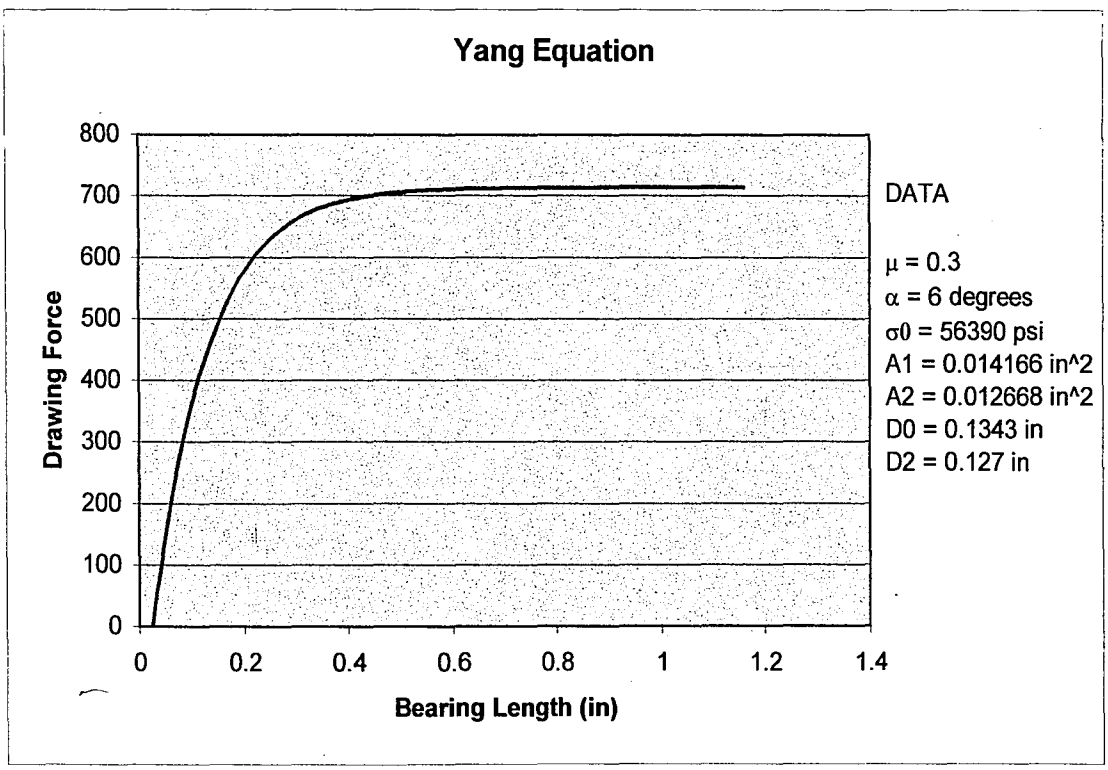

Figure 6.2. Calculated drawing force versus bearing length using the Yang equation and data as presented on the figure.

Because of the limited amount of material for both the A286 and the T430 wires, the majority of the wire drawing study was completed on 302HQ. As can be seen in Tables 9.5, 9.6, and 9.9 in Appendix C, the ranking of coefficient of friction (from lowest to highest) for the 302HQ samples tested on the 31, 96, and 127% bearing dies is exactly the same for all these cases and is listed below:

1. S72674
2. S72676
3. S72675
4. S72677
5. Ws2
6. S72678
7. S72679
8. Oxalate
9. Cu + Black coating B
10. Black coating B

The ratings are listed in order of the increasing coefficient of friction as calculated using drawing force and the Yang equation. This provides a validation as to the method of ranking the coatings in the drawing test, but does not validate the numerical values assigned to coefficient of friction by the Yang analysis. Since three dies provided the same rankings, it was determined that the 96% bearing length provides the best die for testing (out of the original 4 dies: 31, 96, 127, and 148%). The bearing of the die is nearly the same as the drawn diameter of the wire. For the 148% bearing length die, there was a slight change in order of ranking of several of the coatings and they are listed below:

1.S72674
2.S72675
3.S72676
4.S72677
5.Ws2
6.Black coating B

7.Cu + Black coating B
8.S72679
9.Oxalate
10. S72678

The first half of the list (1 – 5) remains relatively unchanged in the ranking of the coatings, while bottom half is more re-arranged. This suggests several interesting points. The non-coated and the copper only coated samples are not affected as much by the bearing length portion of the die, also evident in Figure 6.1 where drawing force does not increase with increasing bearing length on the 302HQ material. The more "friable" coatings, such as Black coating A, Black coating B, and Oxalate are more affected by increasing bearing lengths. It also appears that at a bearing approximately 1.5 times the diameter of the drawn wire, friction characteristics change and the data is not comparable to the lower bearing length dies, evident by the proposed stripping of coating leading to sudden increase in drawing force (Figure 6.1).

One explanation to the surprising ranking of the dies showing that the uncoated sample exhibiting the lowest coefficient of friction is that there is simply lower deformation taking place due to the smaller diameter of the undeformed wire. The wires that were coated were of not of the same diameter because of the coating on top of the original substrate. There is less incompressible material such as the additives in some of the other, higher ranked coatings such as Black coating A and Black coating B. This argument is also supported by the copper coated samples, where the ranking for the 3 lower bearing length dies (31, 96, and 127%), the thinnest copper coating of 50 microinches (S72676) has lower μ than 100 microinch copper coating

(S72675) which has a lower μ than 200 microinch copper (S72677). For the largest bearing length die, the coefficient of friction for the 50 and 100 microinch copper samples were essentially the same (Appendix C – Table 9.10), and both were lower than coefficient of friction calculated for the sample with 200 microinch Cu coating.

Drawing tests for the A286 and T430 substrate materials was only performed on the 96% bearing length die because of the limited amount of material. This die was chosen for reasons mentioned above. Coating rankings were somewhat different than for the 302HQ material. One similarity between all three series is that the Black coating B and Black coating B + copper coated samples had the highest coefficient of friction except for A286, where it was the second highest coefficient of friction. Generally, copper only coated samples showed lower coefficients of friction. For the A286, where there were two 100 micro inch copper coated samples, they performed nearly the same, which is to be expected and helps to further validate the data.

More general statements about the coatings on the T430 and A286 cannot be made because the number of samples tested was low due to lack of time and material availability.

Recommendations for the drawing test are as follows. The die geometry to be used should be approximately a 1:1 ratio of bearing length to drawn wire diameter. The die half angle should be 6° and the reduction should be moderate around 10% (in the case of this study it was 10.5%). Starting diameter of wires to be tested should all be the same to minimize any effect of reduction on coating performance. If a secondary lubricant is used, the wire should be completely submerged in it prior to entering the die to insure complete lubrication. Draw force should be measured and

by using the Yang equation, coefficient of friction can be calculated. Comparison of coating performance should be made on the basis of the numerical values of μ, however, the value of μ cannot be assumed to be the true coefficient of friction for the process because it changes (decreases) with increasing bearing length because of an inherent flaw in the equation. Ideally, the coefficient should not change or change very little with minimal changes in bearing length in the drawing dies, not decrease.

6.2 Extrusion test

The extrusion test gives much more relevant and useful data about each coating's performance during deformation that is related to cold heading than the drawing test. It is a very close simulation of one of the most common steps in the actual heading process and thusly is very useful to evaluate materials. Extrusion is integral to almost all final cold headed part geometries. It is simple and quick to perform and is able to be used to generate a table of data that can be used to make a recommendation for a coating based upon a given process geometry in heading.

Three different extrusions were done for each coating/substrate combination: long, medium, and short. Because of the uncertainty associated with the short extrusions due to the lack of reaching steady state extrusion the data will not be discussed. The reason that steady state extrusion may not have been reached in the shortest extrusion is that when the extrusion blank is placed into the die, it does not completely fill the radiused deformation zone of the die. Because of the short extrusion stroke and the bearing length of the extrusion die, the sample may not

completely be extruded past the bearing. The stroke is mainly used to fill the die for the shortest extrusion.

For the long and medium extrusions, four main data points that give different information for each are gathered. They are as follows:

1. **Maximum extrusion force:** The maximum extrusion force occurs at the beginning portion of the extrusion curve. It is the *breakthrough pressure* (or force as it is presented in the results). This maximum is a result of the large amount of un-deformed material in the die chamber that must move to be extruded and the friction along the die wall. The maximum value gives a measure of the coating effectiveness in minimizing frictional forces against the container and bearing of the die. Headability is generally considered to be inversely proportional to peak load.
2. **Area under the extrusion curve:** The area under the extrusion load versus stroke curve shows the energy necessary to deform the material and also accounts friction associated with the material moving in the die. It is estimated that more than 50-percent of the energy required in cold-forming goes not to actually deforming the steel but to overcoming frictional forces.[9]
3. **Shape or footprint of the extrusion curve:** Three distinct shapes were observed for the extrusion test. A typical one peaked extrusion curve shows a maximum force at the breakthrough, and decreasing force as the stroke continues. This is because there is less material in contact with the upper bore of the die, resulting in progressively less frictional force. Figure 4.8 also shows the "two peaked curve" that is associated with the part becoming stuck

in the die. It is believed that this two-peaked curve occurs because during the initial portion of the extrusion, the coating does not adhere to the part and begins to fill the deformation portion of the die. Then, a much higher breakthrough force is needed to extrude the same part. However, without the ability to separate the die mid-deformation and preserve the coating condition, this cannot be directly verified. Also, in the curves where a double peak is noted, the initial portion of the curve leading up to the first peak is the same as when a double peak is not present. The third curve shape, where no explicit breakthrough is visible and there is not a steadily decreasing force is more complicated to explain. Possible explanations are noted later.

4. **Standard deviation of maximum force:** Additionally, the amount of standard deviation for the maximum extrusion force and the area under the extrusion curve provides insight to the uniformity of the coating. If there is a problem with coating adherence, the standard deviation will be more significant. As defined below, three ratings are used: fully adherent, semi-adherent, and non-adherent.

Standard deviations and differences in area under the curve are not as easily attributed to coating performance. This is a result of several different sources of error inherent in the test. The blank cut-off lengths are not 100% uniform for samples because they were cut by hand. If run on an automated heading machine, it can be more assured that they are the correct length and same length much easier. The length of the stroke of the test has some variability based both on the length of the blank and the set-up for the test. It is difficult to insure that the sample is completely

at the bottom of the die and that the same portion of the deformation zone of the die was filled prior to running the test. Both cut-off length and stroke length problems can be seen in several sets of data (S72678 medium in the extrusion footprint atlas for example, Appendix F, Figure 9.10). The curves are spread apart from each other and do not seem to take off from the same point. Although this creates an error in the area under the curve, it does not affect the general footprint of the curve nor does it affect the maximum extrusion force and standard deviation. Finally, there is some error associated with calculating the area under the curve because of the limited number of data points and difficulty in isolating exactly where the curve begins and making a uniform measurement across the many different testing conditions that arise from the various coating materials, substrate materials, and extrusion geometries.

Differences in steady state extrusion behavior can be attributed to a non-uniform coatings, gradual die packing that does not result in a stuck part or a double peak, or the dynamic loss of coating performance.

When the part became stuck in the die during extrusion and needed a notable effort to remove from the die, the resulting load versus stroke was two-peaked. After the peak of the curve is reached, two distinct tapers are evident in the curves. The negative, gentle sloped taper is indicative of proper lubrication carry through for the whole process, visible in the A-type curve, and is a result of the decreasing amount of surface area contact in the upper bore of the die as the material is extruded. The flat, non-sloped taper is indicative changing friction conditions, which may be related to poor lubricant carry through (C-type). Also, a characteristic breakthrough force is not evident in the C-type curve.

It is proposed that the following ranking for "adherence" of coating, based upon standard deviation of the maximum extrusion force, will be used:

Table 6.1 Coating Adherence Ratings Definition

Standard Deviation	Adherence Rating
< 3.0%	Fully Adherent Coating
3.0% < Standard deviation < 6.0%	Semi-Adherent Coating
> 6.0%	Non-Adherent Coating

Large standard deviations in maximum load are related to a series of curves that do not correspond with each other for a given coating. This means that either die packing occurs giving a double peak with a maximum at a much higher value, there is a non-sticking related difference in maximum peaks, or there is a difference in the steady state extrusion behavior. Figures 6.3, 6.4, and 6.5 show an example of each adherence ranking.

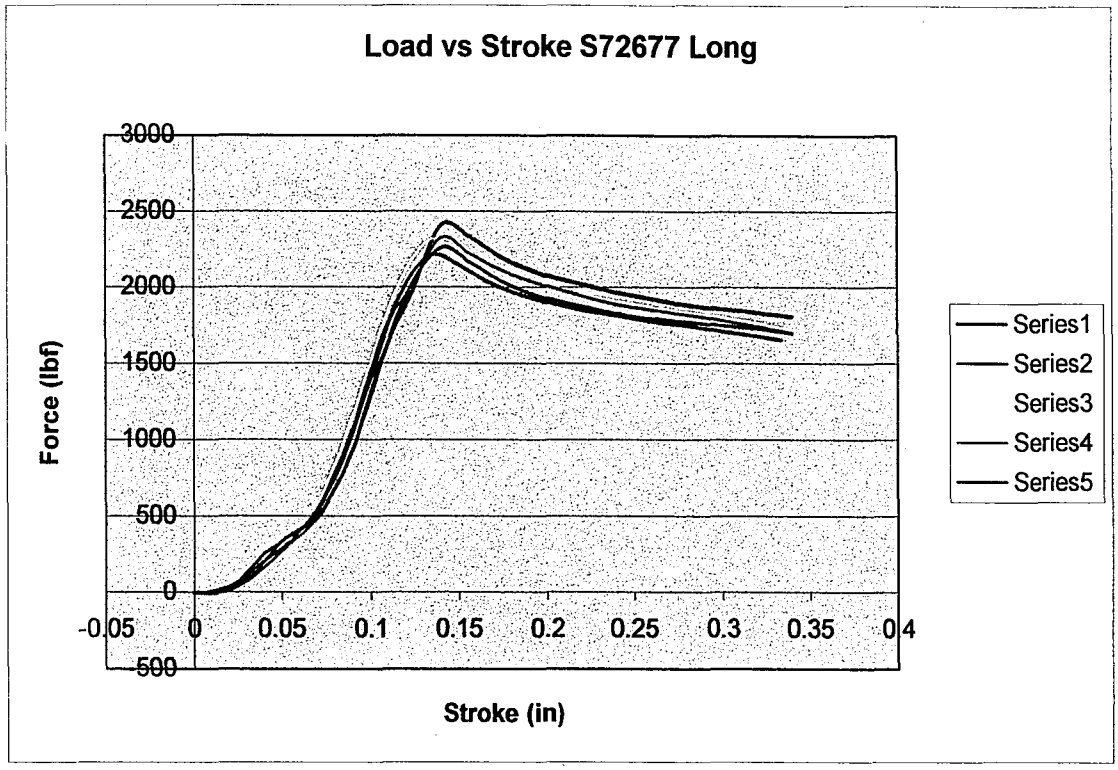

Figure 6.3. Curves showing standard deviation < 3.0% - Fully Adherent Rating. See Appendix F for exact data for this series of curves.

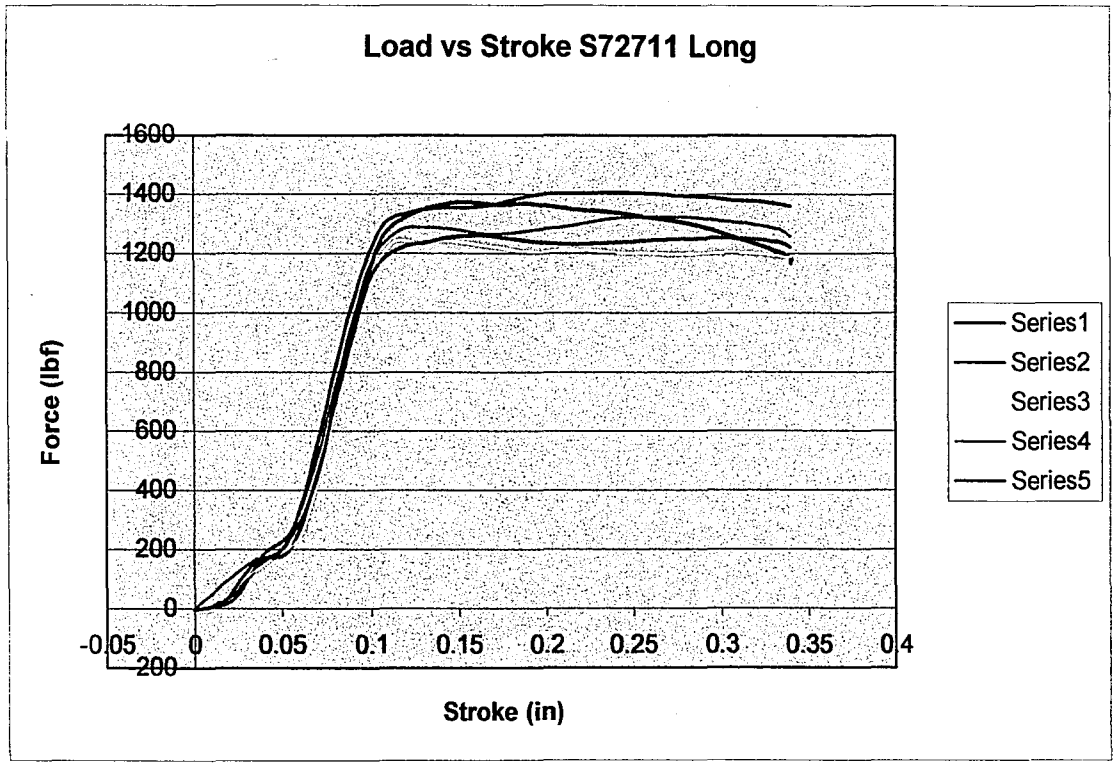

Figure 6.4. Curves showing standard deviation between 3.0% and 6.0% - Semi-Adherent Rating. See Appendix F for exact data for this series of curves.

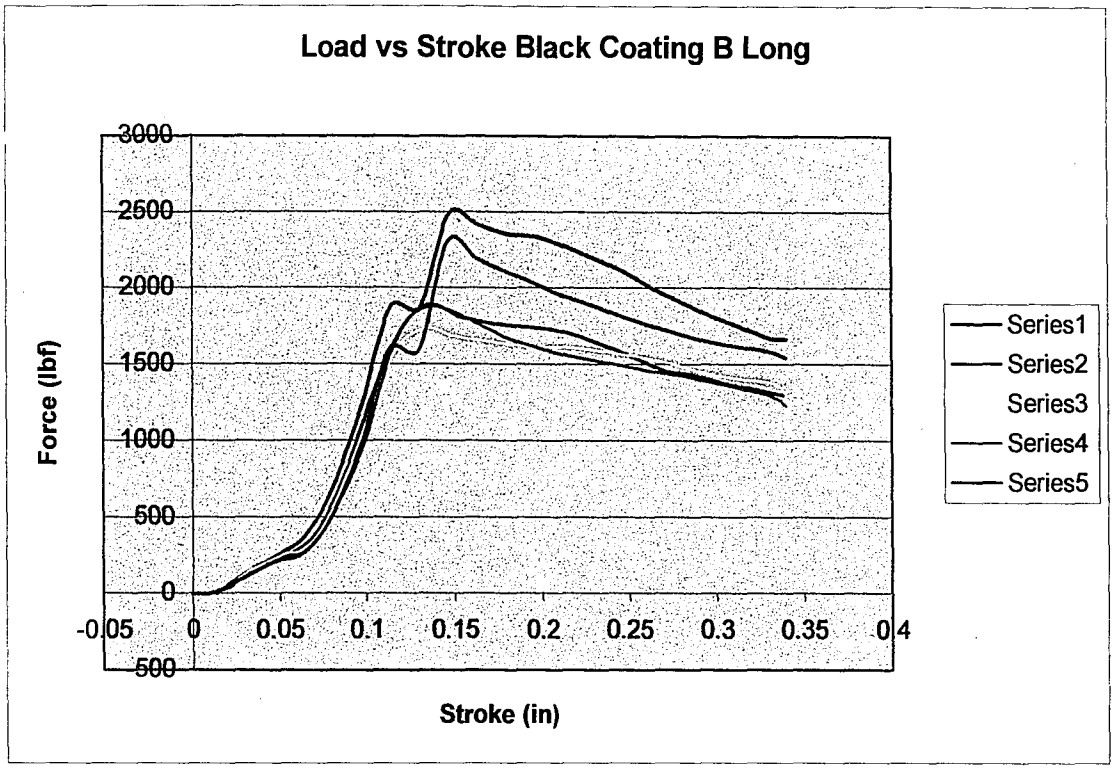

Figure 6.5. Curves showing standard deviation > 6.0% - Non-Adherent Rating. See Appendix F for exact data for this series of curves.

When comparing the S72711 long extrusion to the S72721 long extrusion (C-type curve and A-type curve, respectively), several points should be noted. The S72711 has a higher maximum force (however, no distinct breakthrough point) than the S72721. To explain the lack of the distinct breakthrough point and steadily decreasing force, there may be another force that is greater than the frictional and mechanical deformation terms. This could be caused by the gradual packing of the die during the initial upsetting of the billet that causes the extrusion force to be greater than the friction from the blank in the container and deformation components.

A non-uniform coating after drawing to the initial extrusion diameter would likely be a result of the handling process. If the coating becomes either friable or non-adherent it could be removed when being prepared as an extrusion blank. In the

actual heading process, the heading unit performs the cut-off step and thusly it is less likely that the coating will be disturbed. This is why it is recommended that a standard deviation of 6% be still considered as fair or acceptable.

To properly rank and identify coatings, three separate data will be presented. These can be used in conjunction to make a coating recommendation based upon the specifics of the given application of cold-heading. The main ranking will be based upon maximum extrusion force, followed by its ranking for standard deviation/adherence, and the footprint of the curve. Tables 6.2 and 6.3 summarize the coating rankings based upon maximum extrusion force, footprint, and adherence rating. If two letters are listed for the "Footprint," curves of each type of letter listed were present in the five tests, examples can be seen in Figures 9.15, 9.16, 9.17, 9.18, 9.19, 9.20, 9.25, 9.26, 9.36, 9.37, 9.38, 9.39, and 9.40. For each footprint, see Appendix G.

Table 6.2: Coating rankings for long extrusion

Maximum Extrusion Force (listed in increasing force by ID)	**Adherence rating**	**Footprint (A: standard extrusion shape, B: double peaked, C: non-decreasing after maximum)**
TYPE 302HQ		
S72678	Semi-adherent	A
WS2	Adherent	A
S72675	Semi-adherent	A
S72679	Non-adherent	A
Black coating B	Non-adherent	A-B
S7274	Non-adherent	A
Cu_Black coating B	Non-adherent	A-B
Oxalate	Non-adherent	A-B
S72677	Adherent	A
S72676	Non-adherent	A
TYPE T430		
S72714	Adherent	C
S72710	Non-adherent	A
S72712	Non-adherent	A-B

S72713	Semi-adherent	A
S72721	Non-adherent	A
S72711	Semi-adherent	C
TYPE A286		
S72720	Semi-adherent	A
S72717	Non-adherent	C
S72718	Semi-adherent	A-B
S72719	Non-adherent	A-B
S72715	Semi-adherent	A
S72722	Non-adherent	A
S72716	Semi-adherent	A

Table 6.3: Coating rankings for medium extrusion

Maximum Extrusion Force (listed in increasing force by ID)	**Adherence rating**	**Footprint (A: standard extrusion shape, B: double peaked, C: non-decreasing after maximum)**
TYPE 302HQ		
S72678	Adherent	A
WS2	Adherent	A
S72679	Semi-adherent	A
S72675	Adherent	A
Cu_Black coating B	Semi-adherent	A-B
S7274	Semi-adherent	A
Oxalate	Semi-adherent	A-B
Black coating B	Non-adherent	A-B
S72676	Semi-adherent	A
S72677	Adherent	A
TYPE T430		
S72713	Adherent	A
S72710	Semi-adherent	A
S72714	Semi-adherent	A
S72712	Non-adherent	A-B
S72721	Non-adherent	A
S72711	Adherent	A
TYPE A286		
S72720	Non-adherent	A
S72717	Non-adherent	A-C
S72719	Non-adherent	A-B
S72722	Semi-adherent	A
S72718	Non-adherent	A-B
S72716	Semi-adherent	A
S72715	Adherent	A

When comparing coating adherence rating to footprint, it can be noted that any coating that exhibited the double peaked curve (type-B) also exhibited a standard deviation in maximum extrusion force that was larger than 3%, which corresponds to

either a semi-adherent or a non-adherent rating. However, it is also important that an adherent coating ranking does not necessarily imply that the coating will have lower extrusion forces associated with it and vice versa. For example, the S72677 samples for both long and medium extrusion exhibit type-A curves and receive adherent ratings, yet fall into the highest extrusion force rankings. However, it can be noted from their footprint that their performance is consistent.

Another important observation to note is that adherence ranking can improve from the long extrusion test geometry to the medium extrusion test geometry. Some coatings that receive non-adherent and semi-adherent rankings in the long extrusion test receive semi-adherent and adherent rankings in the medium extrusion test. The value of having two different geometries is evident as that it can distinguish performance for different manufacturing processes.

The coatings that had the highest coefficient of friction in the drawing test (Black coating B) also exhibited type B curves in the extrusion test. This result suggests several different characteristics. The coating is fairly thick, and may pack the die easily because it does not adhere to the wire well. Also, because of its thickness, more material is being deformed in the drawing test resulting in a higher rated coefficient of friction. Although some coating is lost during the drawing test and through blank preparation for the extrusion test, enough lasts that die-packing is still an issue. If no coating remained on the wire, it would have exhibited behavior similar to the uncoated materials (S72674, S72721, and S72722).

Some final recommendations can be made for the process of evaluating coating and lubricant performance for a given substrate material. First, both the wire

drawing step and the heading step must be considered in the evaluation. Often, the first step in heading is a pre-drawn of a small reduction to insure a good surface finish and a straight wire to go on to be headed. If a coating cannot pass the drawing step, it will not be effective in increasing headability. If die wear is a problem, comparisons should be made between maximum extrusion forces of the different coatings. When there is a problem with punch breakage, the extrusion footprint atlas should be referenced to insure a coating that does not exhibit die packing (double peak) is not being used for the given application.

It is evident from the work that has been presented that no one single test has the ability to capture the complex relationship between friction conditions in deformation and various coatings response to processing parameters. General relationships can be determined, but no one specific relationship can be proposed.

6.3 Future work

Several important considerations should be made when concerning future work. For the wire drawing testing, several additional techniques may be used to further elucidate the results that were obtained. By using electron microscopy, the surface finish of the drawn wires can be investigated. Consideration of the appearance of the wire after drawing along with drawing force data can be used to more specifically determine the friction conditions for each coating. Further work investigating the effect of varying both strain rate and reduction on friction conditions would also provide a more comprehensive understanding of the process. More research is needed to determine the mechanism or mechanisms causing the non-increasing drawing force phenomena for certain coatings, while other coatings show a

sharp increase in drawing force. Finite element modeling (FEM) may help in this analysis by limiting the number of physical tests that need to be run by providing numerical solutions modeling the process.

For the extrusion test, several more aspects could be considered for future work. A new method for preparing extrusion blanks and loading them into the die needs to be determined so that the variations that were observed in this work are eliminated. This may be achieved by using a carefully instrumented commercial heading machine, although previously it was believed that this did not provide accurate or repeatable data. More die geometries could be investigated, along with different extrusion steps, although the author believes that the trapped forward extrusion provides the simplest, most representative step in the process, since both deformation and high surface contact are present. To full investigate the proposed die packing phenomenon, a novel die design is needed so that the test can be interrupted when the packing is observed on the load versus stroke data. The die would then need to be able to be separated so that any damage or packing of the coating can be observed.

7.0 Conclusions

Based on the performed experiments and analysis of their results the following conclusions have been formulated:

1. To accurately capture a coating / lubricant's performance for a particular forming operation, the process must be simulated as closely as possible. Temperature, strain rate, and deformation zone geometry all affect performance. "Book" values for coefficient of friction may not be applicable to the specific forming operation and may lead to problems or un-expected formability. Lubricant performance must be evaluated for the specific substrate that it is being used on. Each tested lubricant performed differently with different substrate materials. This is a combination of effects from flow stress and work hardening characteristics.
2. Coefficients of friction calculated using the Yang relationship might not be entirely accurate. However, relative rankings of the evaluated coatings based upon that value can be made.
3. The ability of applying a simple drawing test to the complex cold-heading operation is limited, but useful. Coefficient of friction from wire drawing results does not directly port to headability. However, the coatings exhibiting the highest coefficient of friction in the wiredrawing test also exhibited some instances of die packing and low adherence ratings in the wire extrusion test.
4. Although maximum extrusion force is inversely proportional to headability, the footprint of the extrusion curve and the standard deviation of the

maximum extrusion force are also both needed to properly rate a coating. A double peaked extrusion curve may occur when the coating packs the deformation zone of the die, effectively increasing the extrusion ratio and increasing extrusion force. A non-sloped curve after the maximum extrusion force is indicative of changing friction conditions that may be related to the ability of a coating to carry through the extrusion lubricant or by the stripping of the coating and packing the die, which again causes a higher extrusion ratio, R.

5. Area under the curve or extrusion energy measurements can only be used when strict testing conditions are met. These include a uniform method to cut extrusion blanks and a set-up allowing for the same extrusion stroke each time.
6. To compare coatings for a given cold heading operation, several approaches can be used: a) a comparison between maximum extrusion force between different coatings can be made if there is a friction related problem in the operation such as excessive die wear or surface finish defects, b) if a given heading geometry results in broken punches or die packing, a coating that exhibits better adherence and Type-A extrusion footprint should be substituted.

8.0 References

1. *Heading Hints, A Guide to Cold Forming Speciality Alloys.* 2001, CRS Holdings, Inc.: U.S.A. p. 59.

2. Bowers, N., *A High-yield Approach to Cold-Heading.* Wire Journal, 1979. **12**(9): p. 156 - 159.

3. Petrescu, D., Savage, S.C., Hodgson, P.D., *Simulation of the fastener manufacturing process.* Journal of Materials Processing Technology, 2002. **125-126**: p. 361-368.

4. Avitzur, B., *Metal Forming: Processes and Analysis.* 1968, New York: McGraw-Hill.

5. Dieter, G.E., *Mechanical Metallurgy.* 1986, New York: McGraw-Hill.

6. Schey, J.A., *Metal Deformation Processes - Friction and Lubrication.* 1970, New York: Marcel Dekker.

7. Tevaarwerk, J.L., Plumtree, A., Sowerby, R., *The Role of Lubrication in the Cold Heading of Mild Steel.* Transactions of the ASME, 1975: p. 144 - 150.

8. Lee, P.W., Kuhn, H. A., *Fracture in Cold Upset Forging - A Criterion and Model.* Metallurgical Transactions, 1973. **4**(4): p. 969 - 974.

9. N. Muzack, K.N., C. Osborne, *New Methods for Assessing Cold Heading Quality.* Wire Journal International, 1996. **29**(10): p. 66-72.

10. Sarruf, Y., Cao, B., Jonas, J.J., Nickoletopoulos, N., *Criteria and Tests for Cold Headability.* Wire Journal International, 1999. **32**(2): p. 98 - 105.

11. Savage, S.C., Barnett, M.R., Hodgson, P.D. *Investigation into Cold Heading Lubricants.* in *Metal Forming 2000.* 2000. Rotterdam.

12. Tevaarwerk, J.L., Sowerby, R., Plumtree, A., *Warm and Cold Heading of Stainless Steel.* Journal of Engineering Materials and Technology, 1975. **97**(2): p. 136 - 143.

13. Vickers, G.W., Plumtree, A., Sowerby, R., Duncan, J.L., *Simulation of the Heading Process.* J. Eng. Mater. Technol., 1975. **97**(2): p. 127 - 135.

14. Dubois, A., Lazzarotto, L., Dubar, L., Oudin, J., *A multi-step lubricant evaluation strategy for wire drawing-extrusion-cold heading sequence.* Wear, 2002. **249**: p. 951-961.

15. Lazzarotto, L., Dubar, L., Dubois, A., Ravassard, P., Oudin, J., *Identification of Coulomb's Friction Coefficient in Real Contact Conditions Applied to a Wire Drawing Process.* Wear, 1997. **211**(1): p. 54 - 63.

16. Wright, R.N. *Characterizing Friction in Metalworking.* in *Metal Forming 2000.* 2000.

17. El-Domiaty, A., Kassab, Sadek Z., *Termperature Rise in Wire-drawing.* Journal of Materials Processing Technology, 1998. **83**: p. 72-83.

18. O. Hoffman, G.S., *Theory of Plasticity.* 1953, New York: McGraw-Hill.

19. Yang, C.T., *On the Mechanics of Wire Drawing.* Journal of Engineering for Industry, 1961. **86**(4): p. 305 - 316.

20. Avitzur, B., Misiolek, W. Z., *Encyclopedia of Materials: Science and Technology.* 2001, New York: Elsevier Science Ltd. 5506-5510.

21. Kuhn, H.A., Dieter, G.E.,. *Workability in Bulk Forming Processes.* in *Proceedings of the 4th International Conference on Fracture.* 1977. Waterloo, Canada.

22. Dieter, G.E.e., *Workability Testing Techniques.* 1984, Metals Park, Ohio: American Society for Metals.

23. Bakhshi-Jooybari, M., *A theoretical and experimental study of friction in metal forming by the use of the forward extrusion process.* Journal of Materials Processing Technology, 2002. **125-126**: p. 369-374.

24. Stenger, H., Laue, K., *Extrusion: Processes, Machinery, Tooling.* 1 ed. 1981, Metals Park, Ohio: American Society for Metals. 457.

9.0 Appendices

9.1 Appendix A: Coating Identifications

Table 9.1. Coating Identifications

ID	Coating
TYPE 302HQ	
S72674	Bare 302HQ
S72675	302HQ + 100 microinch copper
S72676	302HQ + 50 microinch copper
S72677	302HQ + 200 microinch copper
S72678	302HQ + 100 microinch copper + black coating A
S72679	302HQ + black coating A
WS2	302HQ + tungsten disulfide
Oxalate	302HQ + oxalate
Black coating B	302HQ + black coating B
Cu_Black coating B	302HQ + 100microinch + black coating B
TYPE T430	
S72710	T430 + 100 microinch copper + black coating A
S72711	T430 + 100 microinch copper + black coating B
S72712	T430 + black coating B
S72713	T430 + black coating A
S72714	T430 + precoat soap pre-drawn to 0.131 inch
S72721	Bare T430
TYPE A286	
S72715	A286 + 100 microinch copper
S72716	A286 + 100 microinch copper #2
S72717	A286 + 100 microinch copper + black coating A
S72718	A286 + 200 microinch copper + black coating B
S72719	A286 + black coating B
S72720	A286 + black coating A
S72722	Bare A286

9.2 Appendix B: Mechanical Test Results

Table 9.2. Undrawn Tensile Mechanical Data

ID	0.2% Offset Yield Strength (ksi)	Ultimate Tensile Strength (ksi)
TYPE 302HQ		
S72674	35.08	77.52
S72675	34.88	78.14
S72676	37.10	78.22
S72677	35.37	77.15
S72678	37.59	77.23
S72679	33.76	76.58
WS2	34.95	81.65
Oxalate	34.94	81.42
Black coating B	35.82	82.17
Cu_Black coating B	35.26	74.29
TYPE T430		
S72710	42.9	65.4
S72711	37.5	62.9
S72712	32.8	60.2
S72713	35.4	60.7
S72714	59.7	66.1
S72721	31.0	59.6
TYPE A286		
S72715	38.1	89.8
S72716	37.9	88.7
S72717	39.2	87.7
S72718	37.1	86.6
S72719	31.7	89.6
S72720	33.3	85.4
S72722	31.0	88.2

Table 9.3. Drawn Tensile Mechanical Data

ID	0.2% Offset Yield Strength (ksi)	Ultimate Tensile Strength (ksi)
TYPE 302HQ		
S72674	77.70	89.28
S72675	77.73	89.46
S72676	78.52	89.90
S72677	77.60	89.08
S72678	78.50	89.42
S72679	78.29	89.50
WS2	80.54	93.49
Oxalate	82.63	94.34
Black coating B	83.31	94.76
Cu_Black coating B	75.60	86.39
TYPE T430		
S72710	71.5	73.8
S72711	69.7	72.0
S72712	69.0	71.8
S72713	70.4	72.3

S72714	69.8	73.3
S72721	71.3	73.0
TYPE A286		
S72715	85.5	101.6
S72716	83.1	99.4
S72717	86.5	100.0
S72718	88.9	104.2
S72719	86.4	102.6
S72720	79.7	97.2
S72722	83.8	102.5

Table 9.4. Mean Wire Tensile Data

ID	0.2% Offset Yield Strength (ksi)	Ultimate Tensile Strength (ksi)
TYPE 302HQ		
S72674	56.39	83.40
S72675	56.30	83.80
S72676	57.81	84.06
S72677	56.48	83.12
S72678	58.04	83.32
S72679	56.03	83.04
WS2	57.75	87.57
Oxalate	58.78	87.88
Black coating B	59.57	88.47
Cu_Black coating B	55.43	80.34
TYPE T430		
S72710	57.2	69.6
S72711	53.6	67.45
S72712	50.9	66.0
S72713	52.9	66.5
S72714	64.75	69.7
S72721	51.15	66.3
TYPE A286		
S72715	61.8	95.7
S72716	60.5	94.05
S72717	62.85	93.85
S72718	63.0	95.4
S72719	59.05	96.1
S72720	56.5	91.3
S72722	57.4	95.35

9.3 Appendix C: Drawing Test Calculated Coefficients of Friction

Results for calculation of coefficient of friction for the various bearing length dies can be seen in Tables 9.5 – 9.10. Samples are listed in order from lowest coefficient of friction to the highest value in each table. The A286 and T430 were only tested on the 96% bearing length die because there was not sufficient material to test on multiple dies, and 96% bearing length was the most intermediate die, where the bearing portion is nearly the same length as the diameter of the drawn wire.

Table 9.5. Coefficient of Friction Data for 302HQ – 31% Bearing Length Die

ID	Calculated Coefficient of Friction (μ)
S72674	0.0986
S72676	0.0996
S72675	0.1012
S72677	0.1014
Ws2	0.1070
S72678	0.1158
S72679	0.1160
Oxalate	0.1293
Cu_Black coating B	0.1374
Black coating B	0.1386

Table 9.6. Coefficient of Friction Data for 302HQ – 96% Bearing Length Die

ID	Calculated Coefficient of Friction (μ)
S72674	0.0551
S72676	0.0582
S72675	0.0595
S72677	0.0608
Ws2	0.0632
S72678	0.0668
S72679	0.0695
Oxalate	0.0754
Cu_Black coating B	0.0818
Black coating B	0.0870

Table 9.7. Coefficient of Friction Data for T430 – 96% Bearing Length Die

ID	Calculated Coefficient of Friction (μ)
S72714	0.0485
S72710	0.0723
S72713	0.0797
S72721	0.0838
S72712	0.0871
S72711	0.0941

Table 9.8. Coefficient of Friction Data for A286 – 96% Bearing Length Die

ID	Calculated Coefficient of Friction (μ)
S72717	0.0477
S72716	0.0517
S72715	0.0600
S72722	0.0602
S72720	0.0624
S72719	0.0657
S72718	0.0710

Table 9.9. Coefficient of Friction Data for 302HQ – 127% Bearing Length Die

ID	Calculated Coefficient of Friction (μ)
S72674	0.0400
S72676	0.0426
S72675	0.0435
S72677	0.0448
Ws2	0.0468
S72678	0.0526
S72679	0.0555
Oxalate	0.0646
Cu_Black coating B	0.0680
Black coating B	0.0687

Table 9.10. Coefficient of Friction Data for 302HQ – 148% Bearing Length Die

ID	Calculated Coefficient of Friction (μ)
S72674	0.0369
S72675	0.0379
S72676	0.0380
S72677	0.0396
Ws2	0.0847
Black coating B	0.1034
Cu_Black coating B	0.1088
S72679	0.1136
Oxalate	0.1152
S72678	0.1235

9.4 Appendix D: Extrusion Test Maximum Forces and Standard Deviations

Each table lists the maximum extrusion force for each material in increasing order. The tables are organized by substrate material and in increasing maximum extrusion force.

Table 9.11. Maximum force: 302HQ Long Extrusion

Type	Max force (lbs)	Standard Deviation (lbs)	% Standard Deviation
S72678	1418.67	43.6	3.1
WS2	1641.45	40.4	2.5
S72675	1808.76	106.5	5.9
S72679	1933.54	271.5	14.0
Black coating B	2061.43	287.4	13.9
S7274	2093.86	198.8	9.5
Cu_Black coating B	2228.84	228.4	10.2
Oxalate	2251.41	381.8	17.0
S72677	2305.29	66.4	2.9
S72676	2387.34	190.6	8.0

Table 9.12. Maximum force: 302HQ Medium Extrusion

Type	Max force (lbs)	Standard Deviation (lbs)	% Standard Deviation
S72678	1424.65	6.6	0.5
WS2	1640.28	23.7	1.4
S72679	1708.03	98.1	5.7
S72675	1833.24	33.0	1.8
Cu_Black coating B	1997.75	105.2	5.3
S7274	2003.87	95.5	4.8
Oxalate	2057.13	120.9	5.9
Black coating B	2101.91	152.3	7.2
S72676	2135.74	84.0	3.9
S72677	2236.79	27.1	1.2

Table 9.13. Maximum force: 302HQ Short Extrusion – Not included in analysis

Type	Max force (lbs)	Standard Deviation (lbs)	% Standard Deviation
S7274	1516.14	30.8	2.0
S72675	1627.17	44.2	2.7
S72676	1675.39	55.2	3.3
S72677	1742.39	55.3	3.2
S72678	1792.09	83.5	4.7
S72679	1946.42	34.1	1.8
WS2	1948.25	118.5	6.1
Oxalate	1954.80	112.5	5.8

Black coating B	1984.22	28.7	1.4
Cu_Black coating B	2095.25	161.5	7.7

Table 9.14. Maximum force: T430 Long Extrusion

Type	Max force (lbs)	Standard Deviation (lbs)	% Standard Deviation
S72714	1216.01	15.8	1.3
S72710	1238.53	88.6	7.2
S72712	1241.89	147.6	11.9
S72713	1257.46	40.0	3.2
S72721	1271.31	99.2	7.8
S72711	1321.99	62.9	4.8

Table 9.15. Maximum force: T430 Medium Extrusion

Type	Max force (lbs)	Standard Deviation (lbs)	% Standard Deviation
S72713	1241.99	21.6	1.7
S72710	1263.68	52.2	4.1
S72714	1284.73	47.8	3.7
S72712	1297.61	114.1	8.8
S72721	1300.30	85.2	6.6
S72711	1371.92	12.9	0.9

Table 9.16. Maximum force: T430 Short Extrusion – Not included in analysis

Type	Max force (lbs)	Standard Deviation (lbs)	% Standard Deviation
S72710	1030.34	106.8	10.4
S72721	1088.65	85.7	7.9
S72713	1117.86	72.8	6.5
S72712	1265.62	87.4	6.9
S72711	1269.00	97.4	7.7
S72714	1399.63	52.3	3.7

Table 9.17. Maximum force: A286 Long Extrusion

Type	Max force (lbs)	Standard Deviation (lbs)	% Standard Deviation
S72720	1645.21	84.9	5.2
S72717	1849.35	185.9	10.1
S72718	1883.82	104.7	5.6
S72719	1940.30	143.1	7.4
S72715	1945.45	91.1	4.7
S72722	1969.73	130.9	6.6
S72716	2016.54	115.2	5.7

Table 9.18. Maximum force: A286 Medium Extrusion

Type	Max force (lbs)	Standard Deviation (lbs)	% Standard Deviation
S72720	1710.00	124.0	7.2
S72717	1815.52	111.3	6.1
S72719	1850.42	143.3	7.7
S72722	1892.09	65.2	3.4
S72718	1917.11	118.6	6.2
S72716	1948.46	58.9	3.0
S72715	1977.13	41.2	2.1

Table 9.19. Maximum force: A286 Short Extrusion – Not included in analysis

Type	Max force (lbs)	Standard Deviation (lbs)	% Standard Deviation
S72720	1517.11	41.4	2.7
S72717	1534.18	47.8	3.1
S72718	1601.29	19.8	1.2
S72719	1661.75	27.8	1.7
S72716	1880.81	29.5	1.6
S72722	1969.73	130.9	6.6
S72715	2005.05	42.9	2.1

9.5 Appendix E: Extrusion Test Areas under the Curve and Standard Deviation

Results for extrusion energy (area under extrusion curve) are listed below. Each table has one substrate and extrusion condition, and results are listed in increasing energy under the curve.

Table 9.20. Area under curve: 302HQ Long Extrusion

Type	Energy (lb – in)	Standard Deviation (lb – in)	% Standard Deviation
S72678	337.6880646	5.152337752	1.525768392
WS2	359.0541626	11.60921158	3.233275863
S72675	374.7813171	83.60464083	22.30757965
S72674	414.2652283	33.41685762	8.066536928
S72679	430.5214844	59.4904206	13.81822342
Cu_Black coating B	431.6230286	27.93925904	6.473069599
Black coating B	441.6256226	45.96486932	10.40810745
S72676	493.3770386	25.86723118	5.242893195
S72677	494.037738	11.42431986	2.312438702
Oxalate	508.5904114	105.242885	20.69305331

Table 9.21. Area under curve: 302HQ Medium Extrusion

Type	Energy (lb – in)	Standard Deviation (lb – in)	% Standard Deviation
S72678	181.20	9.1	5.0
S72675	222.62	39.9	17.9
WS2	235.06	35.8	15.2
S72679	279.42	18.4	6.6
Cu_Black coating B	289.42	15.9	5.5
S72674	301.21	16.7	5.6
Oxalate	307.98	9.1	2.9
S72676	328.38	11.3	3.4
Black coating B	330.75	27.3	8.3
S72677	337.43	7.5	2.2

Table 9.22. Area under curve: T430 Long Extrusion

Type	Energy (lb – in)	Standard Deviation (lb – in)	% Standard Deviation
S72710	291.46	14.8	5.1
S72713	298.14	13.2	4.4
S72712	308.55	26.3	8.5
S72721	317.00	23.4	7.4
S72714	324.30	12.7	3.9
S72711	341.09	19.2	5.6

Table 9.23. Area under curve: T430 Medium Extrusion

Type	Energy (lb – in)	Standard Deviation (lb – in)	% Standard Deviation
S72710	161.66	39.7	24.5
S72711	207.52	28.8	13.9
S72713	211.77	4.5	2.1
S72712	212.14	17.9	8.5
S72721	232.45	16.4	7.1
S72714	240.33	8.9	3.7

Table 9.24. Area under curve: A286 Long Extrusion

Type	Energy (lb – in)	Standard Deviation (lb – in)	% Standard Deviation
S72720	372.56	27.7	7.4
S72719	441.40	30.9	7.0
S72717	449.49	43.9	9.8
S72722	450.79	6.1	1.4
S72718	457.26	23.2	5.1
S72715	463.94	23.8	5.1
S72716	467.46	24.0	5.1

Table 9.25. Area under curve: A286 Medium Extrusion

Type	Energy (lb – in)	Standard Deviation (lb – in)	% Standard Deviation
S72720	288.05	22.4	7.8
S72719	298.62	14.2	4.8
S72718	310.47	30.6	9.8
S72715	311.55	22.6	7.3
S72722	313.37	40.6	12.9
S72716	325.52	11.9	3.7
S72717	328.49	29.7	9.1

9.6 Appendix F: Extrusion Footprint Atlas

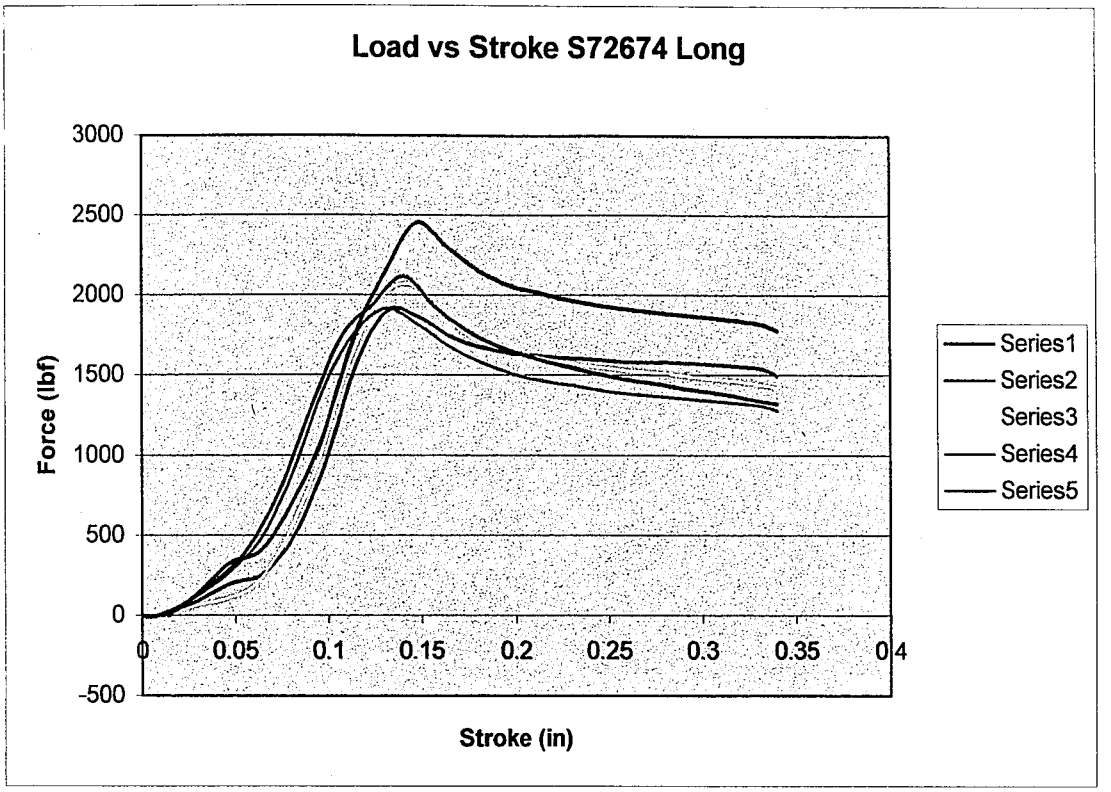

Figure 9.1. Load versus Stroke for S72674 Long Extrusion Test

Table 9.26. Extrusion Data for S72674 Long Extrusion Test

ID	S72674
Extrusion	Long
Substrate	302 HQ
Coating	None
Drawing Lubricant	Hammidraw 1846-B
Extrusion Lubricant	Hasco Stealth
Avg. Max	2093.86
Std. Dev. Max	198.8
% Std. Dev. Max	9.5
Avg. Area	414.27
Std. Dev. Area	33.4
% Std. Dev. Area	8.1
Notes/Comments	A type curves

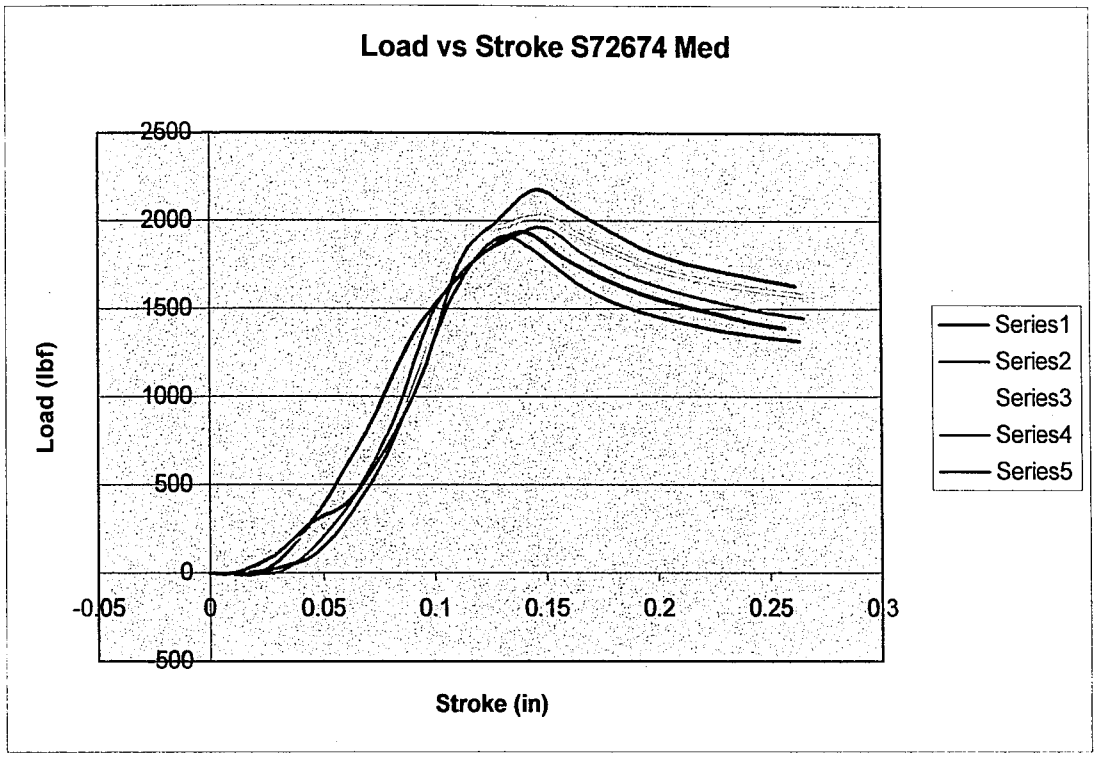

Figure 9.2. Load versus Stroke for S72674 Medium Extrusion Test

Table 9.27. Extrusion Data for S72674 Medium Extrusion Test

ID	S72674
Extrusion	Medium
Substrate	302 HQ
Coating	None
Drawing Lubricant	Hammidraw 1846-B
Extrusion Lubricant	Hasco Stealth
Avg. Max	2003.87
Std. Dev. Max	95.5
% Std. Dev. Max	4.8
Avg. Area	301.21
Std. Dev. Area	16.7
% Std. Dev. Area	5.6
Notes/Comments	A type curves

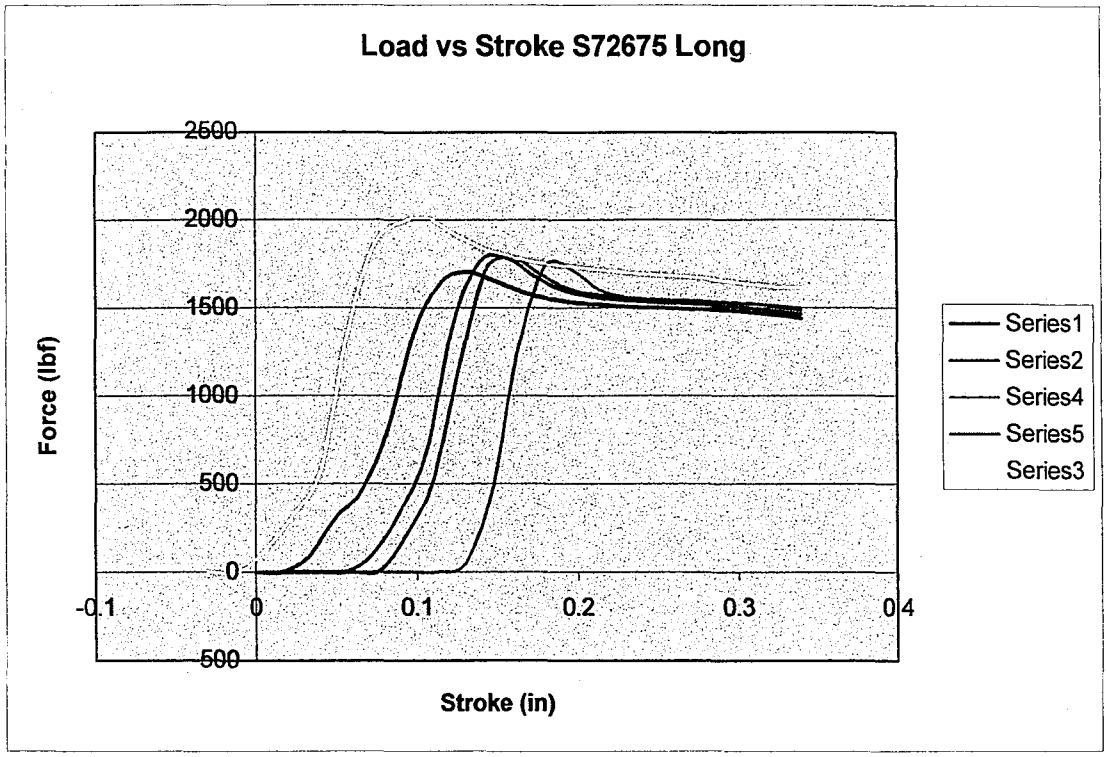

Figure 9.3. Load versus Stroke for S72675 Long Extrusion Test

Table 9.28. Extrusion Data for S72675 Long Extrusion Test

ID	S72675
Extrusion	Long
Substrate	302 HQ
Coating	100 microinch copper
Drawing Lubricant	Sun Waylube
Extrusion Lubricant	Hasco Stealth
Avg. Max	1808.76
Std. Dev. Max	106.5
% Std. Dev. Max	5.9
Avg. Area	374.78
Std. Dev. Area	83.6
% Std. Dev. Area	22.3
Notes/Comments	A type curves, some lateral spread as an effect of zeroing the press

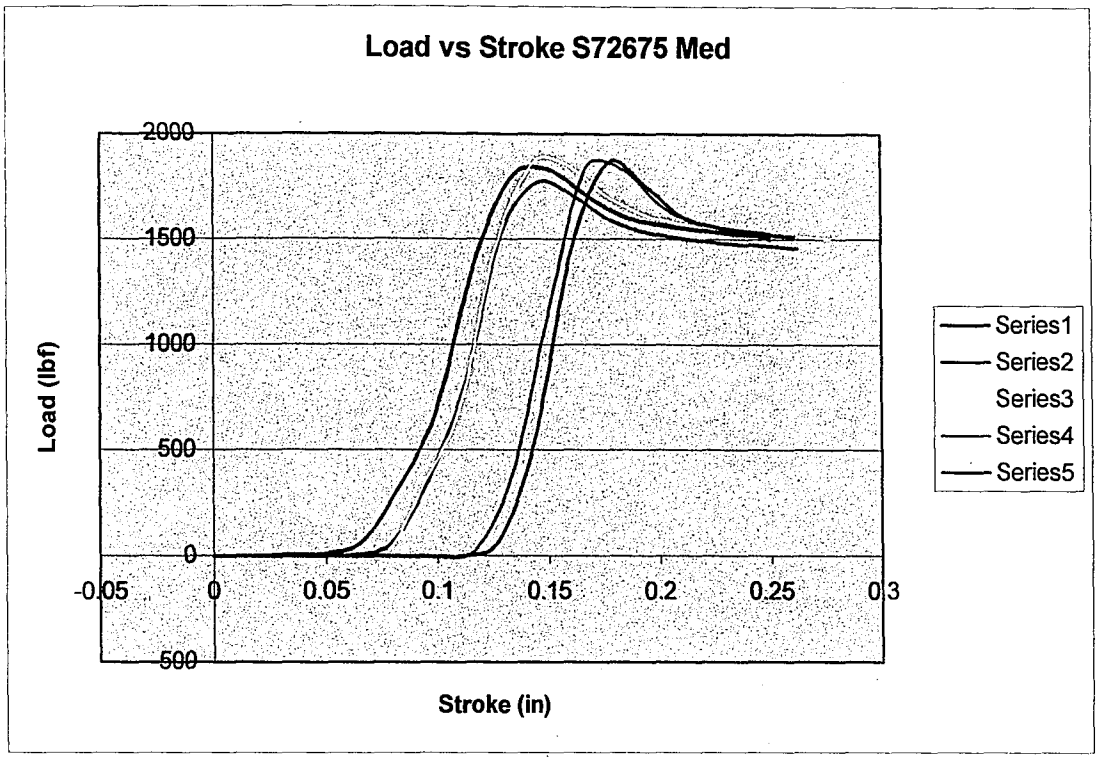

Figure 9.4. Load versus Stroke for S72675 Medium Extrusion Test

Table 9.29. Extrusion Data for S72675 Medium Extrusion Test

ID	S72675
Extrusion	Medium
Substrate	302 HQ
Coating	100 microinch copper
Drawing Lubricant	Sun Waylube
Extrusion Lubricant	Hasco Stealth
Avg. Max	1833.24
Std. Dev. Max	33.0
% Std. Dev. Max	1.8
Avg. Area	222.62
Std. Dev. Area	39.9
% Std. Dev. Area	17.9
Notes/Comments	A type curves, some lateral spread as an effect of zeroing the press

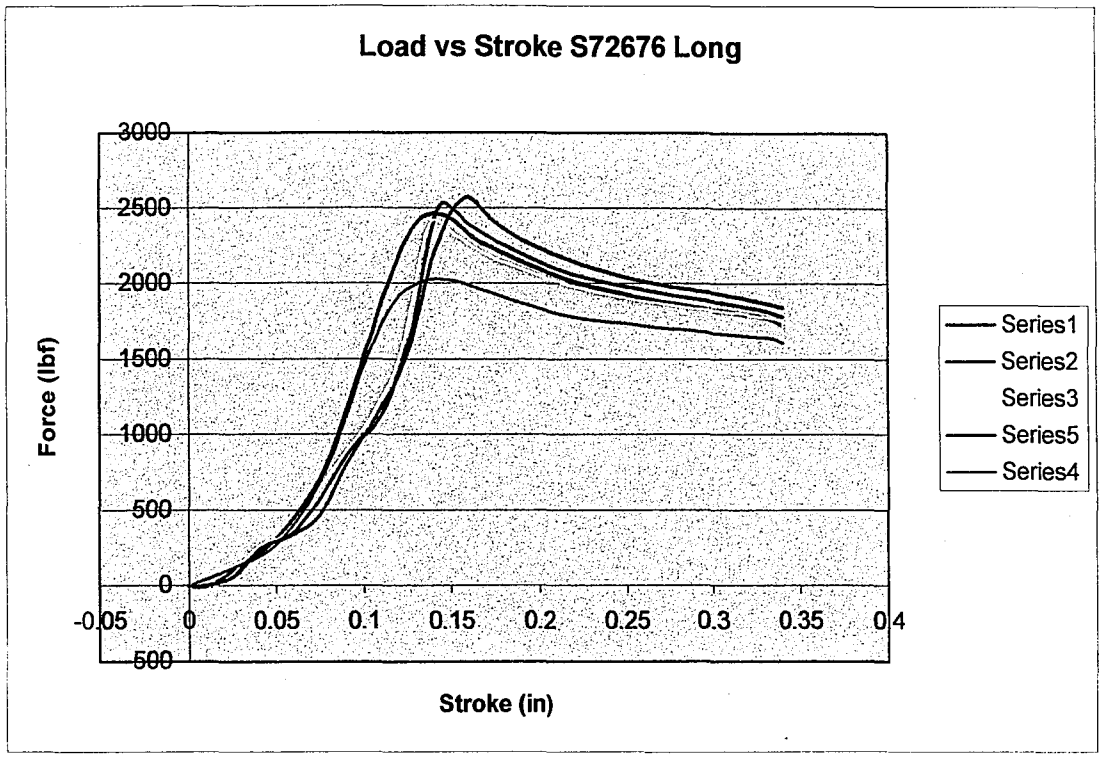

Figure 9.5. Load versus Stroke for S72676 Long Extrusion Test

Table 9.30. Extrusion Data for S72676 Long Extrusion Test

ID	S72676
Extrusion	Long
Substrate	302 HQ
Coating	50 microinch copper
Drawing Lubricant	Hammidraw 1846-B
Extrusion Lubricant	Hasco Stealth
Avg. Max	2387.34
Std. Dev. Max	190.6
% Std. Dev. Max	8.0
Avg. Area	493.38
Std. Dev. Area	25.9
% Std. Dev. Area	5.2
Notes/Comments	A type curves, one low maximum

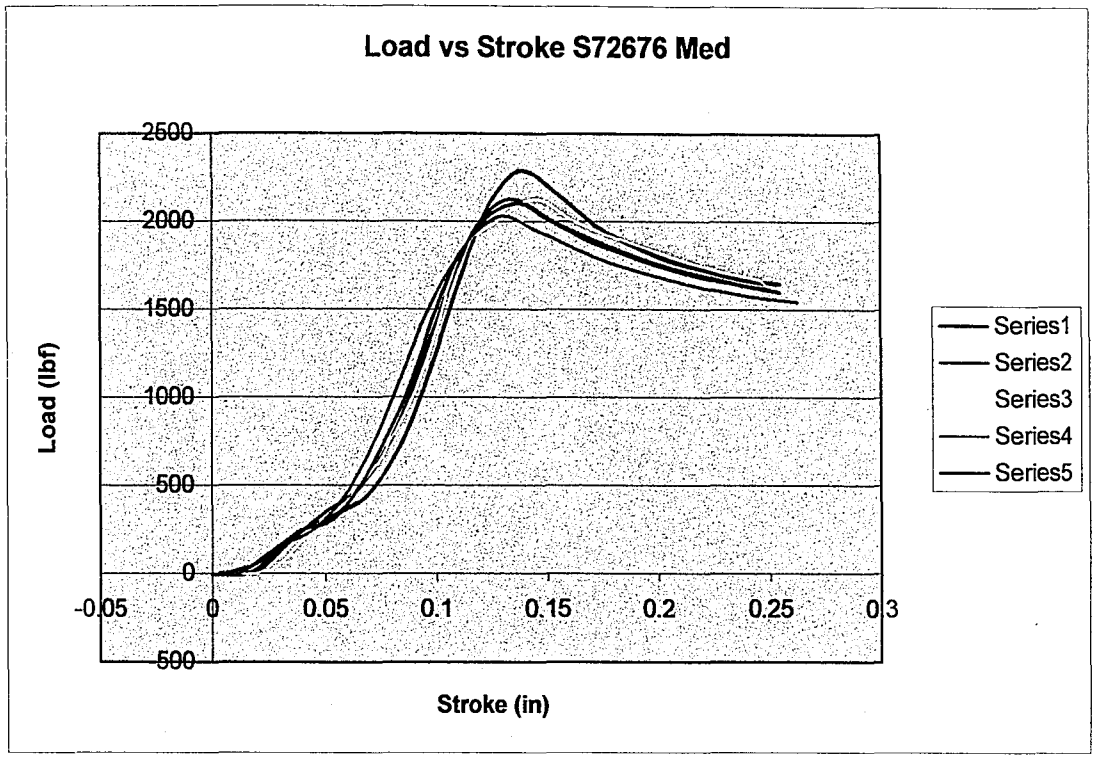

Figure 9.6. Load versus Stroke for S72676 Medium Extrusion Test

Table 9.31. Extrusion Data for S72676 Medium Extrusion Test

ID	S72676
Extrusion	Medium
Substrate	302 HQ
Coating	50 microinch copper
Drawing Lubricant	Hammidraw 1846-B
Extrusion Lubricant	Hasco Stealth
Avg. Max	2135.74
Std. Dev. Max	84.0
% Std. Dev. Max	3.9
Avg. Area	328.38
Std. Dev. Area	11.3
% Std. Dev. Area	3.4
Notes/Comments	A type curves

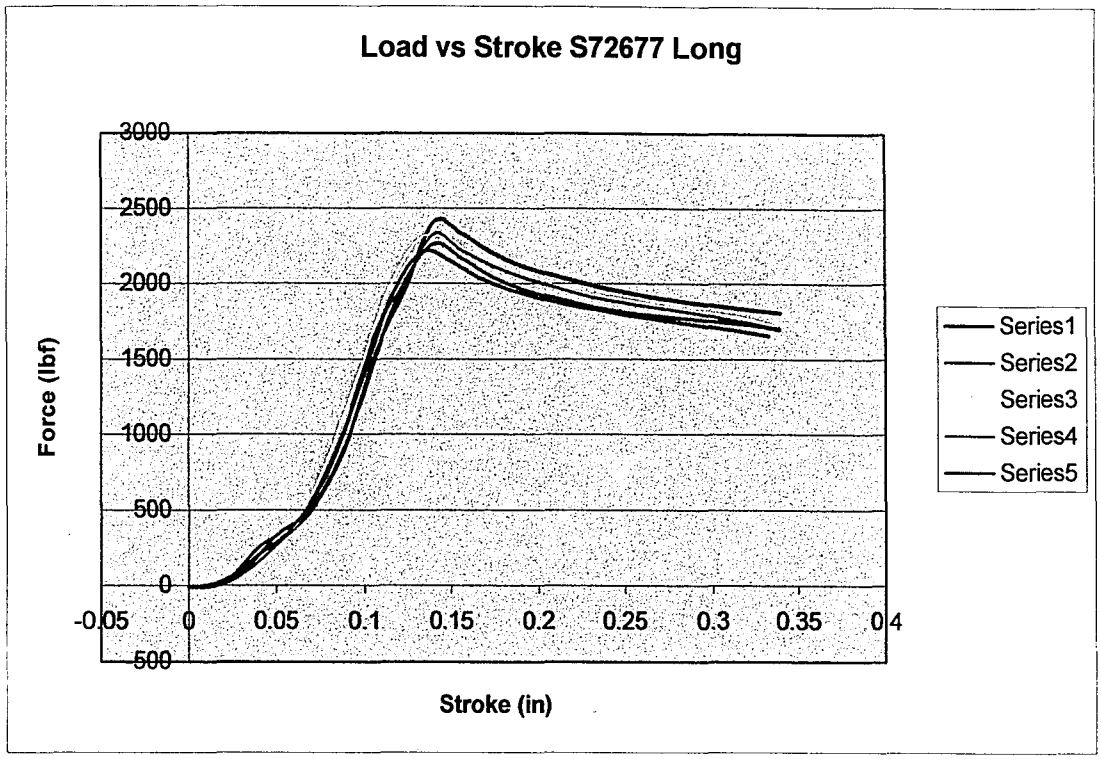

Figure 9.7. Load versus Stroke for S72677 Long Extrusion Test

Table 9.32. Extrusion Data for S72677 Long Extrusion Test

ID	S72677
Extrusion	Long
Substrate	302 HQ
Coating	200 microinch copper
Drawing Lubricant	Hammidraw 1846-B
Extrusion Lubricant	Hasco Stealth
Avg. Max	2305.292
Std. Dev. Max	66.3741
% Std. Dev. Max	2.88
Avg. Area	494.037738
Std. Dev. Area	11.42431986
% Std. Dev. Area	2.31
Notes/Comments	A type curves

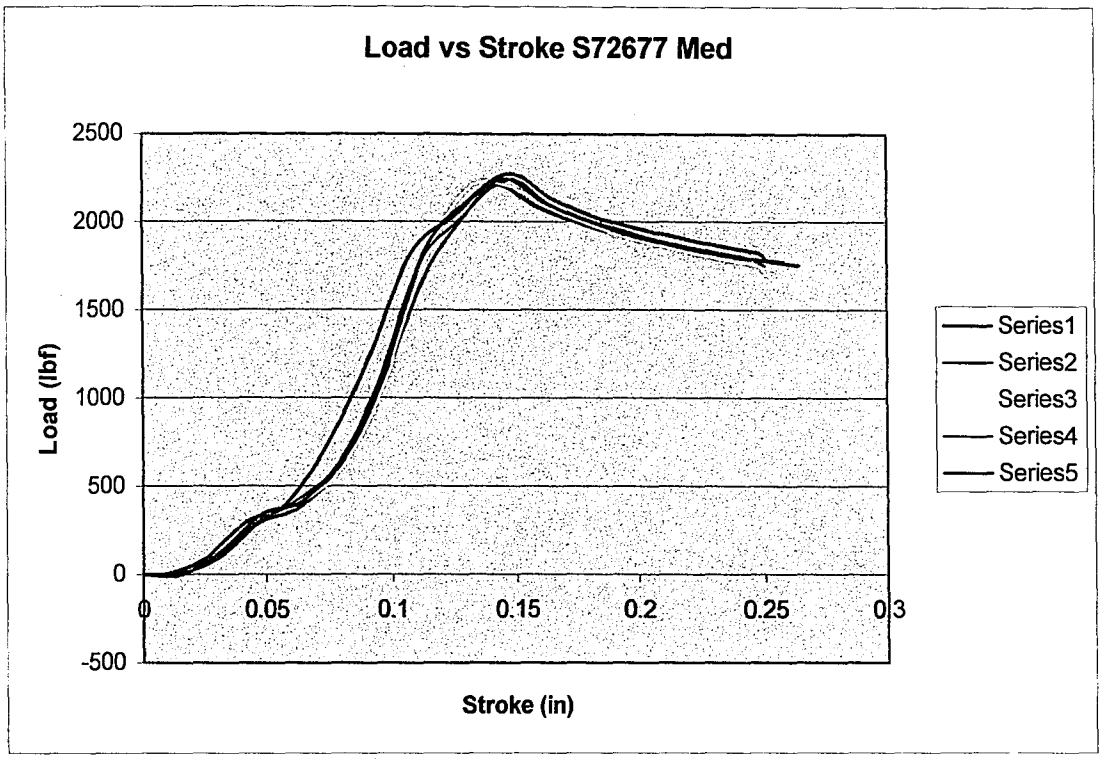

Figure 9.8. Load versus Stroke for S72677 Medium Extrusion Test

Table 9.33. Extrusion Data for S72677 Medium Extrusion Test

ID	S72677
Extrusion	Medium
Substrate	302 HQ
Coating	200 microinch copper
Drawing Lubricant	Hammidraw 1846-B
Extrusion Lubricant	Hasco Stealth
Avg. Max	2236.79
Std. Dev. Max	27.1
% Std. Dev. Max	1.2
Avg. Area	337.43
Std. Dev. Area	7.5
% Std. Dev. Area	2.2
Notes/Comments	A type curves

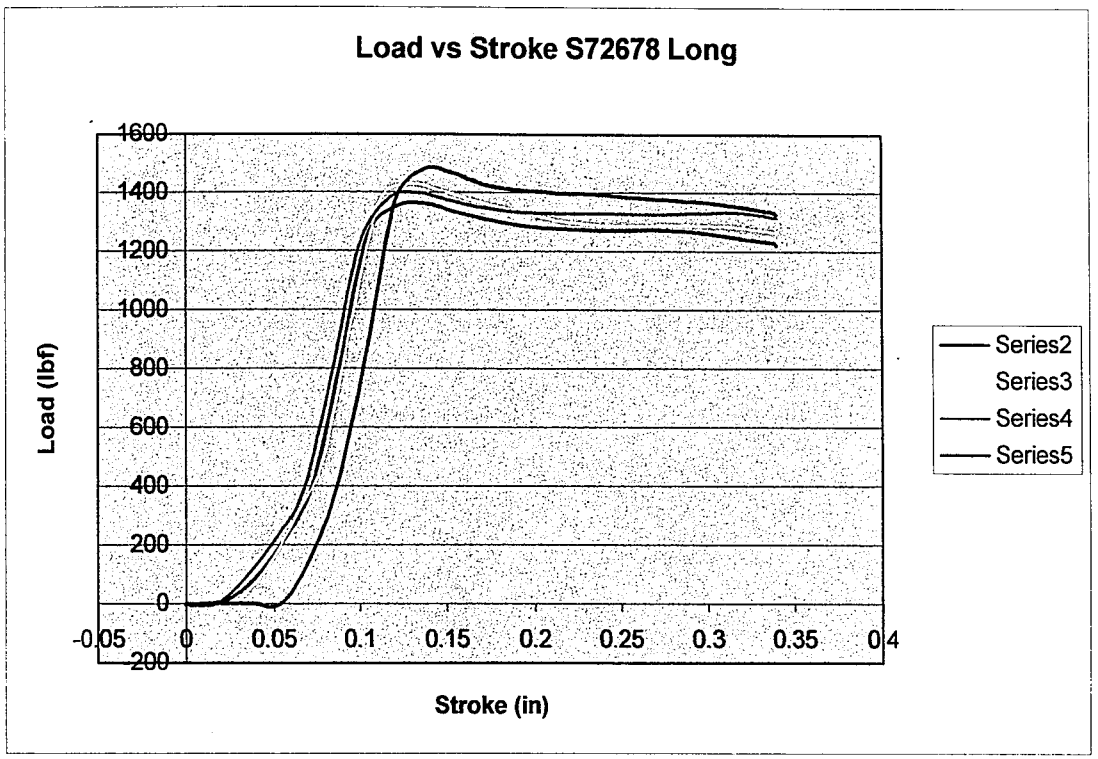

Figure 9.9. Load versus Stroke for S72678 Long Extrusion Test

Table 9.34. Extrusion Data for S72678 Long Extrusion Test

ID	S72678
Extrusion	Long
Substrate	302 HQ
Coating	100 microinch copper plus Black coating A
Drawing Lubricant	Sun Waylube
Extrusion Lubricant	Hasco Stealth
Avg. Max	1418.67
Std. Dev. Max	43.6
% Std. Dev. Max	3.1
Avg. Area	337.69
Std. Dev. Area	5.2
% Std. Dev. Area	1.5
Notes/Comments	A type curves

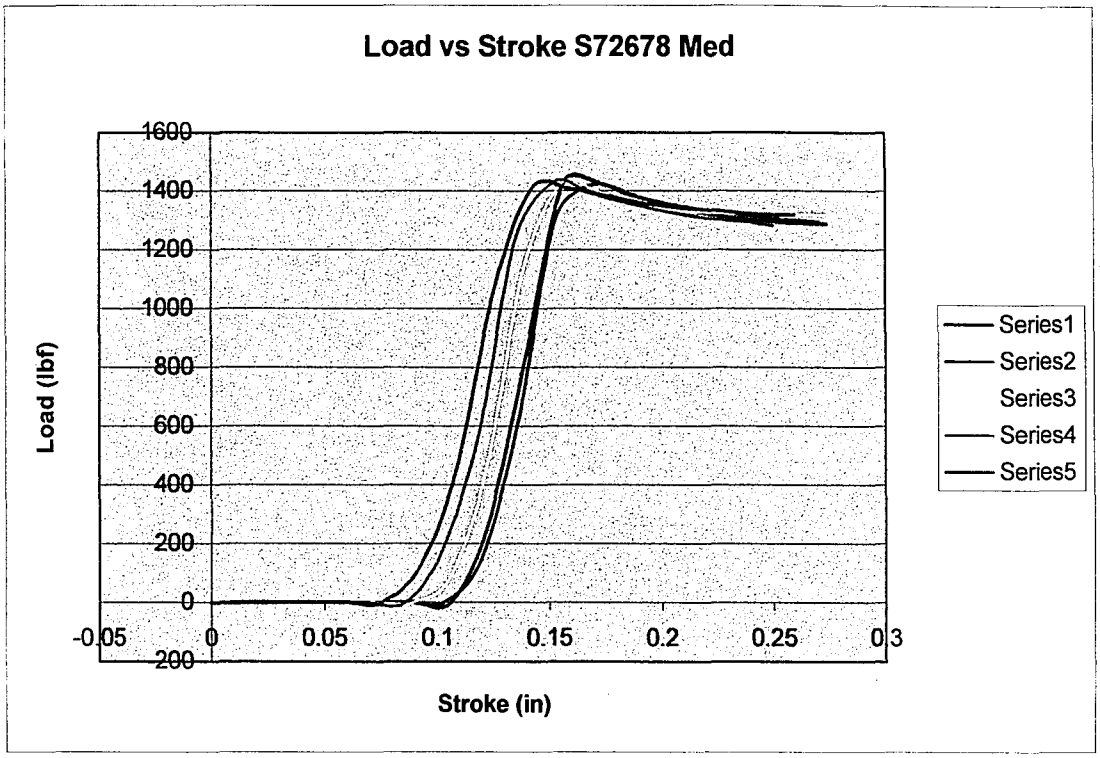

Figure 9.10. Load versus Stroke for S72678 Medium Extrusion Test

Table 9.35. Extrusion Data for S72678 Medium Extrusion Test

ID	S72678
Extrusion	Medium
Substrate	302 HQ
Coating	100 microinch copper plus Black coating A
Drawing Lubricant	Sun Waylube
Extrusion Lubricant	Hasco Stealth
Avg. Max	1424.65
Std. Dev. Max	6.6
% Std. Dev. Max	0.5
Avg. Area	181.20
Std. Dev. Area	9.1
% Std. Dev. Area	5.0
Notes/Comments	A type curves, some lateral spread as an effect of zeroing the press

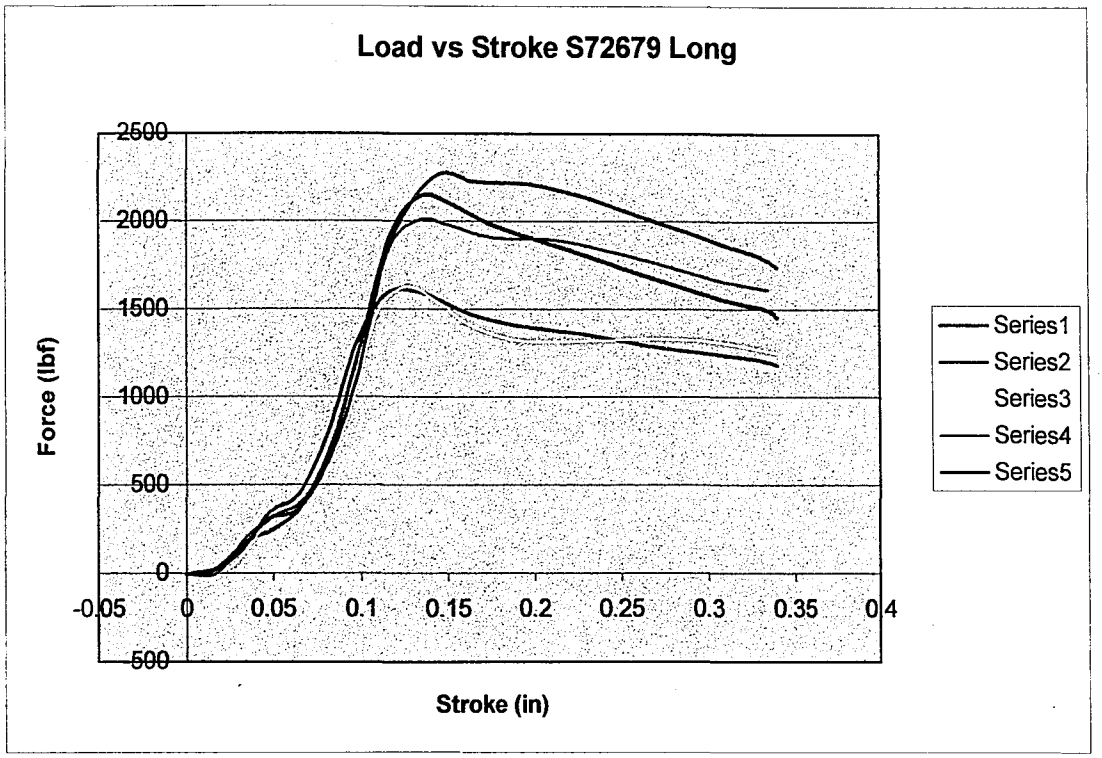

Figure 9.11. Load versus Stroke for S72679 Long Extrusion Test

Table 9.36. Extrusion Data for S72679 Long Extrusion Test

ID	S72679
Extrusion	Long
Substrate	302 HQ
Coating	Black coating A
Drawing Lubricant	Hammidraw 1846-B
Extrusion Lubricant	Hasco Stealth
Avg. Max	1933.54
Std. Dev. Max	271.5
% Std. Dev. Max	14.0
Avg. Area	430.52
Std. Dev. Area	59.5
% Std. Dev. Area	13.8
Notes/Comments	A type curves

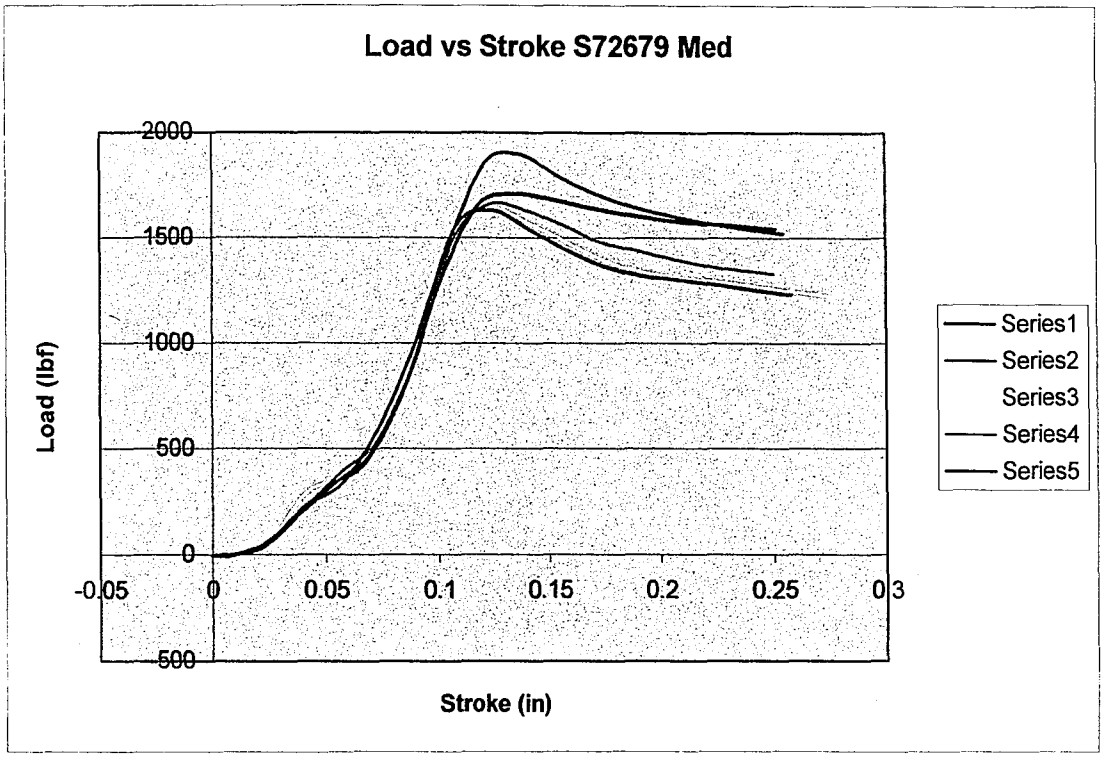

Figure 9.12. Load versus Stroke for S72679 Medium Extrusion Test

Table 9.37. Extrusion Data for S72679 Medium Extrusion Test

ID	S72679
Extrusion	Medium
Substrate	302 HQ
Coating	Black coating A
Drawing Lubricant	Hammidraw 1846-B
Extrusion Lubricant	Hasco Stealth
Avg. Max	1708.03
Std. Dev. Max	98.1
% Std. Dev. Max	5.7
Avg. Area	279.42
Std. Dev. Area	18.4
% Std. Dev. Area	6.6
Notes/Comments	A type curves

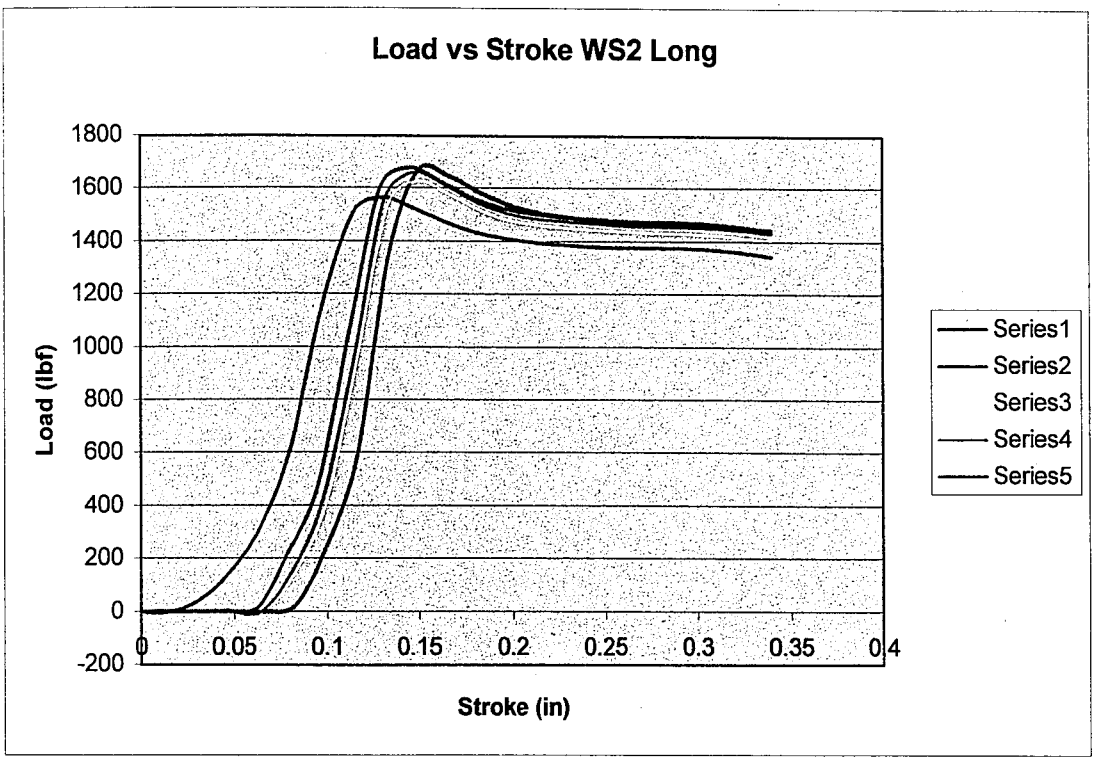

Figure 9.13. Load versus Stroke for WS2 Long Extrusion Test

Table 9.36. Extrusion Data for WS2 Long Extrusion Test

ID	WS2
Extrusion	Long
Substrate	302 HQ
Coating	Tungsten disulfide
Drawing Lubricant	Sun Waylube
Extrusion Lubricant	Hasco Stealth
Avg. Max	1641.45
Std. Dev. Max	40.4
% Std. Dev. Max	2.5
Avg. Area	359.05
Std. Dev. Area	11.6
% Std. Dev. Area	3.2
Notes/Comments	A type curves, some lateral spread as an effect of zeroing the press

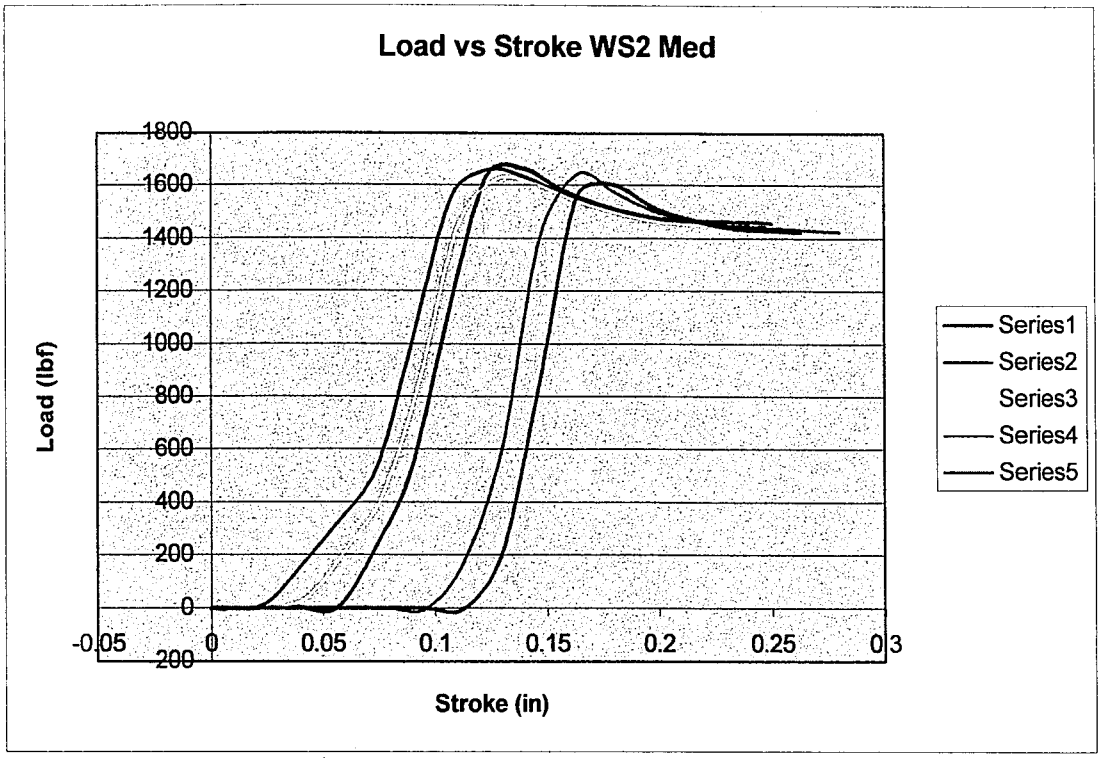

Figure 9.14. Load versus Stroke for WS2 Medium Extrusion Test

Table 9.37. Extrusion Data for WS2 Medium Extrusion Test

ID	WS2
Extrusion	Medium
Substrate	302 HQ
Coating	Tungsten disulfide
Drawing Lubricant	Sun Waylube
Extrusion Lubricant	Hasco Stealth
Avg. Max	1640.28
Std. Dev. Max	23.7
% Std. Dev. Max	1.5
Avg. Area	235.06
Std. Dev. Area	35.8
% Std. Dev. Area	15.2
Notes/Comments	A type curves, some lateral spread as an effect of zeroing the press

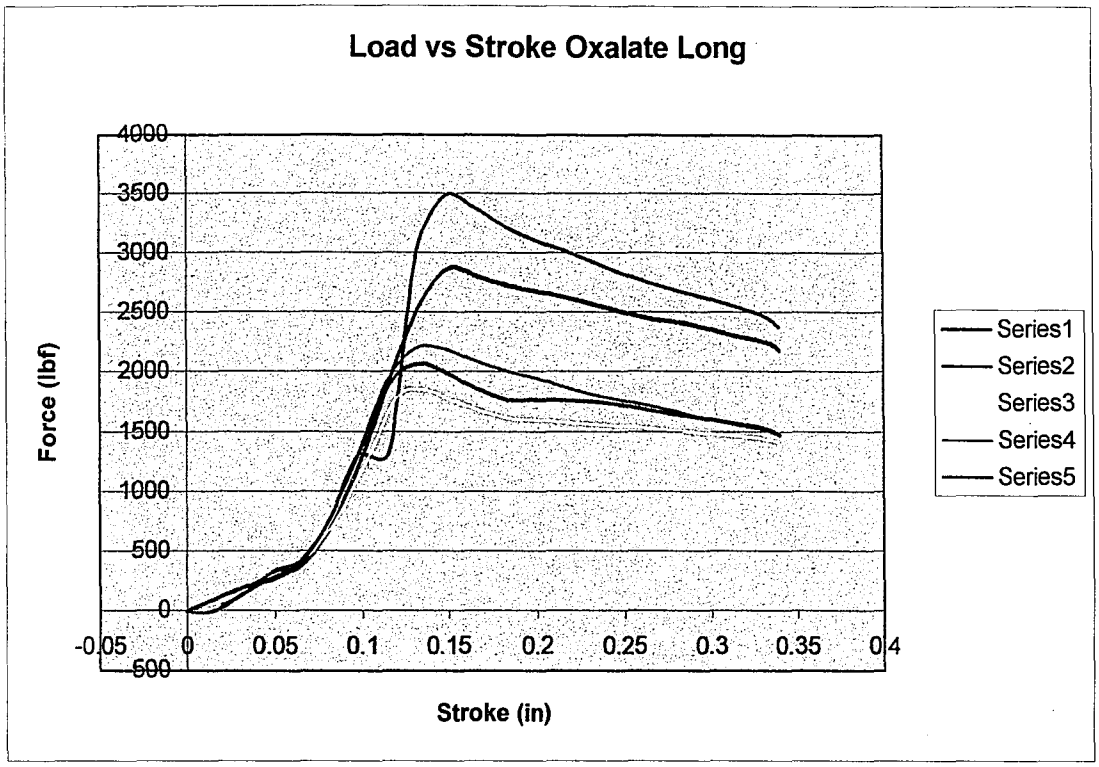

Figure 9.15. Load versus Stroke for Oxalate Long Extrusion Test

Table 9.38. Extrusion Data for Oxalate Long Extrusion Test

ID	Oxalate
Extrusion	Long
Substrate	302 HQ
Coating	Oxalate
Drawing Lubricant	Hammidraw 1846-B
Extrusion Lubricant	Hasco Stealth
Avg. Max	2251.41
Std. Dev. Max	381.8
% Std. Dev. Max	17.0
Avg. Area	508.59
Std. Dev. Area	105.2
% Std. Dev. Area	20.7
Notes/Comments	A and B type curves

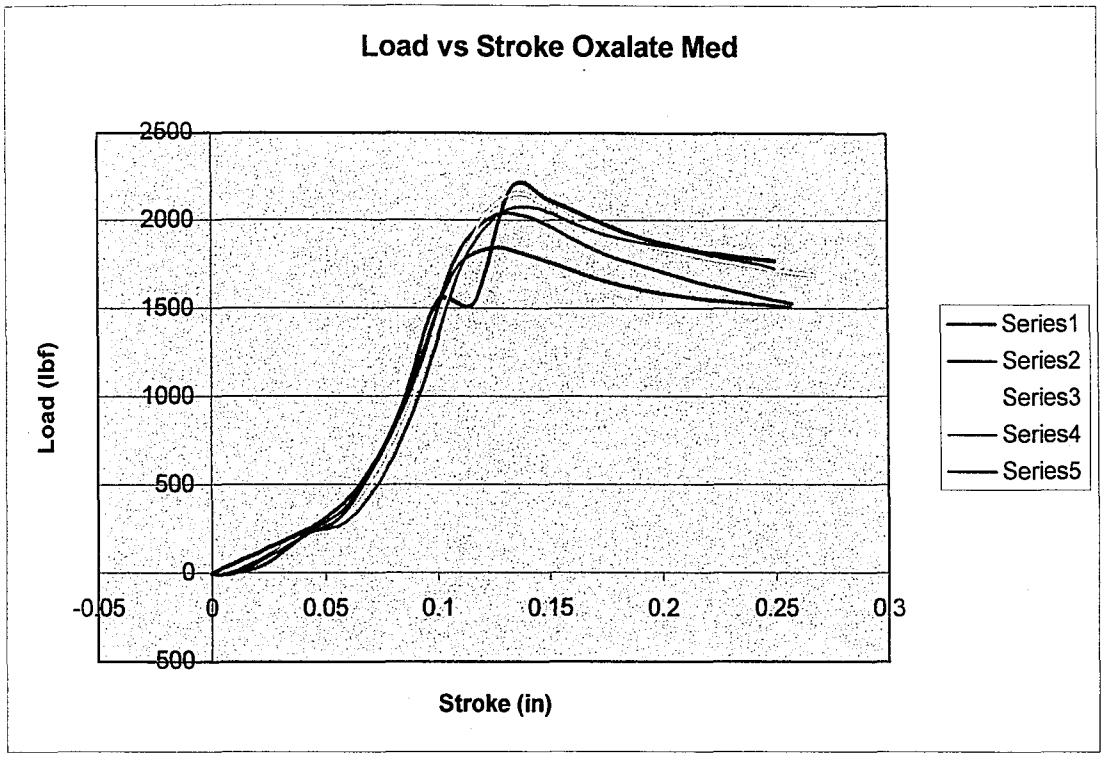

Figure 9.16. Load versus Stroke for Oxalate Medium Extrusion Test

Table 9.39. Extrusion Data for Oxalate Medium Extrusion Test

ID	Oxalate
Extrusion	Medium
Substrate	302 HQ
Coating	Oxalate
Drawing Lubricant	Hammidraw 1846-B
Extrusion Lubricant	Hasco Stealth
Avg. Max	2057.13
Std. Dev. Max	120.9
% Std. Dev. Max	5.9
Avg. Area	307.98
Std. Dev. Area	9.1
% Std. Dev. Area	2.9
Notes/Comments	A and B type curves, less standard deviation than in long extrusion, possibly less coating stripping/buildup because of less severe conditions

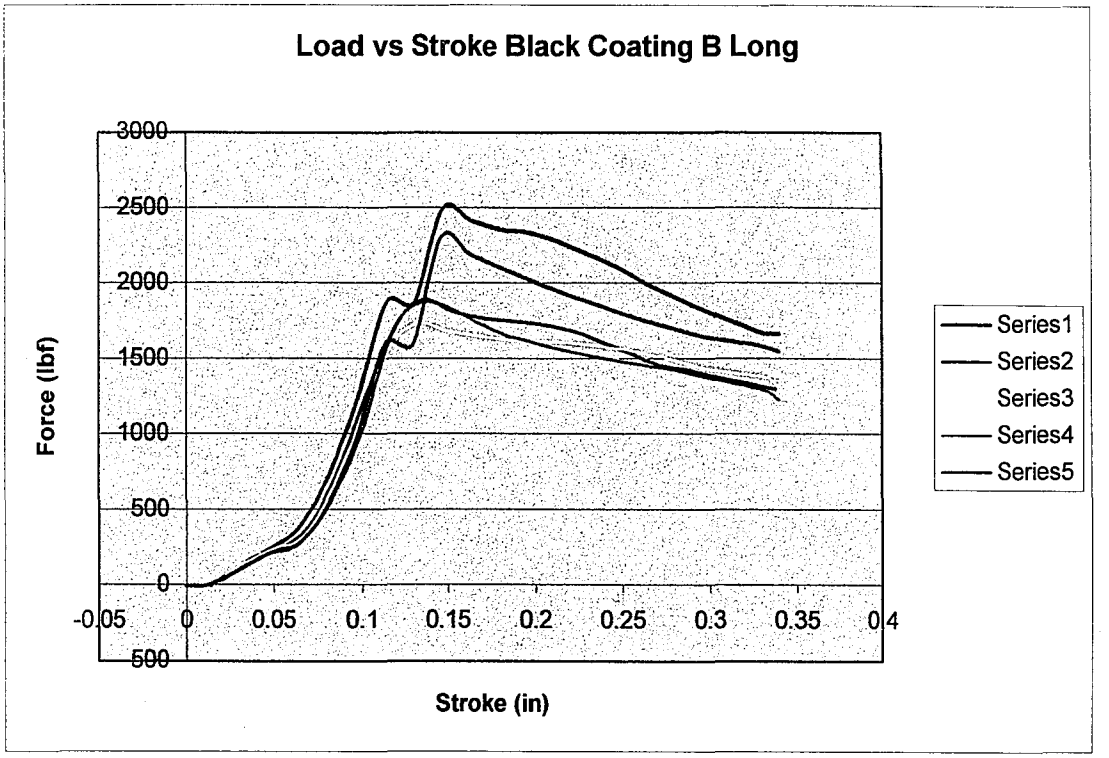

Figure 9.17. Load versus Stroke for Black Coating B Long Extrusion Test

Table 9.40. Extrusion Data for Black Coating B Long Extrusion Test

ID	Black coating B
Extrusion	Long
Substrate	302 HQ
Coating	Black coating B
Drawing Lubricant	Hammidraw 1846-B
Extrusion Lubricant	Hasco Stealth
Avg. Max	2061.43
Std. Dev. Max	287.4
% Std. Dev. Max	13.9
Avg. Area	441.63
Std. Dev. Area	46.0
% Std. Dev. Area	10.4
Notes/Comments	A and B type curves, large standard deviations for both max

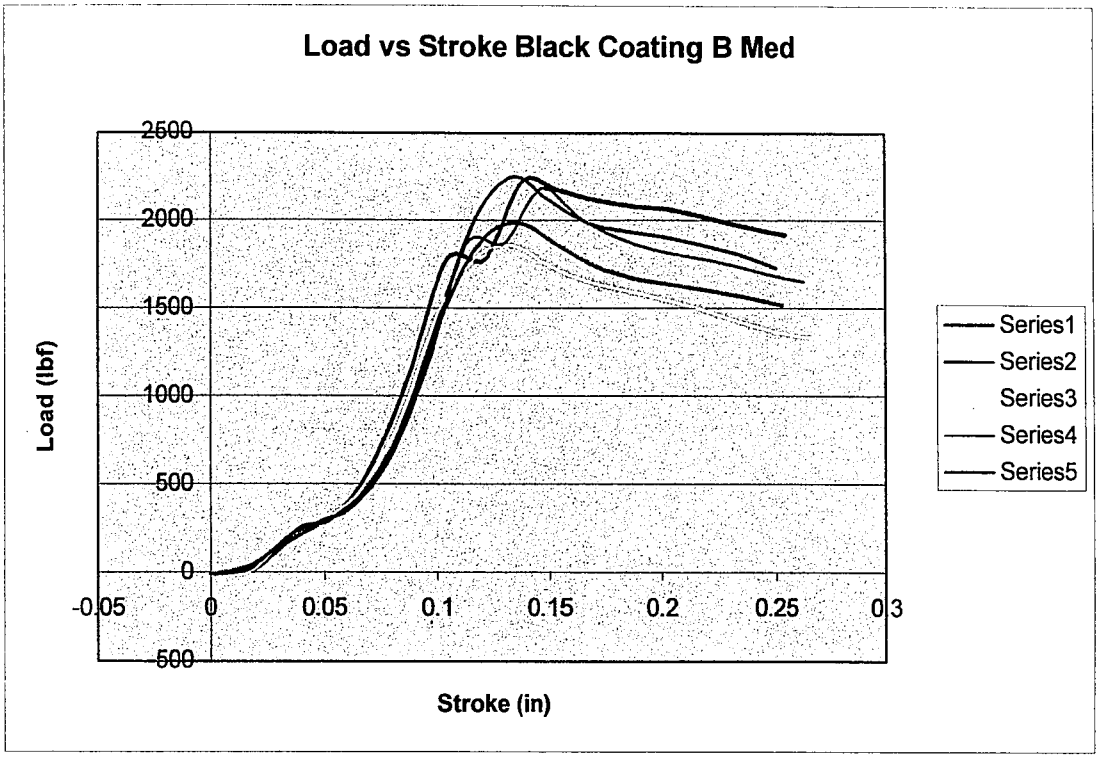

Figure 9.18. Load versus Stroke for Black Coating B Medium Extrusion Test

Table 9.41. Extrusion Data for Black Coating B Medium Extrusion Test

ID	Black coating B
Extrusion	Medium
Substrate	302 HQ
Coating	Black coating B
Drawing Lubricant	Hammidraw 1846-B
Extrusion Lubricant	Hasco Stealth
Avg. Max	2101.91
Std. Dev. Max	152.3
% Std. Dev. Max	7.3
Avg. Area	330.75
Std. Dev. Area	27.3
% Std. Dev. Area	8.3
Notes/Comments	A and B type curves, one max that corresponds with die packing but not double peaked extrusion (series 2)

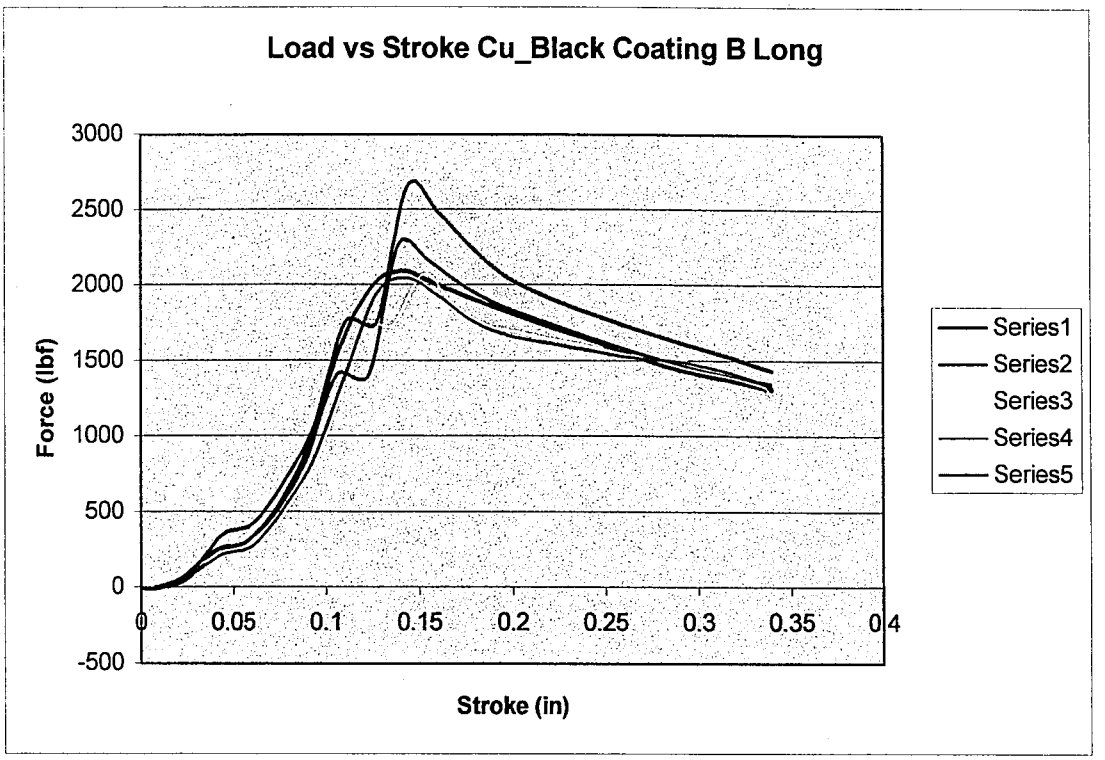

Figure 9.19. Load versus Stroke for Cu + Black Coating B Long Extrusion Test

Table 9.42. Extrusion Data for Cu + Black Coating B Long Extrusion Test

ID	Cu_Black coating B
Extrusion	Long
Substrate	302 HQ
Coating	100 microinch copper plus Black coating B
Drawing Lubricant	Hammidraw 1846-B
Extrusion Lubricant	Hasco Stealth
Avg. Max	2228.84
Std. Dev. Max	228.4
% Std. Dev. Max	10.3
Avg. Area	431.62
Std. Dev. Area	27.9
% Std. Dev. Area	6.5
Notes/Comments	A and B type curves, one B resulting in normal maximum force

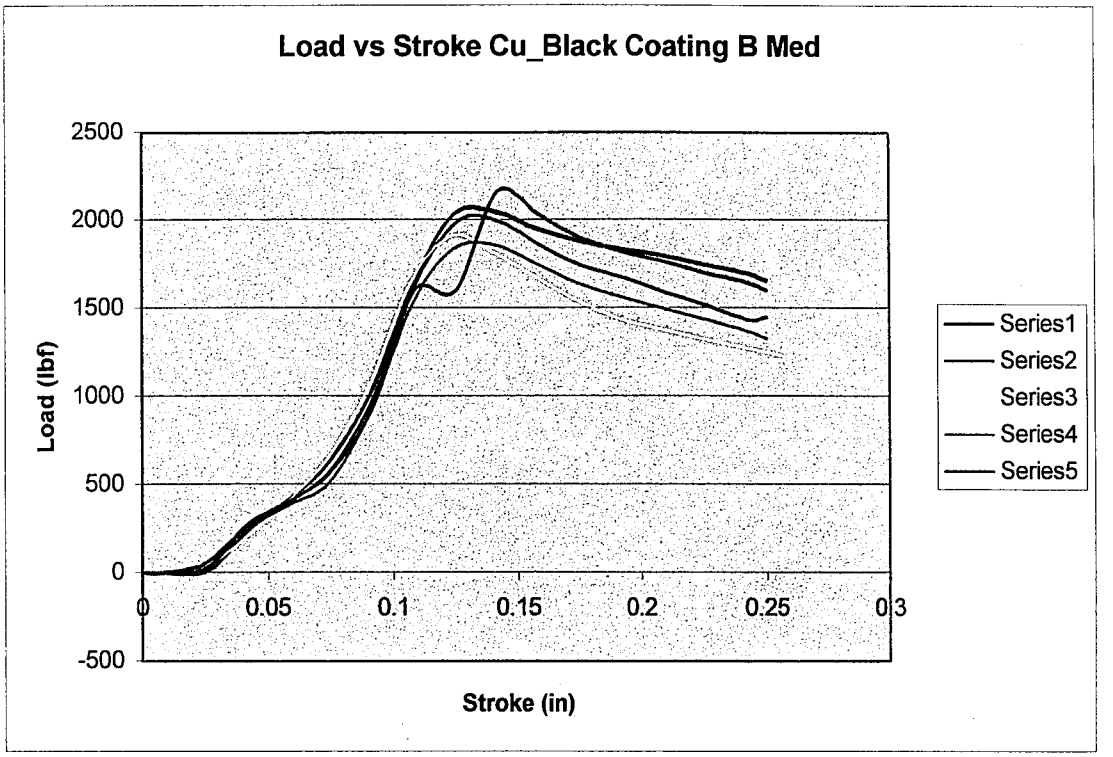

Figure 9.20. Load versus Stroke for Cu + Black Coating B Medium Extrusion Test

Table 9.43. Extrusion Data for Cu + Black Coating B Medium Extrusion Test

ID	Cu_Black coating B
Extrusion	Medium
Substrate	302 HQ
Coating	100 microinch copper plus Black coating B
Drawing Lubricant	Hammidraw 1846-B
Extrusion Lubricant	Hasco Stealth
Avg. Max	1997.75
Std. Dev. Max	105.2
% Std. Dev. Max	5.3
Avg. Area	289.42
Std. Dev. Area	15.9
% Std. Dev. Area	5.5
Notes/Comments	A and B type curves

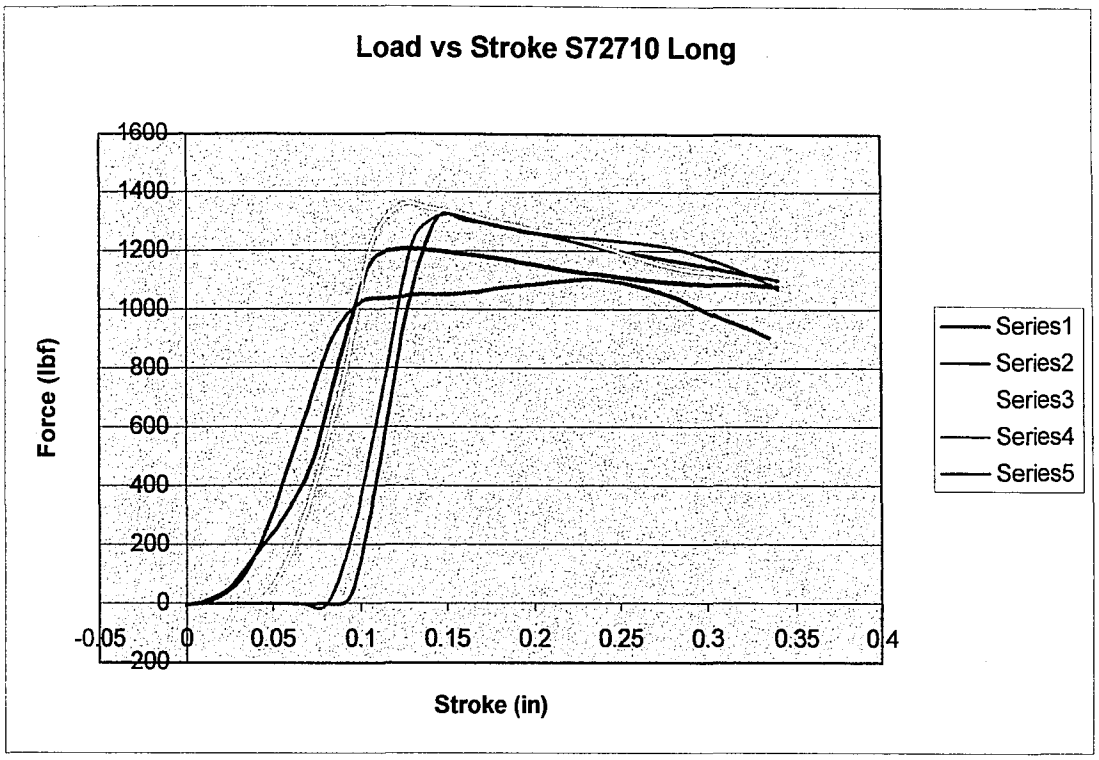

Figure 9.21. Load versus Stroke for S72710 Long Extrusion Test

Table 9.44. Extrusion Data for S72710 Long Extrusion Test

ID	S72710
Extrusion	Long
Substrate	T430
Coating	100 microinch copper plus Black coating A
Drawing Lubricant	Hammidraw 1846-B
Extrusion Lubricant	Hasco Stealth
Avg. Max	1238.53
Std. Dev. Max	88.6
% Std. Dev. Max	7.2
Avg. Area	291.46
Std. Dev. Area	14.8
% Std. Dev. Area	5.1
Notes/Comments	

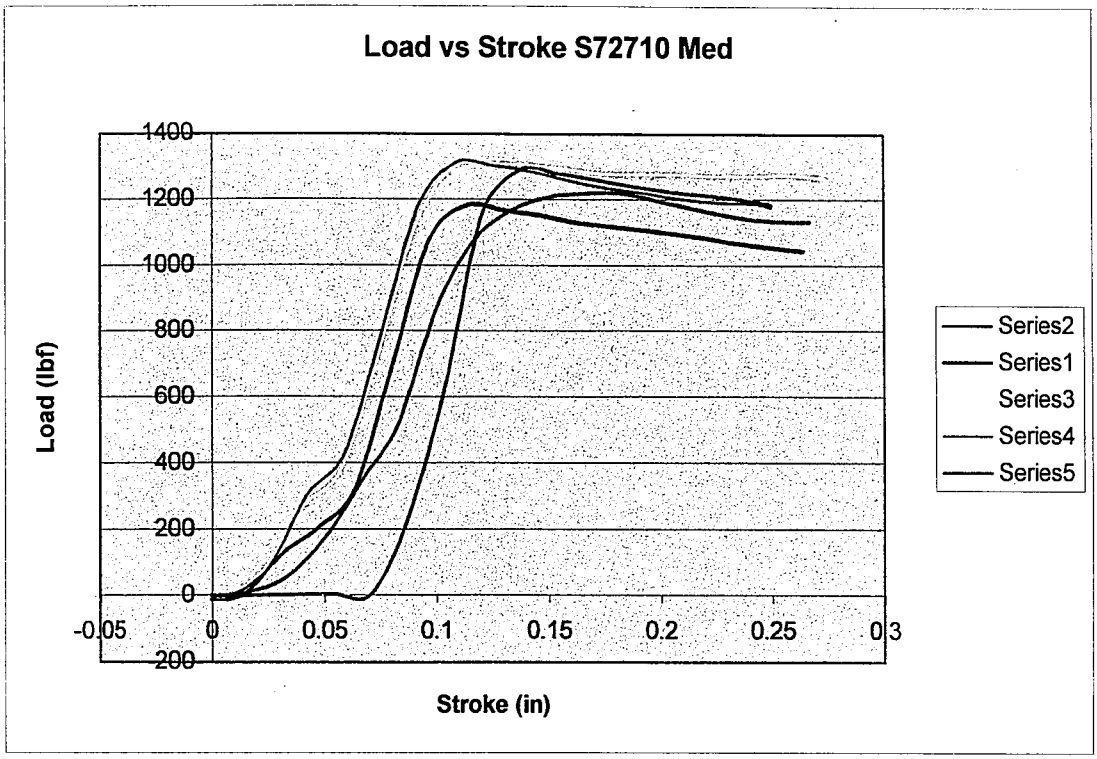

Figure 9.22. Load versus Stroke for S72710 Medium Extrusion Test

Table 9.45. Extrusion Data for S72710 Medium Extrusion Test

ID	S72710
Extrusion	Medium
Substrate	T430
Coating	100 microinch copper plus Black coating A
Drawing Lubricant	Hammidraw 1846-B
Extrusion Lubricant	Hasco Stealth
Avg. Max	1263.68
Std. Dev. Max	52.2
% Std. Dev. Max	4.1
Avg. Area	161.66
Std. Dev. Area	39.6
% Std. Dev. Area	24.5
Notes/Comments	A and C type curves, some lateral spread from zeroing press

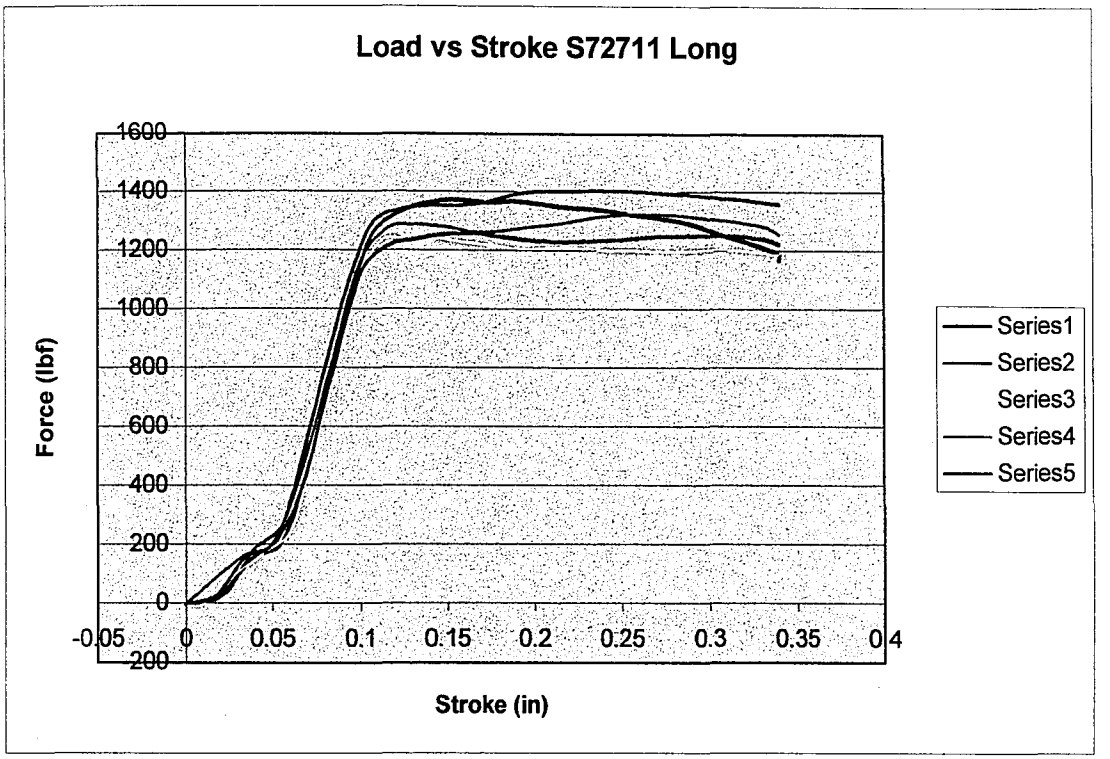

Figure 9.23. Load versus Stroke for S72711 Long Extrusion Test

Table 9.46. Extrusion Data for S72711 Long Extrusion Test

ID	S72711
Extrusion	Long
Substrate	T430
Coating	100 microinch copper plus Black coating B
Drawing Lubricant	Hammidraw 1846-B
Extrusion Lubricant	Hasco Stealth
Avg. Max	1321.99
Std. Dev. Max	62.9
% Std. Dev. Max	4.8
Avg. Area	341.09
Std. Dev. Area	19.2
% Std. Dev. Area	5.6
Notes/Comments	C type curves

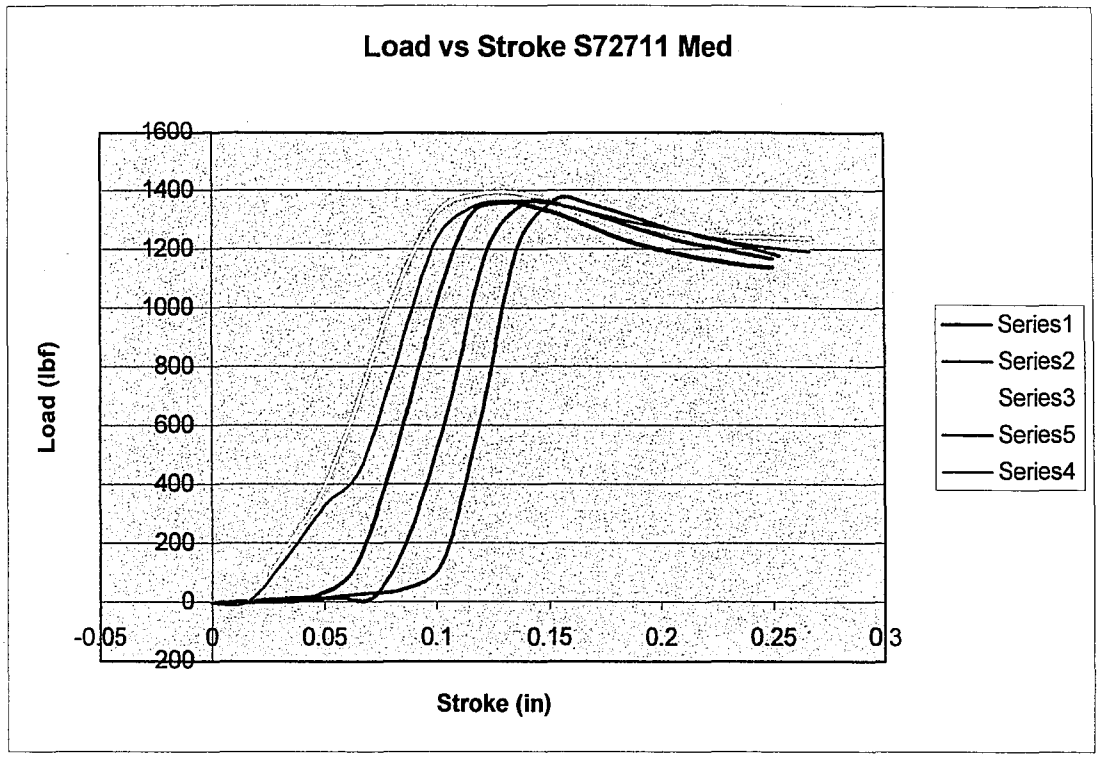

Figure 9.24. Load versus Stroke for S72711 Medium Extrusion Test

Table 9.47. Extrusion Data for S72711 Medium Extrusion Test

ID	S72711
Extrusion	Medium
Substrate	T430
Coating	100 microinch copper plus Black coating B
Drawing Lubricant	Hammidraw 1846-B
Extrusion Lubricant	Hasco Stealth
Avg. Max	1371.92
Std. Dev. Max	12.9
% Std. Dev. Max	0.9
Avg. Area	207.52
Std. Dev. Area	28.75
% Std. Dev. Area	13.9
Notes/Comments	A type curves, some lateral spread as an effect of zeroing the press

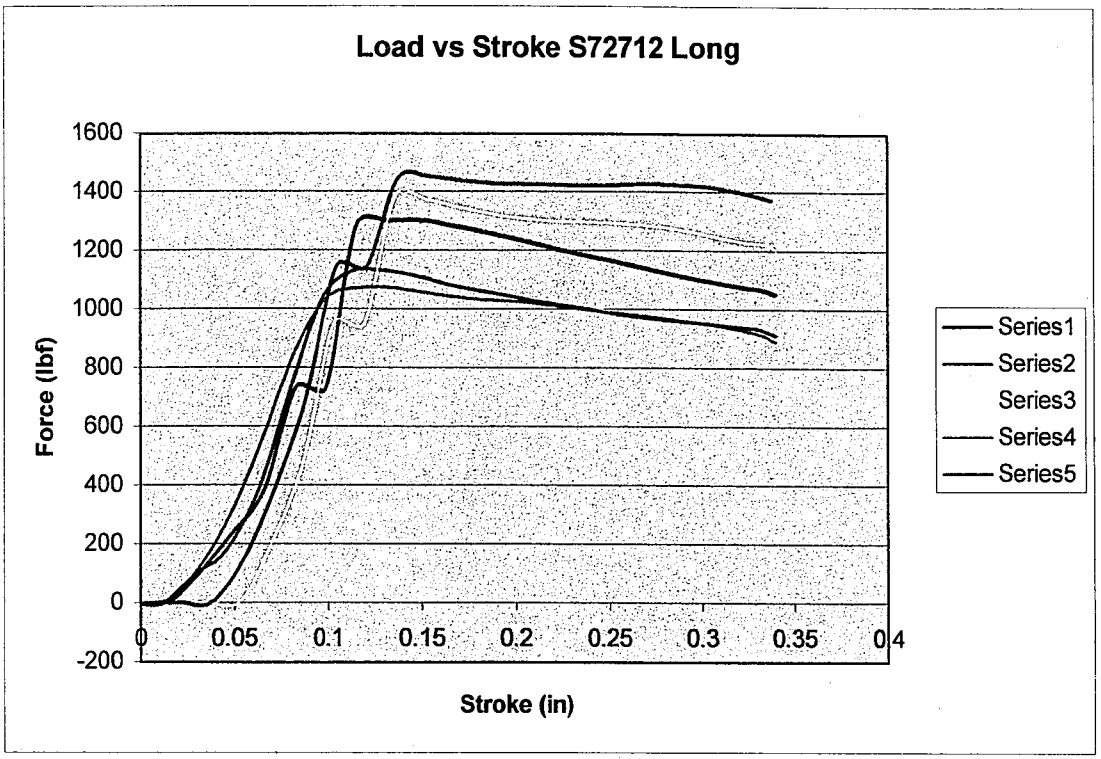

Figure 9.25. Load versus Stroke for S72712 Long Extrusion Test

Table 9.48. Extrusion Data for S72712 Long Extrusion Test

ID	S72712
Extrusion	Long
Substrate	T430
Coating	Black coating B
Drawing Lubricant	Hammidraw 1846-B
Extrusion Lubricant	Hasco Stealth
Avg. Max	1241.89
Std. Dev. Max	147.6
% Std. Dev. Max	11.9
Avg. Area	308.55
Std. Dev. Area	26.3
% Std. Dev. Area	8.5
Notes/Comments	A and B type curves

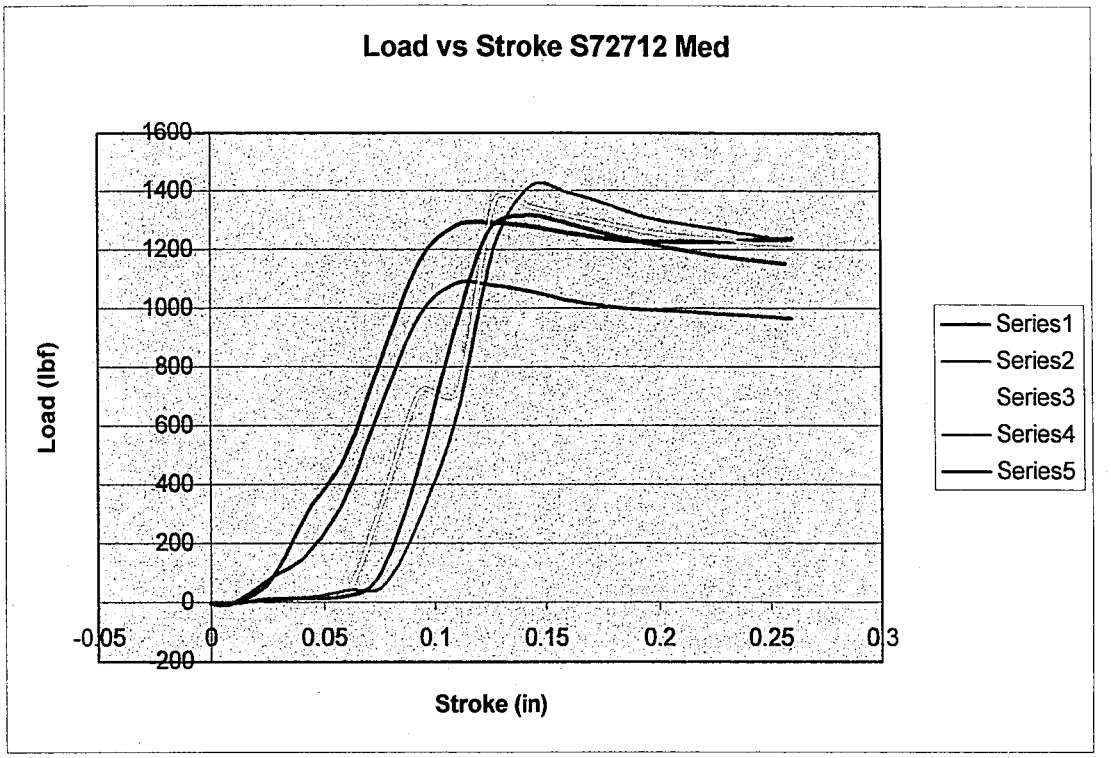

Figure 9.26. Load versus Stroke for S72712 Medium Extrusion Test

Table 9.49. Extrusion Data for S72712 Medium Extrusion Test

ID	S72712
Extrusion	Medium
Substrate	T430
Coating	Black coating B
Drawing Lubricant	Hammidraw 1846-B
Extrusion Lubricant	Hasco Stealth
Avg. Max	1297.61
Std. Dev. Max	114.1
% Std. Dev. Max	8.8
Avg. Area	212.14
Std. Dev. Area	18.0
% Std. Dev. Area	8.5
Notes/Comments	A and B type curves, some lateral spread as an effect of zeroing the press

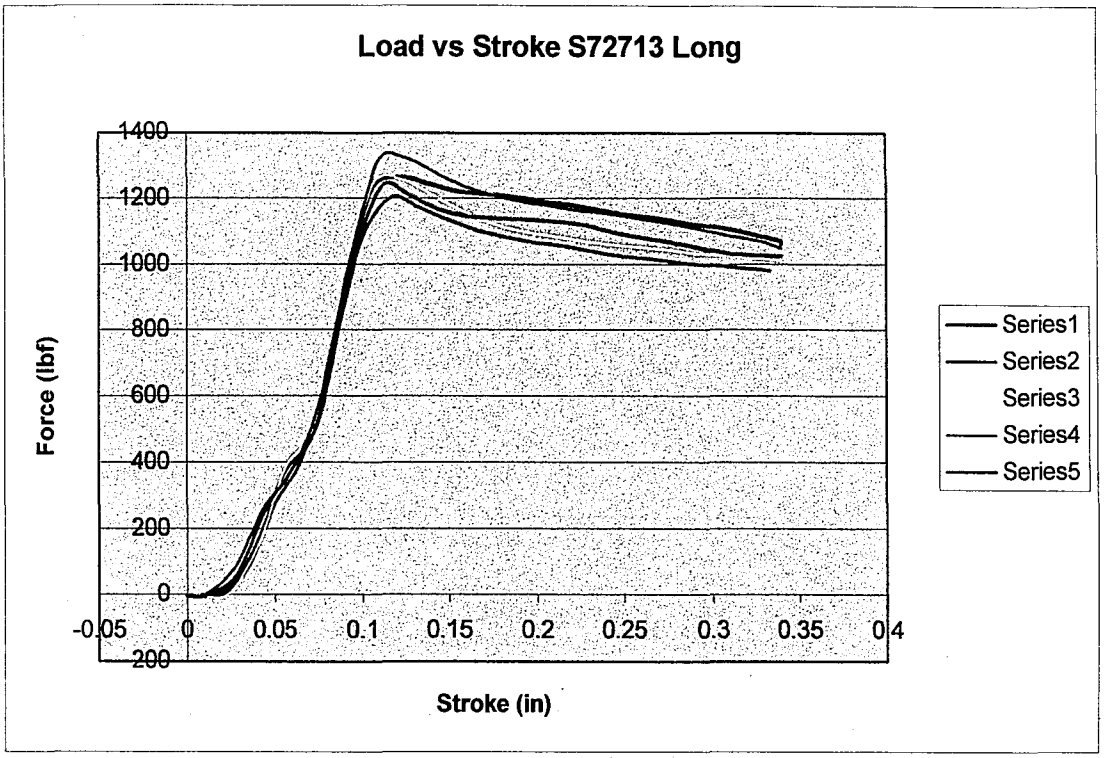

Figure 9.27. Load versus Stroke for S72713 Long Extrusion Test

Table 9.50. Extrusion Data for S72713 Long Extrusion Test

ID	S72713
Extrusion	Long
Substrate	T430
Coating	Black coating A
Drawing Lubricant	Hammidraw 1846-B
Extrusion Lubricant	Hasco Stealth
Avg. Max	1257.46
Std. Dev. Max	40.0
% Std. Dev. Max	3.2
Avg. Area	298.14
Std. Dev. Area	13.2
% Std. Dev. Area	4.4
Notes/Comments	A type curves

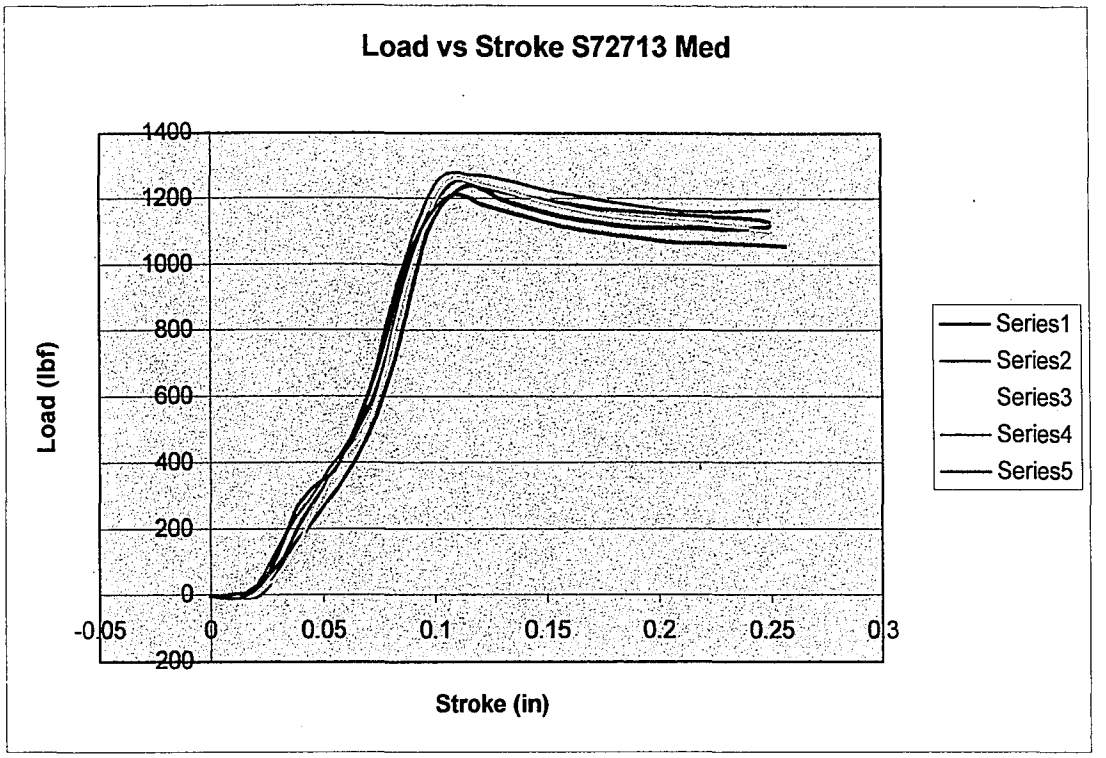

Figure 9.28. Load versus Stroke for S72713 Medium Extrusion Test

Table 9.51. Extrusion Data for S72713 Medium Extrusion Test

ID	S72713
Extrusion	Medium
Substrate	T430
Coating	Black coating A
Drawing Lubricant	Hammidraw 1846-B
Extrusion Lubricant	Hasco Stealth
Avg. Max	1241.99
Std. Dev. Max	21.6
% Std. Dev. Max	1.7
Avg. Area	211.77
Std. Dev. Area	4.5
% Std. Dev. Area	2.1
Notes/Comments	A type curves

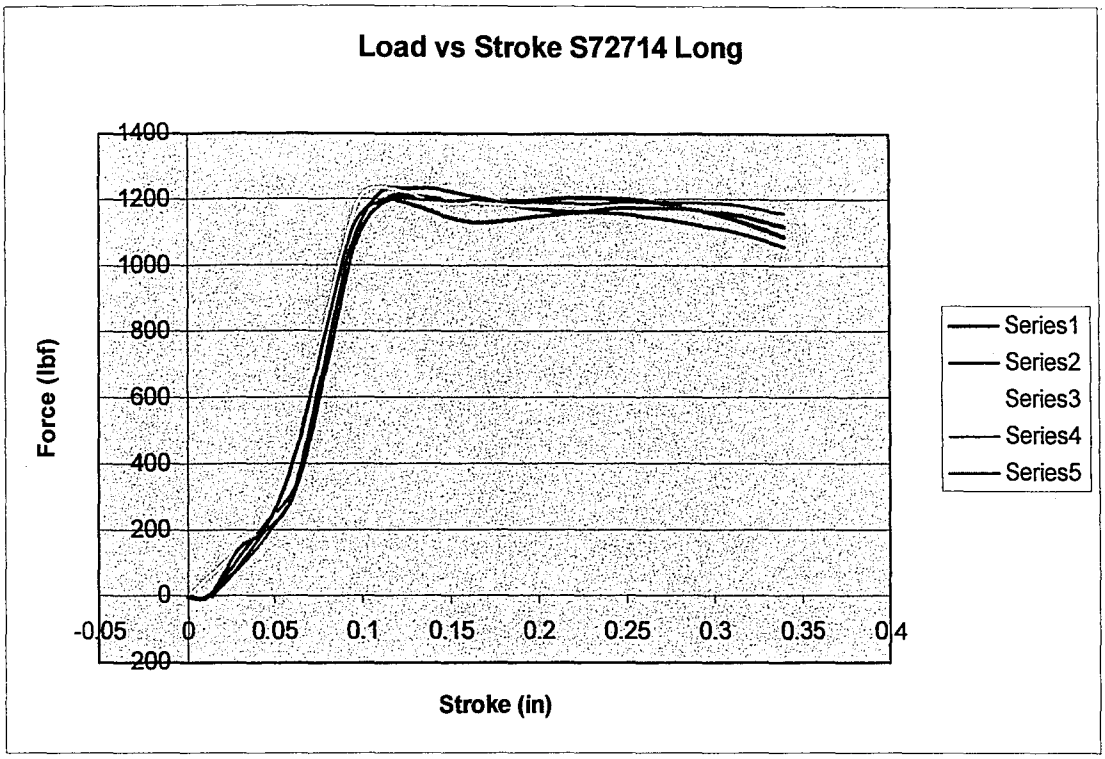

Figure 9.29. Load versus Stroke for S72714 Long Extrusion Test

Table 9.52. Extrusion Data for S72714 Long Extrusion Test

ID	S72714
Extrusion	Long
Substrate	T430
Coating	Precoat soap
Drawing Lubricant	Hammidraw 1846-B
Extrusion Lubricant	Hasco Stealth
Avg. Max	1216.01
Std. Dev. Max	15.8
% Std. Dev. Max	1.3
Avg. Area	324.30
Std. Dev. Area	12.7
% Std. Dev. Area	3.9
Notes/Comments	C type curves

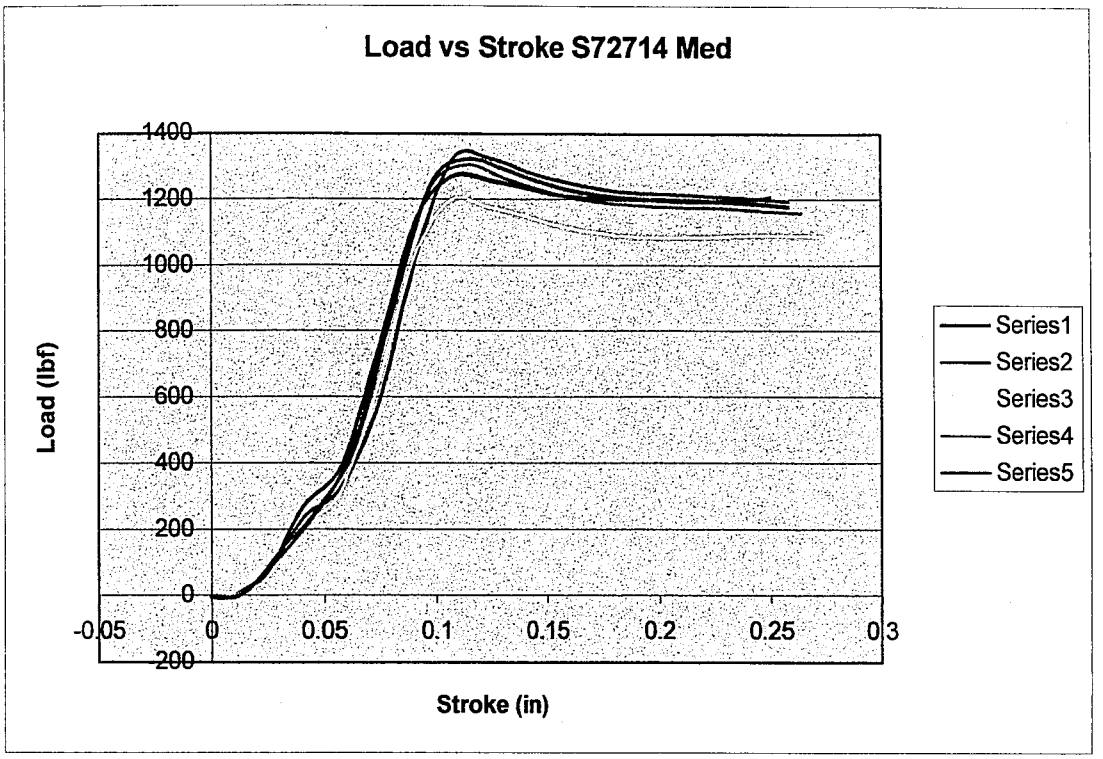

Figure 9.30. Load versus Stroke for S72714 Medium Extrusion Test

Table 9.53. Extrusion Data for S72714 Medium Extrusion Test

ID	S72714
Extrusion	Medium
Substrate	T430
Coating	Precoat soap
Drawing Lubricant	Hammidraw 1846-B
Extrusion Lubricant	Hasco Stealth
Avg. Max	1284.73
Std. Dev. Max	47.8
% Std. Dev. Max	3.7
Avg. Area	240.33
Std. Dev. Area	8.9
% Std. Dev. Area	3.7
Notes/Comments	A type curves

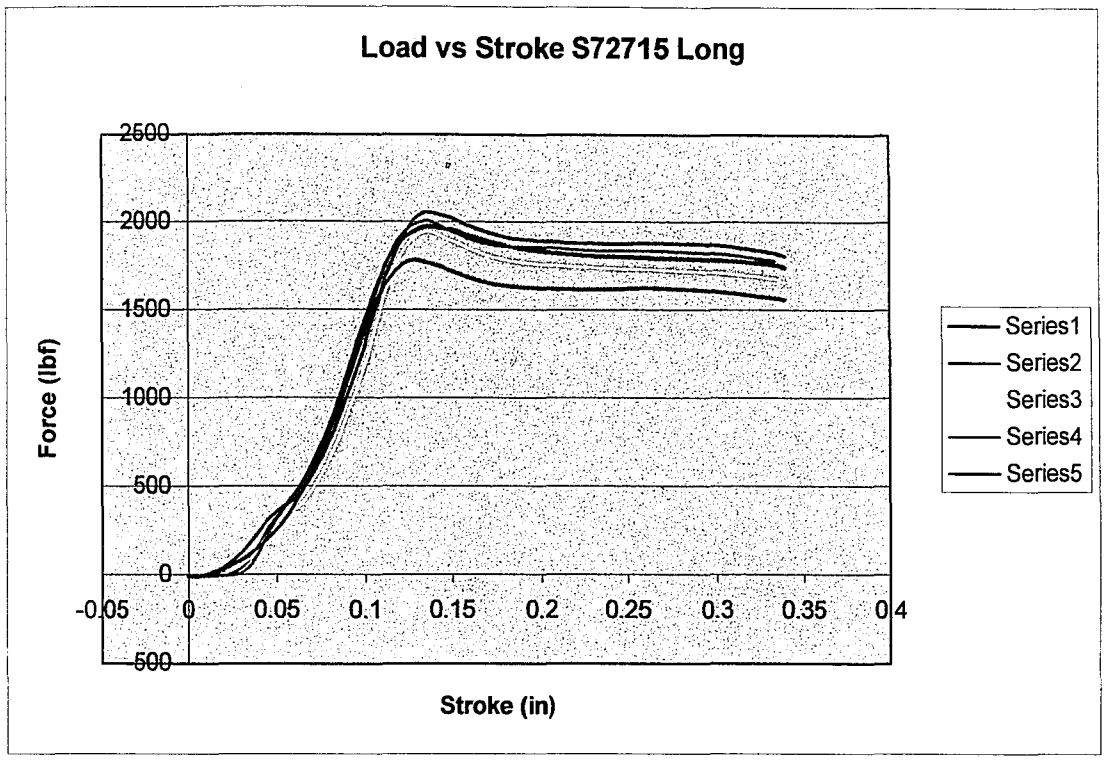

Figure 9.31. Load versus Stroke for S72715 Long Extrusion Test

Table 9.54. Extrusion Data for S72715 Long Extrusion Test

ID	S72715
Extrusion	Long
Substrate	A286
Coating	100 microinch copper
Drawing Lubricant	Hammidraw 1846-B
Extrusion Lubricant	Hasco Stealth
Avg. Max	1945.45
Std. Dev. Max	91.1
% Std. Dev. Max	4.7
Avg. Area	463.94
Std. Dev. Area	23.8
% Std. Dev. Area	5.1
Notes/Comments	A type curves

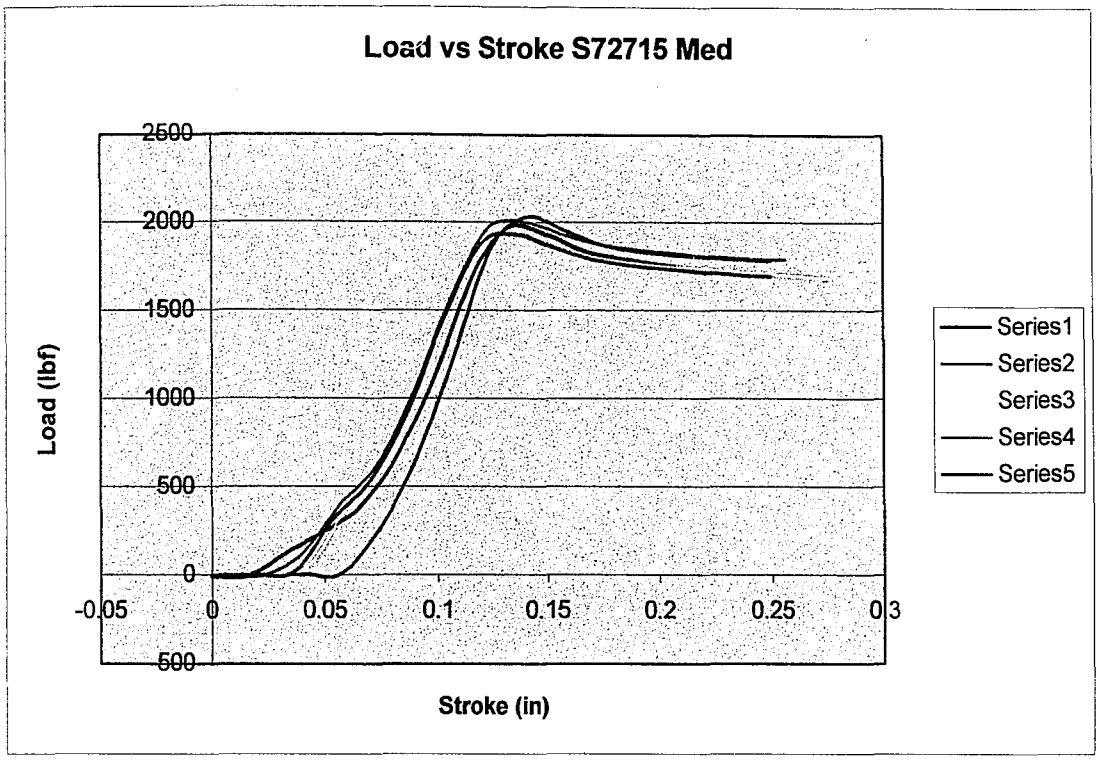

Figure 9.32. Load versus Stroke for S72715 Medium Extrusion Test

Table 9.55. Extrusion Data for S72715 Medium Extrusion Test

ID	S72715
Extrusion	Medium
Substrate	A286
Coating	100 microinch copper
Drawing Lubricant	Hammidraw 1846-B
Extrusion Lubricant	Hasco Stealth
Avg. Max	1977.13
Std. Dev. Max	41.2
% Std. Dev. Max	2.1
Avg. Area	311.55
Std. Dev. Area	22.6
% Std. Dev. Area	7.3
Notes/Comments	A type curves

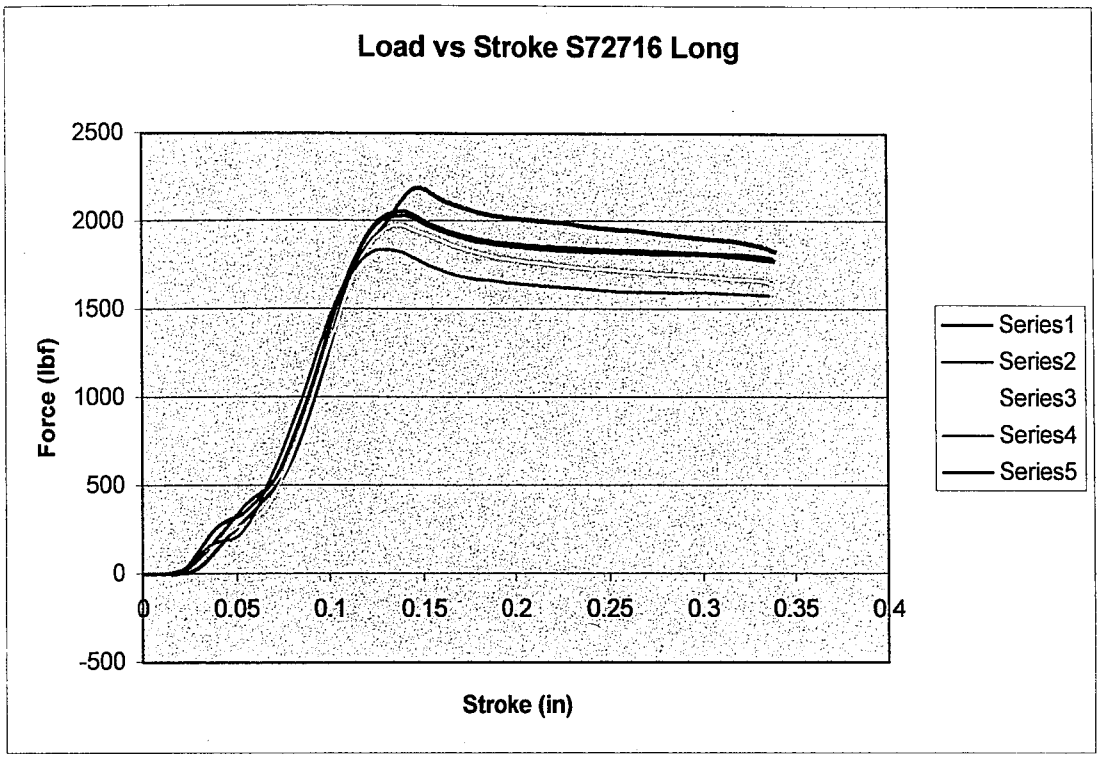

Figure 9.33. Load versus Stroke for S72716 Long Extrusion Test

Table 9.56. Extrusion Data for S72716 Long Extrusion Test

ID	S72716
Extrusion	Long
Substrate	A286
Coating	100 microinch copper
Drawing Lubricant	Hammidraw 1846-B
Extrusion Lubricant	Hasco Stealth
Avg. Max	2016.54
Std. Dev. Max	115.2
% Std. Dev. Max	5.7
Avg. Area	467.46
Std. Dev. Area	24.0
% Std. Dev. Area	5.1
Notes/Comments	A type curves

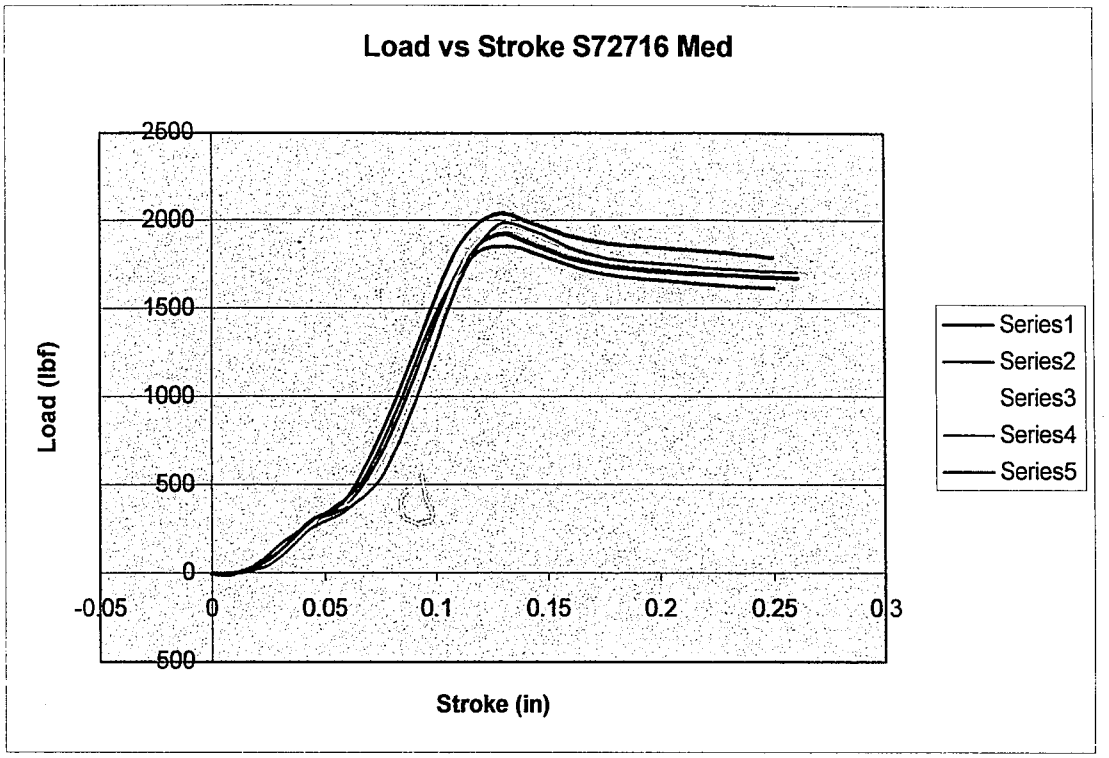

Figure 9.34. Load versus Stroke for S72716 Medium Extrusion Test

Table 9.57. Extrusion Data for S72716 Medium Extrusion Test

ID	S72716
Extrusion	Medium
Substrate	A286
Coating	100 microinch copper
Drawing Lubricant	Hammidraw 1846-B
Extrusion Lubricant	Hasco Stealth
Avg. Max	1948.46
Std. Dev. Max	58.9
% Std. Dev. Max	3.0
Avg. Area	325.52
Std. Dev. Area	11.9
% Std. Dev. Area	3.7
Notes/Comments	A type curves

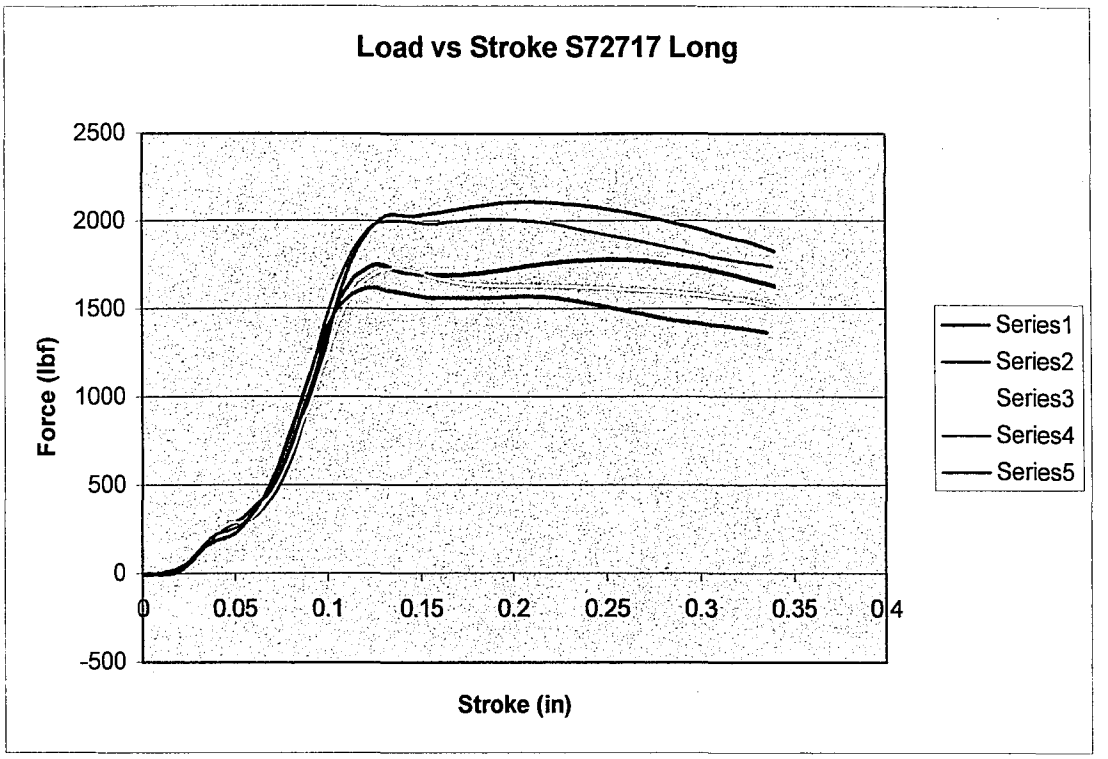

Figure 9.35. Load versus Stroke for S72717 Long Extrusion Test

Table 9.58. Extrusion Data for S72717 Long Extrusion Test

ID	S72717
Extrusion	Long
Substrate	A286
Coating	100 microinch copper plus Black coating A
Drawing Lubricant	Hammidraw 1846-B
Extrusion Lubricant	Hasco Stealth
Avg. Max	1849.35
Std. Dev. Max	185.9
% Std. Dev. Max	10.1
Avg. Area	449.49
Std. Dev. Area	43.9
% Std. Dev. Area	9.8
Notes/Comments	C type curves

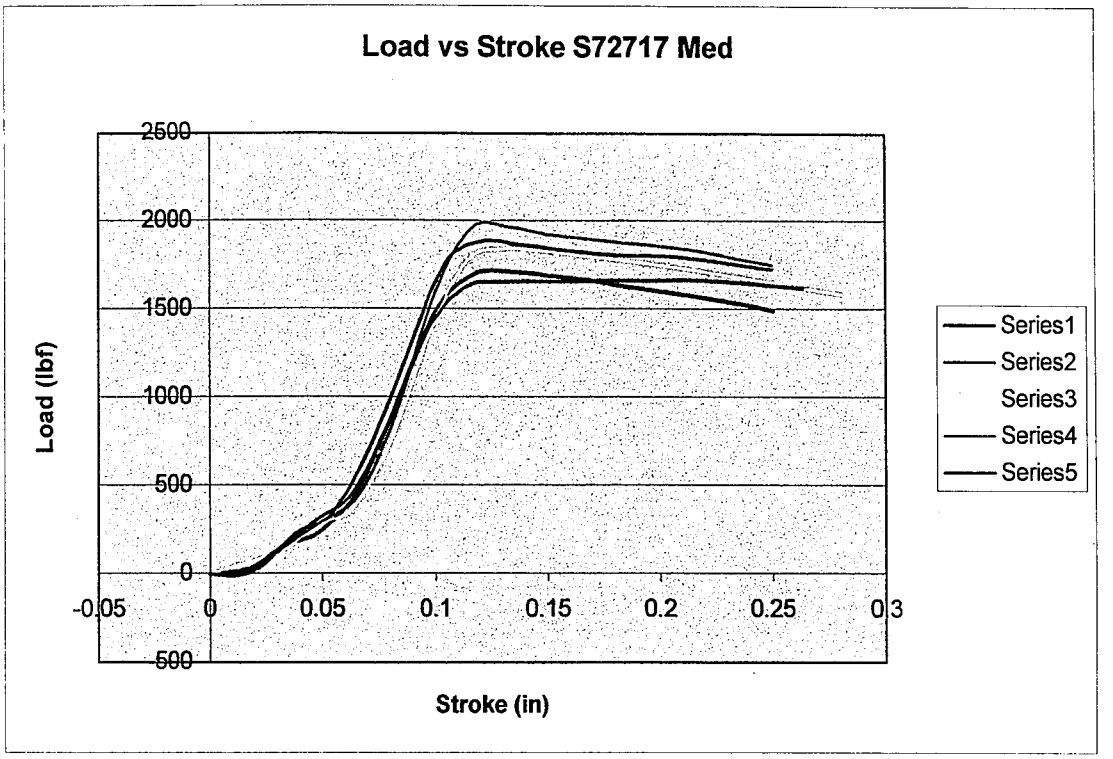

Figure 9.36. Load versus Stroke for S72717 Medium Extrusion Test

Table 9.59. Extrusion Data for S72717 Medium Extrusion Test

ID	S72717
Extrusion	Medium
Substrate	A286
Coating	100 microinch copper plus Black coating A
Drawing Lubricant	Hammidraw 1846-B
Extrusion Lubricant	Hasco Stealth
Avg. Max	1815.52
Std. Dev. Max	111.3
% Std. Dev. Max	6.1
Avg. Area	328.49
Std. Dev. Area	29.7
% Std. Dev. Area	9.1
Notes/Comments	A – C type curves

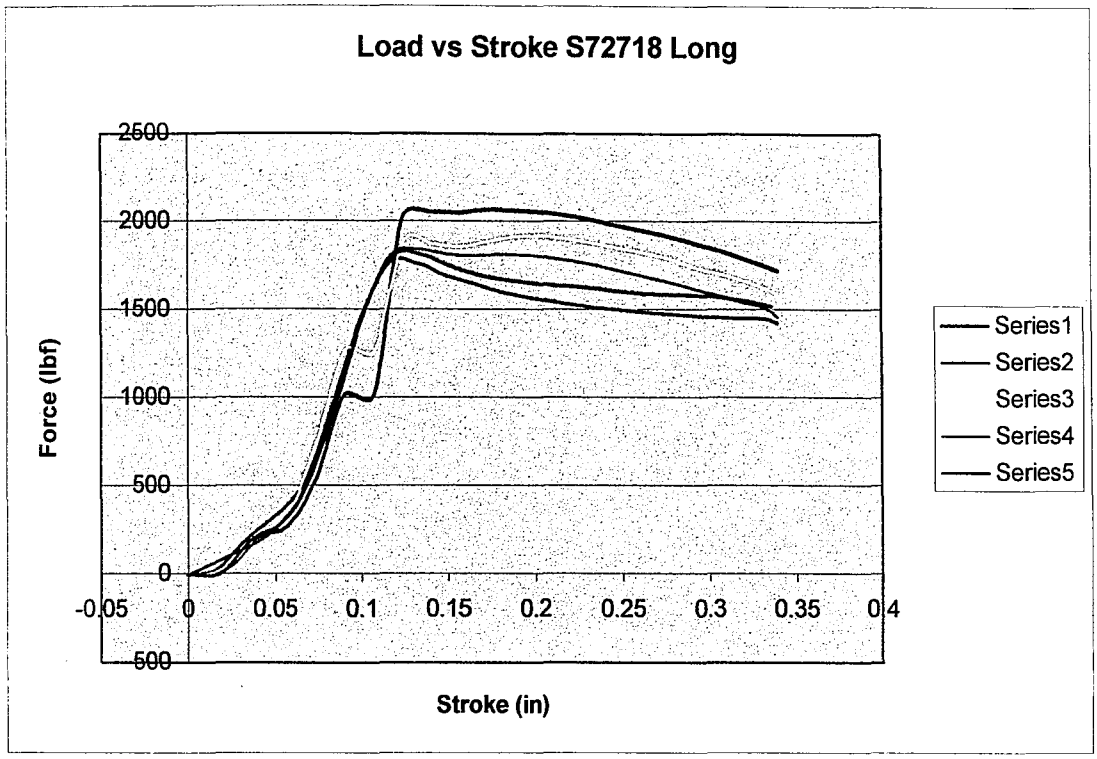

Figure 9.37. Load versus Stroke for S72718 Long Extrusion Test

Table 9.60. Extrusion Data for S72718 Long Extrusion Test

ID	S72718
Extrusion	Long
Substrate	A286
Coating	200 microinch copper plus Black coating B
Drawing Lubricant	Hammidraw 1846-B
Extrusion Lubricant	Hasco Stealth
Avg. Max	1883.82
Std. Dev. Max	104.8
% Std. Dev. Max	5.6
Avg. Area	457.26
Std. Dev. Area	23.2
% Std. Dev. Area	5.1
Notes/Comments	A and B type curves

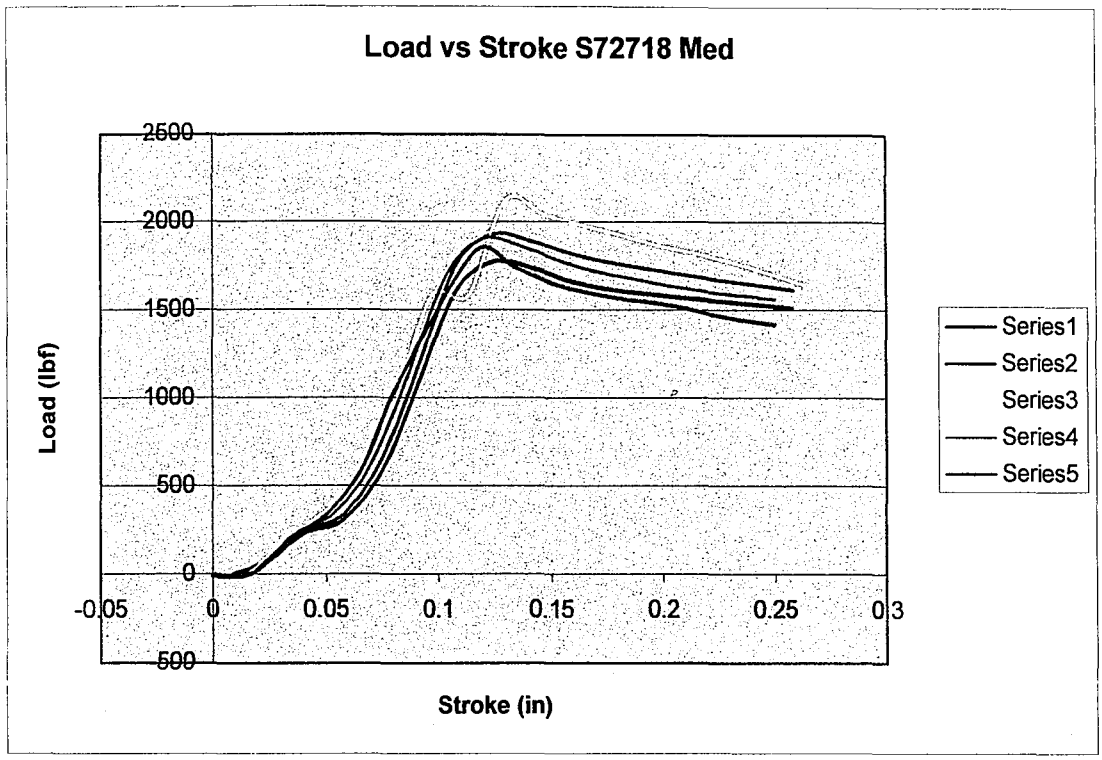

Figure 9.38. Load versus Stroke for S72718 Medium Extrusion Test

Table 9.61. Extrusion Data for S72718 Medium Extrusion Test

ID	S72718
Extrusion	Medium
Substrate	A286
Coating	200 microinch copper plus Black coating B
Drawing Lubricant	Hammidraw 1846-B
Extrusion Lubricant	Hasco Stealth
Avg. Max	1917.11
Std. Dev. Max	118.6
% Std. Dev. Max	6.2
Avg. Area	310.47
Std. Dev. Area	30.6
% Std. Dev. Area	9.8
Notes/Comments	A and B type curves

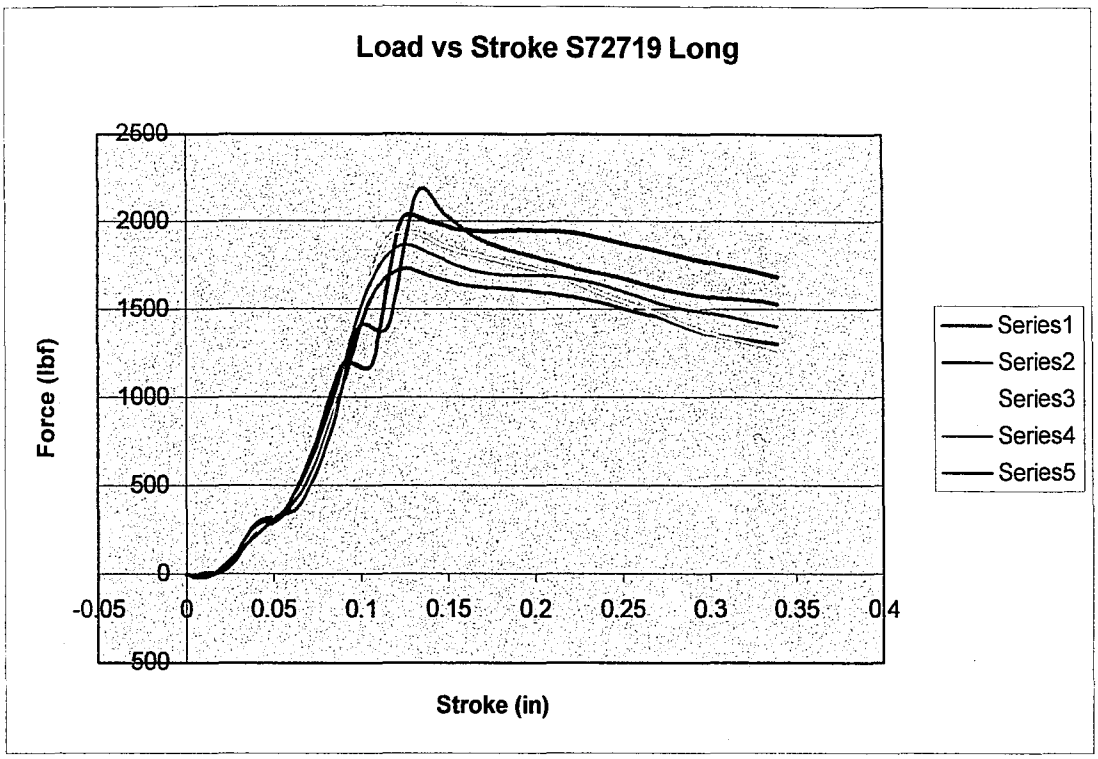

Figure 9.39. Load versus Stroke for S72719 Long Extrusion Test

Table 9.62. Extrusion Data for S72719 Long Extrusion Test

ID	S72719
Extrusion	Long
Substrate	A286
Coating	Black coating B
Drawing Lubricant	Hammidraw 1846-B
Extrusion Lubricant	Hasco Stealth
Avg. Max	1940.30
Std. Dev. Max	143.2
% Std. Dev. Max	7.4
Avg. Area	441.40
Std. Dev. Area	30.9
% Std. Dev. Area	7.0
Notes/Comments	A and B type curves

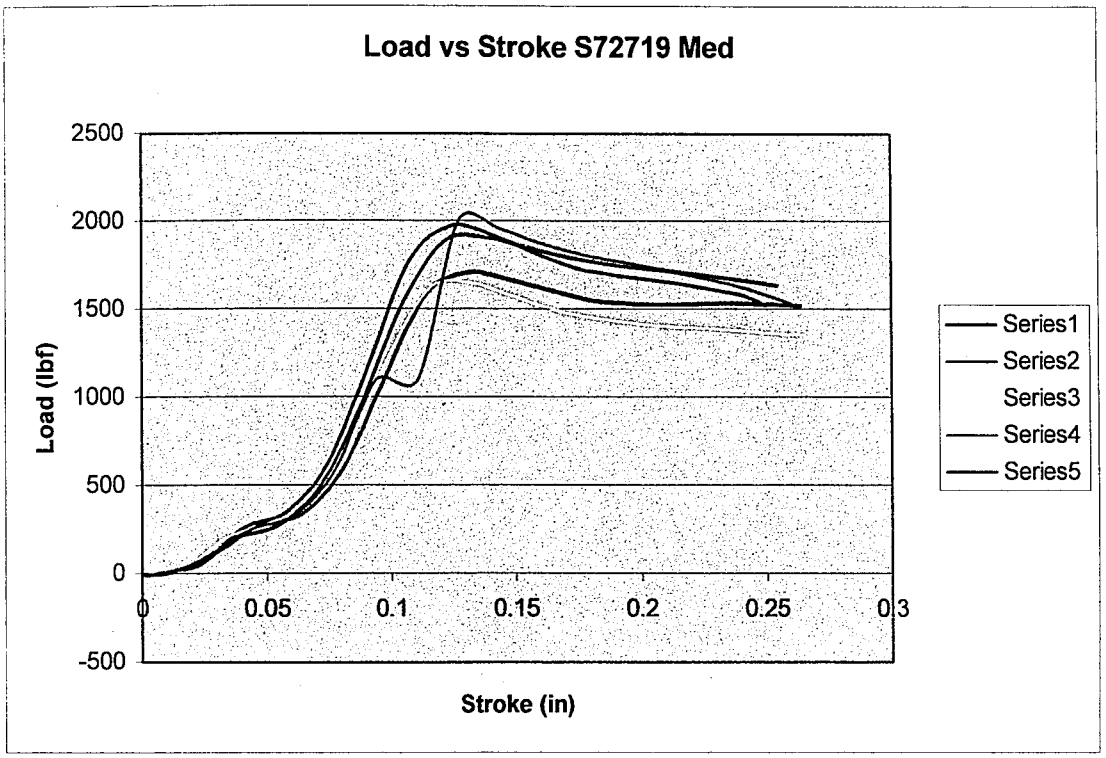

Figure 9.40. Load versus Stroke for S72719 Medium Extrusion Test

Table 9.63. Extrusion Data for S72719 Medium Extrusion Test

ID	S72719
Extrusion	Medium
Substrate	A286
Coating	Black coating B
Drawing Lubricant	Hammidraw 1846-B
Extrusion Lubricant	Hasco Stealth
Avg. Max	1850.42
Std. Dev. Max	143.3
% Std. Dev. Max	7.8
Avg. Area	298.62
Std. Dev. Area	14.2
% Std. Dev. Area	4.8
Notes/Comments	A and B type curves, B type does not have a much larger maximum

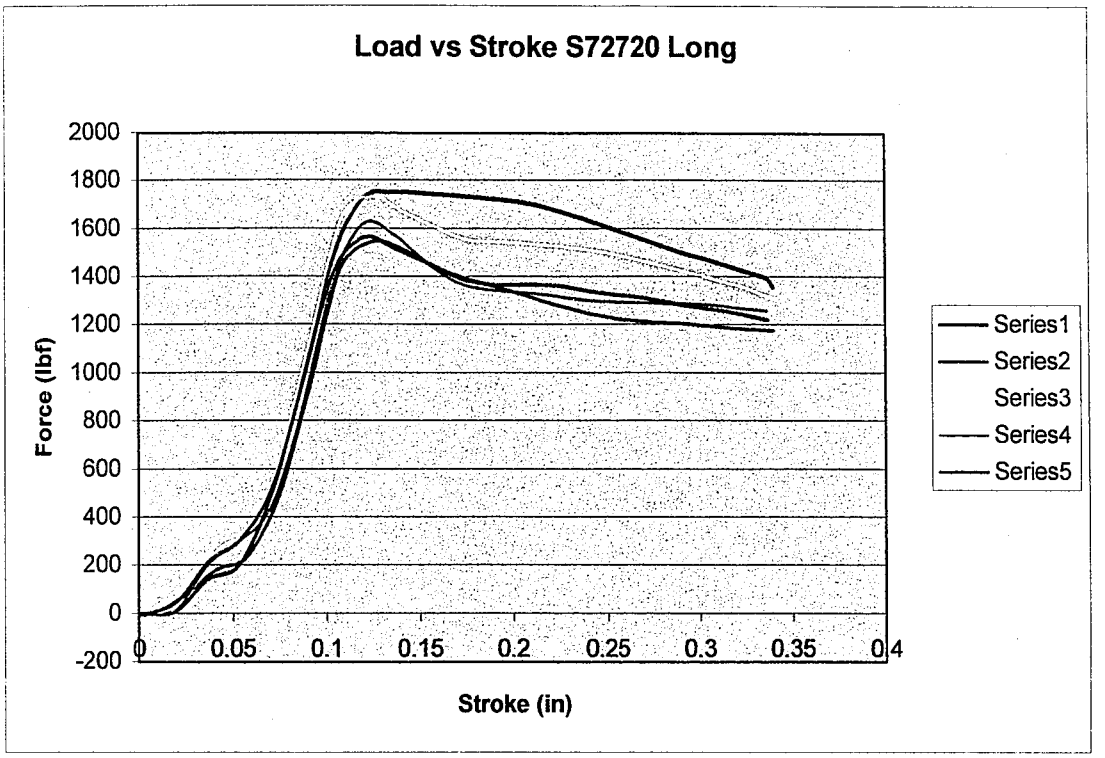

Figure 9.41. Load versus Stroke for S72720 Long Extrusion Test

Table 9.64. Extrusion Data for S72720 Long Extrusion Test

ID	S72720
Extrusion	Long
Substrate	A286
Coating	Black coating A
Drawing Lubricant	Hammidraw 1846-B
Extrusion Lubricant	Hasco Stealth
Avg. Max	1645.21
Std. Dev. Max	84.9
% Std. Dev. Max	5.2
Avg. Area	372.56
Std. Dev. Area	27.7
% Std. Dev. Area	7.4
Notes/Comments	A type curves

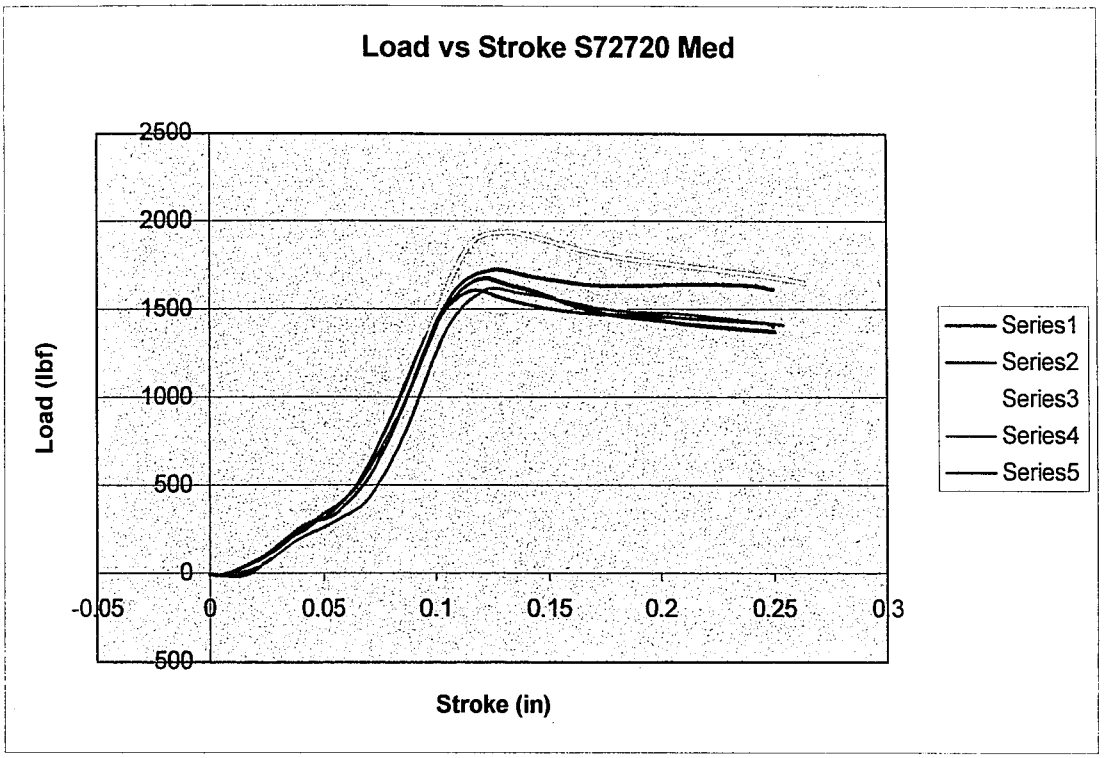

Figure 9.42. Load versus Stroke for S72720 Medium Extrusion Test

Table 9.65. Extrusion Data for S72720 Medium Extrusion Test

ID	S72720
Extrusion	Medium
Substrate	A286
Coating	Black coating A
Drawing Lubricant	Hammidraw 1846-B
Extrusion Lubricant	Hasco Stealth
Avg. Max	1709.96
Std. Dev. Max	124.0
% Std. Dev. Max	7.3
Avg. Area	288.05
Std. Dev. Area	22.4
% Std. Dev. Area	7.8
Notes/Comments	A type curves

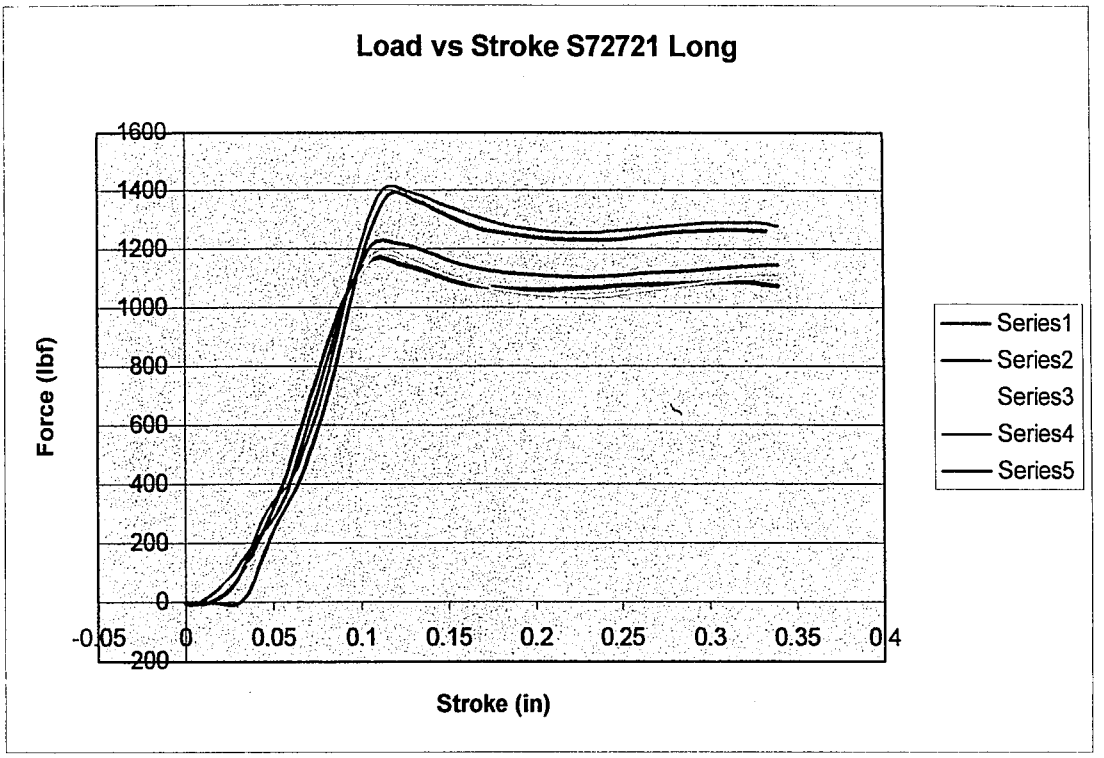

Figure 9.43. Load versus Stroke for S72721 Long Extrusion Test

Table 9.66. Extrusion Data for S72721 Long Extrusion Test

ID	S72721
Extrusion	Long
Substrate	T430
Coating	Bare
Drawing Lubricant	Hammidraw 1846-B
Extrusion Lubricant	Hasco Stealth
Avg. Max	1271.31
Std. Dev. Max	99.2
% Std. Dev. Max	7.8
Avg. Area	317.00
Std. Dev. Area	23.4
% Std. Dev. Area	7.4
Notes/Comments	A type curves, slight increase in force near end of extrusion

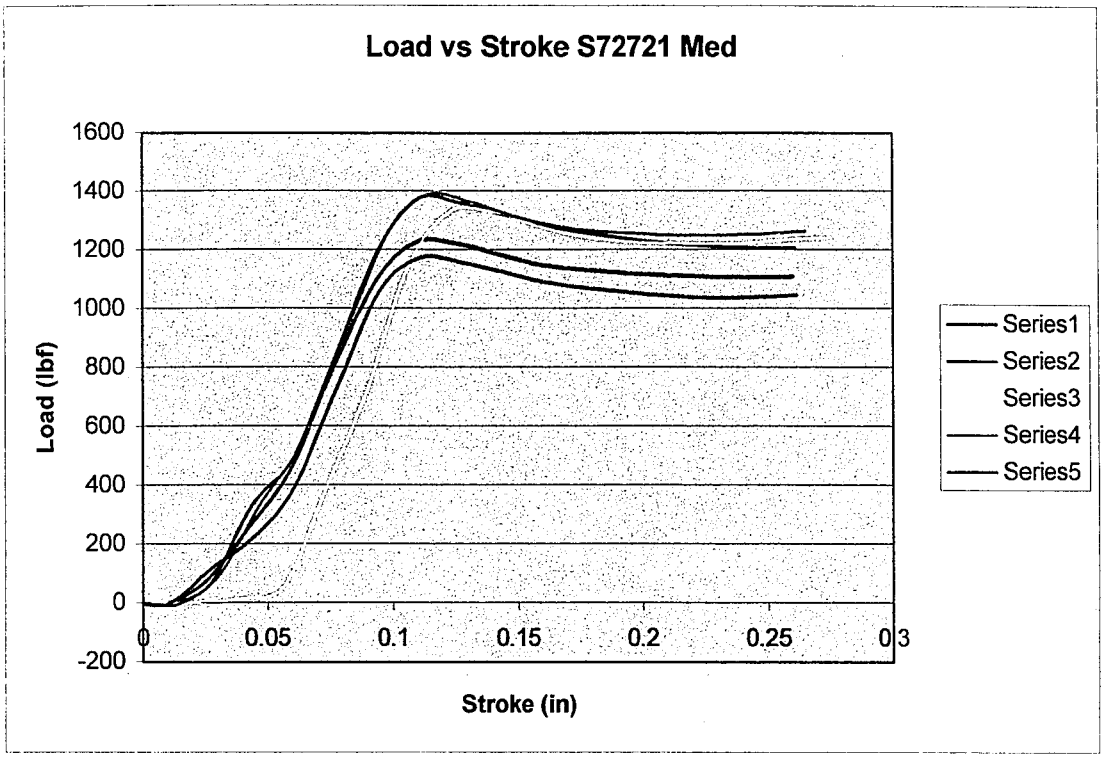

Figure 9.44. Load versus Stroke for S72721 Medium Extrusion Test

Table 9.67. Extrusion Data for S72721 Medium Extrusion Test

ID	S72721
Extrusion	Medium
Substrate	T430
Coating	Bare
Drawing Lubricant	Hammidraw 1846-B
Extrusion Lubricant	Hasco Stealth
Avg. Max	1300.30
Std. Dev. Max	85.2
% Std. Dev. Max	6.6
Avg. Area	232.45
Std. Dev. Area	16.4
% Std. Dev. Area	7.1
Notes/Comments	A type curves, some lateral spread as an effect of zeroing the press

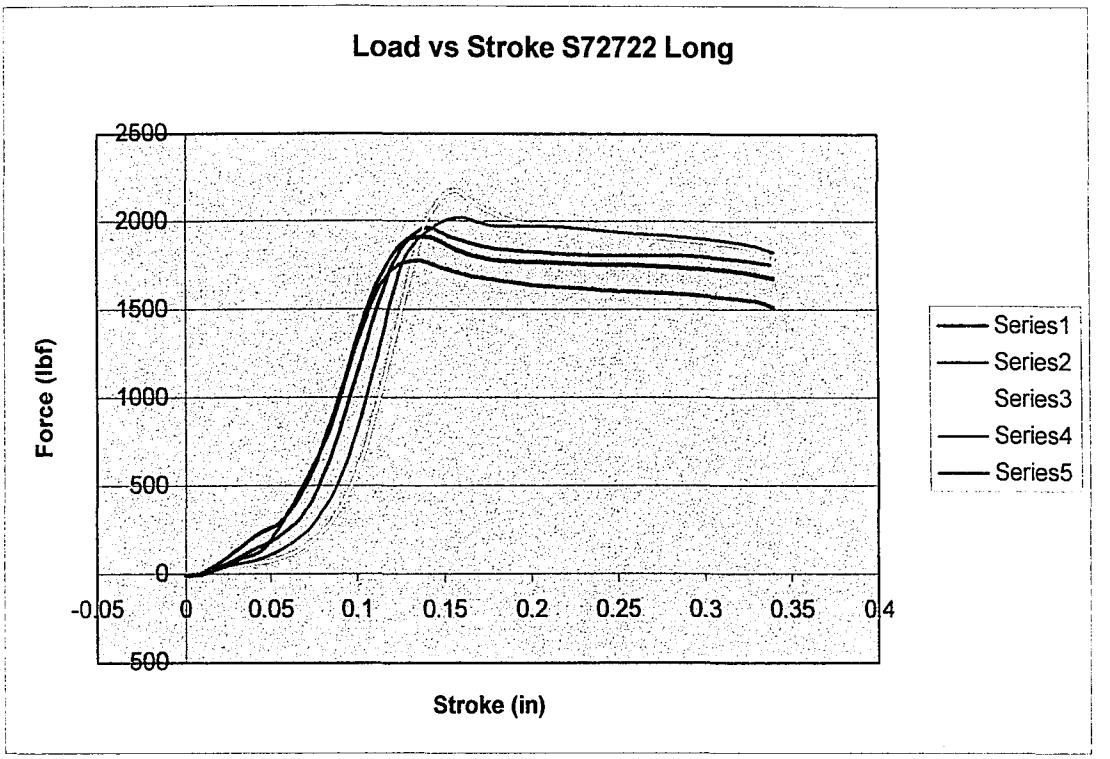

Figure 9.45. Load versus Stroke for S72722 Long Extrusion Test

Table 9.68. Extrusion Data for S72722 Long Extrusion Test

ID	S72722
Extrusion	Long
Substrate	A286
Coating	Bare
Drawing Lubricant	Hammidraw 1846-B
Extrusion Lubricant	Hasco Stealth
Avg. Max	1969.73
Std. Dev. Max	130.9
% Std. Dev. Max	6.7
Avg. Area	450.79
Std. Dev. Area	6.1
% Std. Dev. Area	1.4
Notes/Comments	A type curves

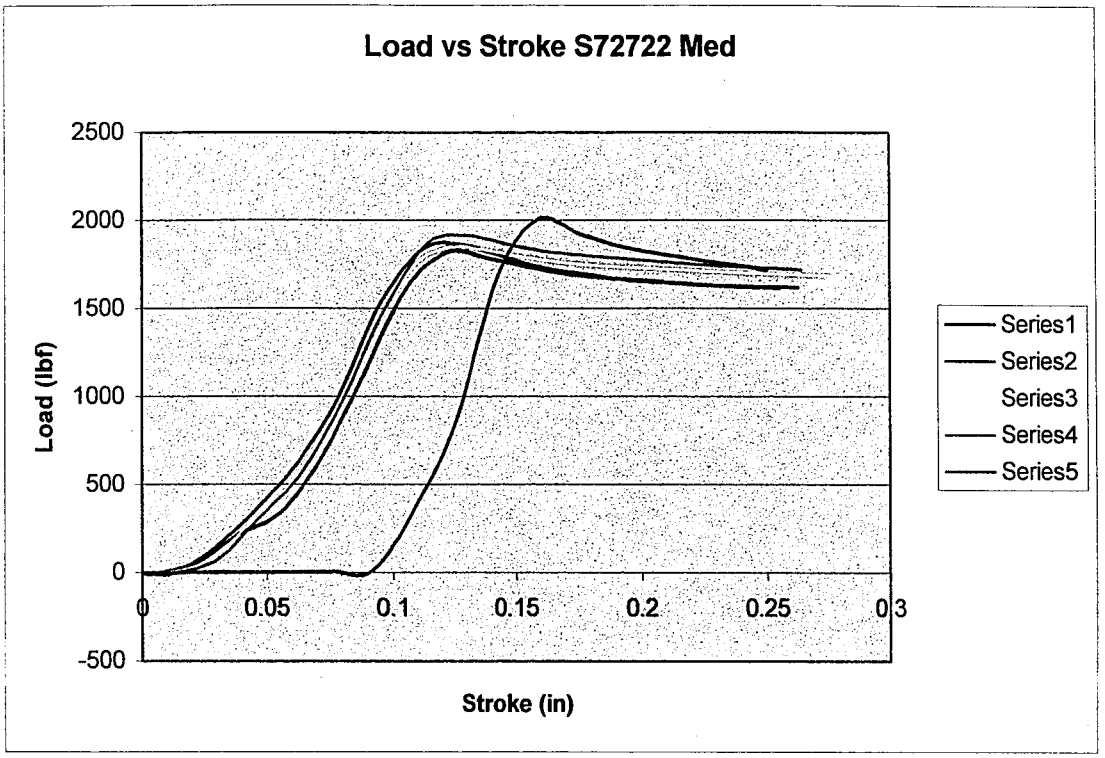

Figure 9.46. Load versus Stroke for S72722 Medium Extrusion Test

Table 9.69. Extrusion Data for S72722 Medium Extrusion Test

ID	S72722
Extrusion	Medium
Substrate	A286
Coating	Bare
Drawing Lubricant	Hammidraw 1846-B
Extrusion Lubricant	Hasco Stealth
Avg. Max	1892.09
Std. Dev. Max	65.2
% Std. Dev. Max	3.5
Avg. Area	313.37
Std. Dev. Area	40.6
% Std. Dev. Area	12.9
Notes/Comments	A type curves, some lateral spread as an effect of zeroing the press

9.7 Appendix G: Equipment Modifications

Wire Drawing Bench Modifications:

The Waterbury-Farrel wire drawing bench was modified in several ways for the testing. Both 500 and 5000 lb load cells manufactured by Entran Devices were used on the wire drawing bench in conjunction with an amplifier also provided by Entran. The signal was then read by a National Instruments data acquisition card using LabView™ software. The data was then saved into a text file that was read and manipulated using Microsoft Excel. Also, a special lubricant box was constructed so that the wire being drawn is completely submerged in the lubricant prior to entering the drawing die.

Instron Tensile Testing Unit Modifications

Only minor modifications were made to the Instron tensile testing unit. A custom extrusion die holder and custom extrusion punch holder were both designed and machined to fit into the existing fittings of the machine.

10.0 Curriculum Vitae

Mario Ernest Epler was born on December 25, 1977 in Lancaster Pennsylvania to Douglas and Marita Epler. He attended Donegal High School prior to his undergraduate studies at Lehigh University. Mario graduated from Lehigh in June of 2000 with honors with a B.S. in Materials Science and Engineering. He decided to continue his studies at Lehigh under the guidance of Wojciech Misiolek, director of the Institute for Metal Forming.

As an undergraduate at Lehigh, Mario spent a summer doing research at Oak Ridge National Lab under the O.R.I.S.E. program. He was the president of the Student Materials Society his senior year, and was awarded (with his student group) first place award for the local ASM chapter student poster contest his junior year.

As a graduate student, he was awarded the Brink Fellowship for his first year of studies. He was part of a team that was awarded second place for the ET design contest in 2001, for the Digital Armor PDA case.

His current research interests include metal deformation characterization and modeling and process engineering. Specific interests include powder metallurgy, welding, and steel forming.

Mario has been a DJ on the school's radio station WLVR 91.3 fm for most of his undergraduate and graduate years at Lehigh, which is his main hobby. Someday, he hopes to be able to fully fabricate his and other custom motorcycles and to be a contestant on Junkyard Wars or Monster Garage, much like one of his idols, Jesse James of West Coast Choppers.

END OF TITLE